The Geometry and Evolution of Supra-Salt Normal Fault Arrays

Anette Broch Mathisen Tvedt

Dissertation for the degree of philosophiae doctor (PhD)

at the University of Bergen

2016

Dissertation date: 22. June 2016

Year: 2016

Title: The Geometry and Evolution of Supra-Salt Normal Fault Arrays

Author: Anette Broch Mathisen Tvedt

Print: AIT Bjerch AS / University of Bergen

Preface

This dissertation has been submitted for the degree of Philosophiae Doctor (PhD) at the Department of Earth Science at the University of Bergen. This study is the result of research collaboration between Centre for Integrated Petroleum Research (Uni CIPR – Uni Research), Department of Earth Science at the University of Bergen, Norway and Imperial College, London, UK. The work has been carried out at CIPR between July 2011 and December 2015. This project is part of the SALTEC project, funded by CIPR and the Research Council of Norway. The SALTEC project focuses on the role that salt plays during tectonics, how salt influences the structural style of a deformed region, and how it sometimes even triggers deformation.

During the research conducted for this PhD dissertation, the candidate has been enrolled in the PhD study program at the Department of Earth Science at the University of Bergen. The candidate has been supervised by Professor Atle Rotevatn (University of Bergen), and co-supervised by Professor Christopher A-L. Jackson (Imperial College), Professor Haakon Fossen (University of Bergen) and Professor Robert Gawthorpe (University of Bergen).

Guide for readers

This thesis follows an article-based format in conformity with most Norwegian doctoral dissertations for natural sciences. The thesis consists of three parts, where Chapter 1 introduces the rationale of the study, research goals, study areas,

approach of the research, background and state of the art. Chapter 2, the main part of the thesis, consists of four scientific articles published in, or submitted to, peer-reviewed scientific journals. Chapter 3 features a summary of the main outcomes, discussion of these results, conclusions, implications and perspectives of this research. The reference list following Chapter 3 includes all references cited within this thesis. The appendix comprises additional contributions in the form of abstracts of presentations and posters presented at international conferences.

For readers accustomed to monographic dissertations, please note that there may be some overlap between the different papers, as they are stand-alone publications, particularly in terms of introduction and background material.

Acknowledgements

During the course of this thesis, I have had the pleasure to meet and work with many inspirational, outstanding scientists. This thesis would not have been possible without the great support from supervisors, colleagues, friends and family.

First, I would like to thank my supervisors Atle Rotevatn, Christopher A-L. Jackson, Haakon Fossen and Robert Gawthorpe, who have provided great support throughout this project. I especially want to thank Atle, as the main supervisor, for excellent discussions, genuine interest, guidance, friendship and great motivation throughout the project. I have really appreciated your scientific input in all different geological wonders, and even when the faults we study have demonstrated they are alive and brutal, you have even fed me with live updates on magnitudes and calmed me down. I would also especially like to thank Chris for always welcoming me to Imperial College. I have really appreciated your inexhaustible scientific input, our great discussions and your constant enthusiasm. I am truly grateful for all your help, guidance and friendship, and I hope we can continue our collaboration in the future. I would also like to thank Haakon Fossen for all the good support. I have really enjoyed that you always challenge me on different subjects and your great scientific input. I would also like to thank Rob Gawthorpe for the support and inspirational scientific discussions. I really appreciate your great knowledge and your uplifting mood.

I am also very grateful to the Research Council of Norway and Uni CIPR for the financial and administrational support through the SALTEC project. PGS and CGG are gratefully acknowledged for providing the excellent 3D seismic reflection data that made this study possible. I would also like to thank Schlumberger for providing access to Petrel software, Badleys Geosciences for their TrapTester modelling software, Midland Valley for providing their Move software, and MathWorks for their Matlab programming software.

I am very fortunate to have been affiliated with both Uni CIPR and the Department of Earth Science at University of Bergen, where the work environment has been great both scientifically and socially. I especially want to thank all colleagues and fellow PhD students both at Uni CIPR and the Department of Earth Science for interesting discussions, fun and support throughout this research. Luisa, Kristian and Svenn, I am truly thankful for all your help, support, discussions, motivation, good times in the office and your friendship. Ingrid, Helge and Espen, you have stood by me since the day we set our feet into the "Matnat" nine years ago. I am truly grateful for your support throughout, inspirational discussions and your friendship. I also would like to thank Becky, Matt, Olly and Tom at Imperial College for good scientific discussions and for taking care of me when I have been over for a visit.

I would also like to thank my colleagues at Petrolia Norway for scientific input, support, friendship and for cheering me on during the inning of manuscript and thesis preparation.

I would especially express my gratitude to my beloved friends and family for their consistent support, understanding, patience and love. You have constantly stayed interested in the wonders of salt and reminded me how cool salt can be when the frustration has breached the surface, and for that, I am truly grateful!

Finally, and most importantly, I would like to thank Ole Joachim for his love, support, and patience. I am now looking forward to spend more time with you!

Anette Broch Mathisen Tvedt

Bergen, January 2016

"You are the salt of the earth"
Matthew 5:13

Abstract

The structural style and evolution of normal fault arrays above mobile salt is less understood compared to those developed in rifts where strong variations in mechanical stratigraphy are absent. This research was performed to refine the understanding of the growth of supra-salt extensional fault arrays and how salt may impact the growth history and structural style of such arrays. To investigate the three-dimensional growth history of supra-salt fault arrays, detailed qualitative and quantitative analyses have been performed of fault geometry/morphology, throw distribution and syn-kinematic strata of fault arrays in two different salt basins (the techniques used in the analyses are presented in Paper I), the Egersund Basin, offshore Norway (Paper II & IV) and Santos Basin offshore Brazil (Paper III).

The first paper discusses how different techniques of fault analyses can be used to determine the style of growth of seismic-scale syn-sedimentary normal faults. It is presently known that normal faults can either grow via sympathetic increase in displacement and length ('isolated model') or by rapid establishment of their near-final length prior to significant displacement accrual ('coherent model'). Application of quantitative techniques exemplified in Paper I can aid the assessment of the relative roles of the isolated and coherent fault models during crustal extension.

Paper II discusses how growth of normal faults in multilayer sequences can occur by the use of a 3D seismic case study of a supra-salt fault array in the Egersund Basin, offshore Norway. The supra-salt fault array was initiated by re-activation of a pre-existing sub-salt fault array during the Late Triassic, mainly through kinematic coupling with the sub-salt fault array, before being buried during the Late Jurassic to Turonian times. Only parts of the fault array were reactivated during the Turonian, in response to salt mobilisation driven by basin inversion. Based on the three-dimensional fault analyses, we conclude that a combination of basement faulting and salt (re-) mobilisation is the driving mechanisms behind fault activation and reactivation. Reactivated faults are located where the underlying salt

is thick, while the non-reactivated faults are found where salt is depleted. Even though the sub- and supra-salt faults are mainly geometrically decoupled through the salt, our findings suggest that a kinematic coupling existed as sub-salt faults still affected nucleation and localization of the cover faults.

Paper III describes the evolution of supra-salt fault arrays within the São Paulo Plateau in the Santos Basin. Kinematic analyses reveal that the fault arrays formed during two discrete phases of deformation (Albian-to-Miocene fault arrays above salt anticlines and -plateau, and Oligocene-to-Present fault arrays above salt-walls). Albian to Miocene faulting likely reflects a combination of thin-skinned overburden extension, which drove reactive diapirism in relatively distal parts of the basin, and outer-arc extension-related faulting driven by regional contraction and overburden shortening. In contrast, the Oligocene-to-Present faults likely formed due to thin-skinned overburden extension above mature salt walls. We show that: (i) supra-salt fault growth can be protracted and polyphasal; (ii) it can be difficult to determine the triggers and drivers for supra-salt normal fault nucleation and growth; and (iii) domains of extension and contraction on salt-bearing passive margin may not be mutually exclusive and may overlap in time and space.

Paper IV discusses the geometry and growth of a normal fault array formed during the birth, growth and death of an array of salt structures. We show that the supra-salt fault array and salt structures developed in response to; (i) movement on a thick-skinned, basin bounding fault in the Late Triassic, causing salt mobilisation by base salt tilting and gliding, which in turn caused the nucleation and initial fault growth by thin-skinned extension. Overburden gravity gliding and stretching drove reactive diapirism and salt wall growth that continued into the Late Jurassic, when the salt stocks nucleated. The faults reached their near-full length during this time. The amount of fault growth during reactive diapirism during the Late Triassic-Late Jurassic was controlled by salt flow into the widening salt walls (though extension was driving the reactive diapirism); (ii) subsequent to reactive diapirism, diapir collapse due to along-strike migration of salt within the wall drove further fault

growth, principally by displacement accrual in the Early Cretaceous, with active diapirism occurring simultaneously along strike; (iii) active diapirism occurring until the Neogene, which drove further salt wall collapse and fault growth near the diapirs. Our study supports physical model predictions, showcasing a three-dimensional example of how protracted, multiphase salt diapirism can influence the structure and growth of normal fault arrays.

This study has demonstrated how qualitative and detailed quantitative fault analyses of supra-salt fault arrays can be used to track the flow of salt and provide a contribution to the understanding of overburden deformation linked to salt mobilisation. Further, this research offers insight into the complex interplay between salt diapirism and faulting, showcasing three-dimensional natural examples of how multiphase salt diapirism can influence the structure and growth of normal fault arrays. Detailed investigation of the dynamics of supra-salt deformation, have implications for the prediction the four-dimensional flow of salt and can thereby provide us with a better understanding of the tectono-stratigraphic evolution of salt-influenced sedimentary basins.

List of publications and authorship statement

The four papers presented in this thesis are a product of cooperation with listed authors. Contributions from others than the listed authors are acknowledged at the end of each paper.

Paper I: Techniques to determine the style of growth of seismic-scale syn-sedimentary normal faults
Submitted to the Geological Society, London, Special Publications
Christopher A-L. Jackson, Rebecca E. Bell, Atle Rotevatn, Anette B.M. Tvedt

Paper I is written by Christopher A-L. Jackson. The paper came out of the work performed, and techniques used, by all of the authors over several years in different study areas. I provided examples used in the paper, including interpretation of seismic data, analyses and interpretations from both the Santos and Egersund basins, in addition to manuscript review.

Paper II: Growth of normal faults in multilayer sequences: A 3D seismic case study from the Egersund Basin, Norwegian North Sea
Published in Journal of Structural Geology, Volume 55, October 2013, Pages 1–20
Anette B.M. Tvedt, Atle Rotevatn, Christopher A.-L. Jackson, Haakon Fossen, Robert L. Gawthorpe

For **Paper II**, I was responsible for interpretation of seismic data and analyses of those interpretations, drafting figures and writing the manuscript. Atle Rotevatn, Christopher A.-L. Jackson, Haakon Fossen and Robert L. Gawthorpe contributed with important discussions and manuscript review.

Paper III: Growth of Supra-Salt Normal Fault Arrays in the Santos Basin
Submitted to Journal of Structural Geology
Anette B.M. Tvedt, Christopher A.-L. Jackson, Atle Rotevatn, Haakon Fossen

For **Paper III**, I was responsible for interpretation of seismic data and analyses of results, drafting figures and writing the manuscript. Christopher A.-L. Jackson, Atle Rotevatn and Haakon Fossen contributed with important discussions and manuscript review.

Paper IV: Supra-salt normal fault growth during the rise and fall of a salt diapir: insights from 3D seismic reflection data
Submitted to Journal of Structural Geology
Anette B.M. Tvedt, Atle Rotevatn, Christopher A.-L. Jackson

For **Paper IV**, I was responsible for interpretation of seismic data and analyses of those interpretations, drafting figures and writing the manuscript. Atle Rotevatn and Christopher A.-L. Jackson engaged in discussions and manuscript review.

Contents

Chapter 1. Introduction

1.1 Rationale

Salt tectonics can be defined as the process of deformation involving flow of salt (Hudec and Jackson, 2007). Salt tectonics is known to differ from deformation in non-salt influenced settings, e.g.; passive margins, where salt is present, displays larger scale of up-dip extension and down-dip shortening than margins unaffected by salt, and salt influenced fold and thrust belts tend to be wider than non-salt influenced fold and thrust belts (Hudec and Jackson, 2007). Salt tectonics play an important role for the structural style in many sedimentary basins worldwide (e.g., in the Gulf of Mexico, North Sea and Persian Gulf) and is relatively well understood when it comes to the overall geometry of salt structures, mechanics of salt flow and the processes controlling the growth of diapirs (e.g., Vendeville and Jackson, 1992b; Vendeville and Jackson, 1992a; Jackson et al., 1994; Hudec and Jackson, 2007; Brun and Fort, 2011; Hudec and Jackson, 2011). Despite recent advances in the understanding of salt mechanisms and how salt move through time by the use of physical analogue models and three dimensional seismic (e.g. Ge and Jackson, 1998; Rowan et al., 1999; Brun and Mauduit, 2009; Hudec and Jackson, 2011; Jackson et al., 2014a; Jackson et al., 2015), cross sectional observations remain a prime source of knowledge on the structural style and evolution of normal fault arrays above mobile salt, compared to those developed in rifts where strong variations in mechanical stratigraphy are absent (e.g. Gupta et al., 1998; Dawers and Underhill, 2000; Gawthorpe and Leeder, 2000; Gupta and Scholz, 2000; McLeod and Underhill, 2000). For example, structures related to the rise and fall of salt diapirs during thin-skinned extension are particularly well studied in cross-sections and physical experiments (Vendeville and Jackson, 1992b; Vendeville and Jackson, 1992a; Ge et al., 1995), but although recent studies focus on the 3D evolution of normal fault growth in salt-influenced settings, the effects of salt on lateral fault growth and map-view fault geometries are clearly far less constrained than those observed in cross-section. Where the three-dimensional segmentation, growth and linkage of different fault arrays related to the different salt structures have mainly been

described qualitatively (e.g. Rowan et al., 1999). Relatively few studies have addressed the three-dimensional temporal and spatial evolution of supra-salt normal fault arrays related to the growth and demise of salt structures by the use of natural examples, by both using a quantitative and qualitative approach. The main aim of the current research is to increase our understanding of the geometry and evolution of extensional fault arrays in salt-influenced settings, with special emphasis on normal fault growth in extensional salt basins and on passive margins where salt is present. A better understanding of the geometry and evolution of supra-salt fault arrays have implications for the understanding of the four-dimensional flow of salt and tectono-stratigraphic evolution of sedimentary salt-basins, which in turn can aid the exploration and production of hydrocarbons.

1.2 Research goals

This study focuses on the geometry and evolution of extensional fault arrays in salt-influenced settings, specifically on the interactive effects of fault evolution and salt flow through time. The main aims of this work have been to:

- Investigate the impact of salt on the nature of, and kinematic coupling between, supra- and sub-salt faulting.
- Investigate the geometry and kinematics of supra-salt normal faults and distinguish the characteristics of faulting
- Test different mechanisms controlling initiation and growth of supra-salt normal wall fault arrays, where salt has influenced both localisation and growth.
- Investigate the interplay between fault evolution and salt-flow through time during multiphase salt diapirism

These main aims are addressed through subsurface case studies of the Egersund Basin (offshore SW Norway) and the Santos Basin (Brazil), by detailed analyses of fault statics (e.g. present-day fault geometry, morphology, segmentation) and dynamics (e.g. initiation, localization, growth patterns, growth rates, displacement distributions,

lateral and vertical linkage and interaction with mobile salt) to unravel the interplay between salt mobilisation and supra-salt faulting.

1.3 Study areas and research approach

1.3.1 Study areas

The main aims of this study are addressed through the analysis of three-dimensional seismic data from the Egersund Basin in the North Sea offshore Norway and the Santos

Fig. 1.1 Location of study areas; Santos Basin offshore Brazil and Egersund Basin offshore Norway.

Basin offshore Brazil (Fig. 1.1). Both data sets are of good to excellent quality, and therefore allow detailed fault investigation in the supra-salt cover.

The Egersund Basin is located in the SW part of the North Sea and represent a salt influenced rift basin (Sørensen et al., 1992; Glennie et al., 2003; Jackson and Lewis, 2016). The superb three-dimensional seismic shows a wide range of supra-salt fault arrays related to the growth of salt walls, salt anticlines and salt stocks (Jackson and Lewis, 2013; Tvedt et al., 2013; Jackson and Lewis, 2016; Tvedt et al., in review). The Egersund Basin has evolved through several stages after initial opening in the Carboniferous - Permian and infill of c. 1000 m Zechstein salt in the Late Permian (Sørensen et al., 1992). The present day remaining salt is relatively thin with the exception of tall salt stocks that are up to c. 2 km. In order to improve our understanding of the basin evolution of the Egersund Basin, the supra-salt fault arrays have been analysed in detail to shed light on the multiphase supra-salt fault growth. Salt mobilisation has clearly influenced fault growth during several phases, even after major tectonic events and thereby had an impact on the structural style of the Egersund Basin.

The Santos Basin is different in terms of both overall tectonic setting and salt thickness. The studied part of the Santos Basin, the São Paulo Plateau is located downslope on the Brazilian passive margin. After rifting and the establishment of the passive margin and deposition of the salt, salt has strongly influenced the deformation of the supra-salt cover (e.g. Demercian et al., 1993; Davison et al., 2012; Jackson et al., 2015; Tvedt et al., in review). The salt in this part of the basin is much thicker (general thickness of the salt is at least 500 m thick between c. 2 km tall flat-topped salt walls) than in the Egersund Basin, and thus also expected to have a larger control on the deformational styles (Duffy et al., 2013). The supra-salt fault arrays have been analysed in detail to investigate the multiphase supra-salt fault growth, as salt mobilisation has clearly influenced fault growth during several phases. Our analyses consider the supra-salt fault arrays, which are located above salt anticlines, plateaus, and wide flat-topped walls, at different stratigraphic levels in the post salt cover.

1.3.2 Methods

The three-dimensional seismic data analyses within the two study areas has employed a wide range of techniques, including: (i) throw-distance (*T*-*x*) plots – these allow us to identify zones of linkage between fault segments and evaluate the growth history in map view (Walsh and Watterson, 1990; Childs et al., 1995; Gawthorpe and Leeder, 2000; Kim and Sanderson, 2005); (ii) throw-depth (*T*-*z*) plots - these allow us to investigate the potential role of dip linkage and physical barriers in the host rock on fault growth (Mansfield and Cartwright, 1996; Hongxing and Anderson, 2007), and can also indicate times of syn-sedimentary faulting and blind fault propagation (e.g. Williams et al., 1989; Nicol et al., 1996; Jackson and Rotevatn, 2013; Tvedt et al., 2013); (iii) strike-projections of fault throw – these illustrate throw distribution across the fault surface and provide insights into the growth and linkage history of segmented normal fault arrays (Walsh and Watterson, 1991); (iv) time-thickness (isochron) maps and expansion indices for key stratigraphic intervals - these illustrate variations in sediment thickness related to faulting and to basin formation, and can shed light on fault growth history and phases of salt-related basin subsidence (Thorsen, 1963; Rouby et al., 2003; Jackson and Rotevatn, 2013; Tvedt et al., 2013); and (v) restoration and balancing of 2D sections in order to investigate the fault history, possible timing of salt mobilisation and large-scale basin geometry, with a specific focus on the timing of tilting and differential subsidence (Rowan, 1993).

Paper I describes the techniques in detail, including their limitations, whereas in Paper II-IV only the relevant methods and how these are utilized to resolve the different case studies, are explained.

1.4 Background and state of the art

1.4.1 Normal fault growth

The overall evolution of normal fault systems occurs as a consequence of crustal extension either by passive or active rifting (e.g.; Jackson and McKenzie, 1983; Gibbs, 1984; McClay, 1990). Normal faults in such systems can grow either by, or a

combination, of the following mechanisms: (i) sympathetic increase in their displacement and length (e.g. Watterson, 1986; Walsh and Watterson, 1988; Dawers et al., 1993; Dawers and Anders, 1995); this is known as the '*isolated fault model*' (*sensu* Walsh et al., 2003) or by (ii) rapid establishment of their near-final length prior to significant displacement accrual (e.g. Morley, 2002; Walsh et al., 2002; Giba et al., 2012; Jackson and Rotevatn, 2013); referred to as the '*coherent fault model*' (*sensu* Walsh et al., 2003).

Normal faults growing via the '*isolated fault model*' develop as individual segments, which then grow, link and amalgamate to form longer, continuous faults (e.g.; Peacock and Sanderson, 1991; Cartwright et al., 1995; Gawthorpe et al., 1997; Gawthorpe and Leeder, 2000; Mansfield and Cartwright, 2001; Rykkelid and Fossen, 2002). As the individual faults develop by lateral growth and overlap and interact, the displacement transfer is accommodated by relay zones (e.g.; Peacock and Sanderson, 1994). Between the fault tips of overlapping fault segments, rotation and enhancement of the local stress field eventually causes failure and relay breaching (Crider and Pollard, 1998; Kattenhorn et al., 2000), resulting in hard linkage of the individual fault segments (e.g.; Peacock and Sanderson, 1991; Trudgill and Cartwright, 1994; Crider and Pollard, 1998).

Normal faults growing via the '*coherent fault model*' initiate and grow as kinematically related segments of a fault array. The fault segments establish their near-final lengths early, resulting in their relay zones evolving by rotation, without lengthening, before relay breaching (Giba et al., 2012; Hemelsdaël and Ford, 2016). Whereas 'isolated faults' display a maximum displacement at the fault centre with gradually decreasing displacement towards the fault tips (e.g.; Muraoka and Kamata, 1983; Gawthorpe and Leeder, 2000; Mansfield and Cartwright, 2001), the 'coherent faults' will have steep fault growth paths on displacement-length graphs (Walsh et al., 2002). The relay zones are established early and the continued evolution mainly involve rotation without further lengthening before relay breaching (Giba et al., 2012; Hemelsdaël and Ford, 2016).

See Paper I for a more detailed description of how normal faults grow via a sympathetic increase in their displacement and length ('isolated fault model') or by rapid establishment of their near-final length prior to significant displacement accumulation ('coherent fault model'). This study focuses on extensional regimes where presence of salt has influenced the evolution of normal fault arrays.

1.4.2 Salt tectonics in rifts and on passive margins

Salt tectonics can be defined as the process of deformation involving flow of salt (Hudec and Jackson, 2007), where salt is defined as rocks composed primarily of halite, which is mechanically weak and behaves as a viscous fluid even at geologically rapid strain rates (*cf.* Hudec and Jackson, 2007). As salt is much weaker and has much lower viscosity than most of its surrounding rocks, salt will be the first to respond to regional stress (Ge et al., 1995). Salt structures related to salt tectonics are diapirs, stocks, pillows, walls, anticlines, walls, canopies etc. (Fig. 1.2).

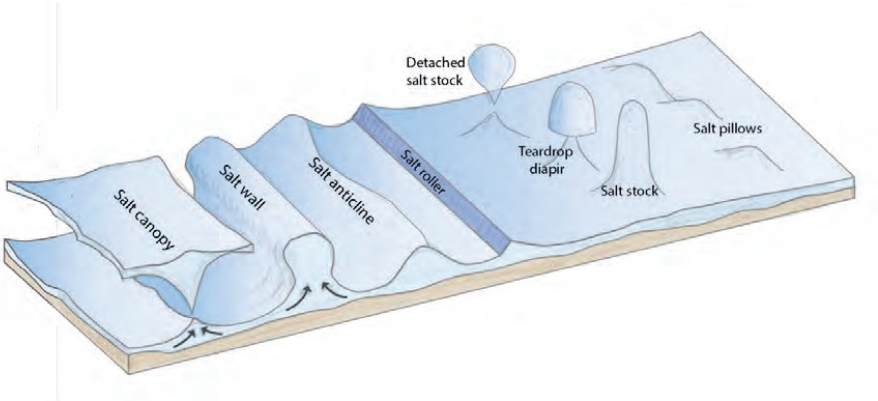

Fig. 1.2. Different types of salt structures, where the salt canopies, diapirs and stocks are the most mature. Modified from Fossen (2010).

Growth of salt structures, as represented in Fig. 1.2, can result in different styles of faulting and growth patterns. The growth of such salt structures is mainly associated with either growth by salt diapirs through reactive, active or passive diapirism (Fig. 1.3). During *reactive diapirism*, salt begins to rise in sharp-crested diapirs in space

created by regional extensional thinning during rifting or gravity spreading (Vendeville and Jackson, 1992b; Hudec and Jackson, 2007). During reactive diapirism oppositely dipping normal faults typically form in the overburden either sequentially or coevally during regional extension, with younger faults towards the crest (Fig. 1.3a) (Vendeville and Jackson, 1992b; Jackson and Vendeville, 1994; Rowan et al., 1999). If sequential faulting occurs, further slip on earlier-formed faults will be inhibited by the salt and overburden and, as a consequence, a second set of faults will form in the hangingwall above the salt diapirs, where the overburden is thinnest and weakest. The second set of faults will continue to grow until fault slip is inhibited by increasing resistance in the salt and overburden. This process continues until extension ceases (Vendeville and Jackson, 1992b). As extension or gravity spreading ceases, diapirism, and hence also fault growth, halts or the diapirs evolve into active or passive diapirs (Vendeville and Jackson, 1992b).

During *active diapirism* salt can force its way through the overburden, initiated by differential, thermal or displacement loading (Vendeville and Jackson, 1992b; Schultz-Ela et al., 1993). During active diapirism the overburden is faulted to accommodate flexure of the overburden during the uplift of the crest of the salt diapir (Vendeville and Jackson, 1992b). Faults related to active diapirism often occur on the crest or the edge of originally flat-crested rising diapirs (Fig. 1.3b) (Schultz-Ela et al., 1993). Schultz-Ela et al. (1993) argue that for active diapirism to occur, the diapir height must be more than two-thirds to three-quarters of the thickness of the surrounding cover. Since active diapirism is controlled by gravitational forces acting on the salt, active diapirism can continue independent of regional extension (Vendeville and Jackson, 1992b). When a salt diapir emerges at the surface, the salt diapir can continue to grow by downbuilding, where sediments accumulate around the diapir; this is referred to as *passive diapirism* (Fig. 1.3c) (Vendeville and Jackson, 1992b; Hudec and Jackson, 2007).

Salt-related extensional fault arrays have been subject of a great interest in the last decades and are most common in either active rift settings or on the outer shelf and upper slope of passive margins (Hudec and Jackson, 2007). Rift basins typically form in areas of crustal extension (Jackson and McKenzie, 1983). When salt is present, salt

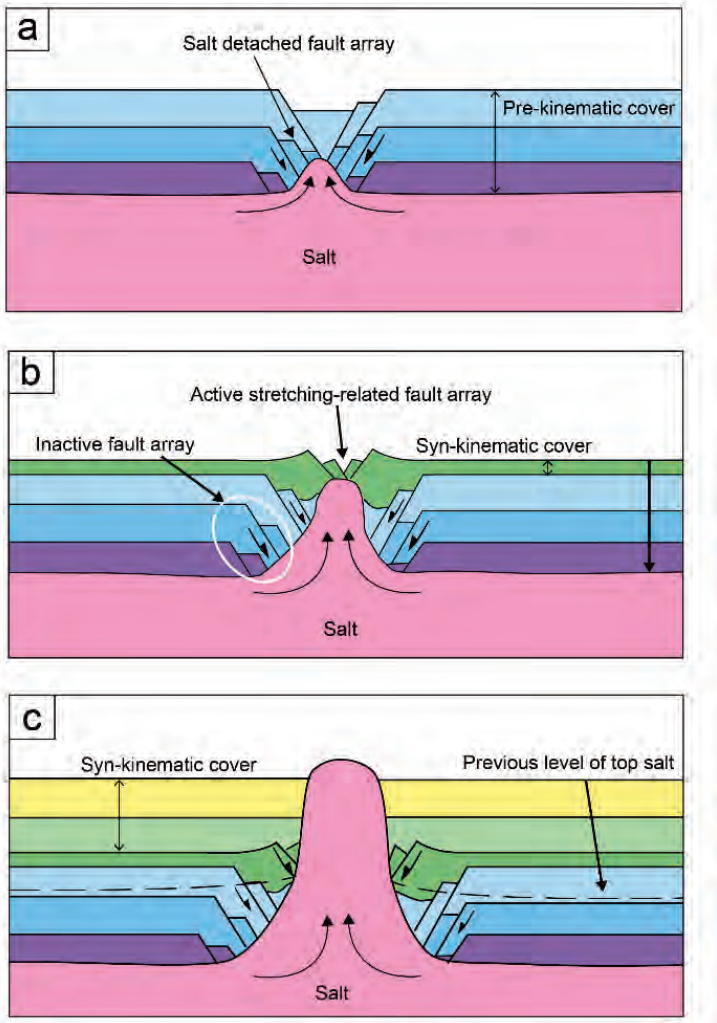

Fig. 1.3. Conceptual figure showing diapir piercement during regional extension. The growth of diapirs may go through some or all of these stages; (a) reactive diapirism; (b) active diapirism, where the supra-salt cover load pressurizes the salt; and (c) passive diapirism where sediment downbuilding occurs while the diapir continues to grow. Modified from Vendeville and Jackson (1992b) and Hudec and Jackson (2007).

can influence the structural styles and growth history of such basins by for example decoupling of basement and supra-salt overburden structures (e.g. Jackson and Vendeville, 1994; Richardson et al., 2005; Marsh et al., 2010; Duffy et al., 2013). In this work we have investigated supra-salt deformation related to mobilisation of the Zechstein Supergroup in the Egersund Basin, a rift basin offshore Norway. On salt bearing passive margins, salt can act as a decollement and result in thin-skinned deformation, including proximal extension and distal contraction (Rowan et al., 2004; Brun and Fort, 2011). In the research, we have investigated fault arrays whose growth is related to the mobilisation the Ariri Formation in the distal parts of the Santos Basin, on the passive margin of Brazil.

During the development of salt basins, a wide range of fault styles can develop in association with different types of salt structures (Stewart et al., 1996; Rowan et al., 1999). Supra-salt normal fault arrays (the focus of the present thesis) are often related to the growth or collapse of salt (Rowan et al., 1999; Davison et al., 2000b; Hudec and Jackson, 2007) and their trigger and driving mechanisms may generally involve one or more of the following: (i) crustal extension (Jackson, 1987; Nalpas and Brun, 1993); (ii) cover extension driven by gravity-gliding or gravity spreading (Gutiérrez, 2004; Hudec and Jackson, 2004; Jackson and Hudec, 2005; Hudec and Jackson, 2007; Dutton and Trudgill, 2009); (iii) differential compaction of cover around structures cored by largely incompressible salt (Anderson and Franseen, 1991; Hudec and Jackson, 2007); (iv) overburden folding and outer arc-related extension driven by either buckle folding above salt detachments or squeezing and active rise of mature diapirs (Pollard and Johnson, 1973; Cosgrove and Hillier, 2000; Hillier and Cosgrove, 2002); and/or (v) overburden collapse due to salt dissolution (Goldstein and Collins, 1984; Ge and Jackson, 1998; Bertoni and Cartwright, 2005).

Crustal extension

Crustal extension in salt basins can cause significantly different styles of supra-salt faulting than basins that lack salt (e.g. Penge et al., 1993; Jackson and Vendeville, 1994; Richardson et al., 2005; Marsh et al., 2010; Duffy et al., 2013). The salt can in such settings result in regionally significant detachment horizons, which again can lead

to decoupling of basement and overburden deformation during early crustal extension (e.g. Jackson and Vendeville, 1994; Jackson et al., 1994; Stewart et al., 1996; Erratt et al., 1999; Withjack and Callaway, 2000; Kane et al., 2010; Jackson and Rotevatn, 2013). Further crustal extension may lead to geometrical coupling as basement faults may breach through the salt and link with supra-salt fault structures (e.g. Vendeville et al., 1995; Tvedt et al., 2013; Wilson et al., 2013).

Gravity-gliding or gravity spreading

Regional or local tectonic events may trigger salt mobilisation, and hence faulting in the supra-salt cover. On passive margins, where salt can act as an intra-stratal detachment, overburden can move by gliding downslope the margin, causing thin-skinned faulting with different structural styles related to the location on the slope (upslope vs. downslope) (Mauduit et al., 1997; Rowan et al., 2004; Mohriak et al., 2008; Brun and Fort, 2011). In such settings, extension is focused in up-dip portions of the margin, and the extension can be accommodated by nappe extrusion in the distal part of the basin (Rowan et al., 2004; Hudec and Jackson, 2006). Regional extension could cause pre-existing diapirs to widen and collapse, thus generating crestal faults. Stretching would focus on the diapirs (if present) because they are weaker than the rocks in the possible flanking mini-basins. However, if salt diapirs are not present, deformation would likely be more distributed with salt rollers being the main structure (Rowan et al., 1999). On a larger regional scale, basin tilting as low as 1° can cause dominant gliding of the salt- sedimentary overburden where salt has acted as a detachment (Bishop et al., 1995; Stewart, 1999; Brun and Fort, 2011). In such settings the faults strike broadly normal to the tilt direction and the faults detach on top of the salt. On tilted margins, extensional structures are often found up dip, while contractional structures are found down dip (Brun and Fort, 2011).

Outer arc extension caused by differential compaction or by differential contraction

Formation of extensional faults may be caused by extension of the overburden due to differential compaction (Schultz-Ela et al., 1993; Jackson et al., 1994; Rowan et al., 1999; Cosgrove and Hillier, 2000; Stovba and Stephenson, 2002) or contraction of the

underlying salt (Stewart and Coward, 1995; Rowan, 1997; Rowan et al., 1999; Stovba and Stephenson, 2002) causing outer arc stretching. Faults formed by outer arc stretching due to differential compaction generally form in the zone of maximum extensional strain; the zone of maximum bending (Cosgrove and Hillier, 2000). These faults are often referred to as keystone faults, which typically do not detach on salt (Rowan et al., 1999). Local extension above the salt walls can also occur due to the differential contraction of salt (incompressible; Anderson and Franseen, 1991; Hudec and Jackson, 2007), and clastic sediments and carbonates in flanking mini-basins. Keystone faults can also form during contraction in the outer arc of salt-cored buckle folds, forming at the fold crest where strata are most curved (Rowan et al., 1999). Faults formed either by differential compaction or contraction have similar characteristics, in terms of geometry, distribution and localisation relative to the salt.

Gravitational deformation caused by salt dissolution

Erosion of overburden and thereby near-surface exposure of the salt is known to result in salt dissolution (Anderson and Knapp, 1993; Cartwright et al., 2001; Hudec and Jackson, 2002). Salt dissolution can also result from fracturing related to, for example, differential compaction, and when the fractures are established they can act as conduits for water and thereby facilitate further dissolution (Goldstein and Collins, 1984; Anderson et al., 1988; Anderson and Knapp, 1993; Ge and Jackson, 1998). Further, karstification of soluble sediments such as salt can cause gravitational deformation of the overburden (Goldstein and Collins, 1984; Gutiérrez, 2004). Structures related to dissolution-induced deformation can include folds, sinkholes, breccia pipes, joints, normal and reverse faults (Goldstein and Collins, 1984).

Distinguishing between these mechanisms (i-v) could be problematic as they often share some of the same characteristics. Although there are some recent studies that focus on the 3D evolution of normal fault growth in salt-influenced settings (Erratt et al., 1999; Baudon and Cartwright, 2008c; Jackson and Rotevatn, 2013), the effects of different initiation and driving mechanisms on the three-dimensional geometry of supra-salt fault geometries are clearly far less constrained than geometries observed in the cross-sectional plane of observation. Further, the use of both quantitative and

qualitative analyses in order to track the interaction between the salt and overburden deformation can lead to a better understanding of the different initiation and driving mechanisms, which again may result in a better understanding of the tectono-stratigraphic evolution of salt basins.

Chapter 2. Manuscript compilation

Paper II: Growth of normal faults in multilayer sequences: A 3D seismic case study from the Egersund Basin, Norwegian North Sea

II

Anette B.M. Tvedt, Atle Rotevatn, Christopher A.-L. Jackson, Haakon Fossen, Robert L. Gawthorpe

Published in Journal of Structural Geology, Volume 55, October 2013, Pages 1–20

Journal of Structural Geology 55 (2013) 1–20

Contents lists available at ScienceDirect

Journal of Structural Geology

journal homepage: www.elsevier.com/locate/jsg

Growth of normal faults in multilayer sequences: A 3D seismic case study from the Egersund Basin, Norwegian North Sea

Anette B.M. Tvedt [a,b,*], Atle Rotevatn [a,b], Christopher A.-L. Jackson [c], Haakon Fossen [a,b], Robert L. Gawthorpe [b]

[a] Centre for Integrated Petroleum Research, University of Bergen, Allégaten 41, 5007 Bergen, Norway
[b] Department of Earth Science, University of Bergen, Allégaten 41, 5007 Bergen, Norway
[c] Department of Earth Science & Engineering, Imperial College, London SW7 2BP, UK

ARTICLE INFO

Article history:
Received 2 November 2012
Received in revised form
29 July 2013
Accepted 7 August 2013
Available online 14 August 2013

Keywords:
Salt tectonics
Fault reactivation
Throw-length distribution
Expansion index
Fault linkage
Vertical throw-distribution

ABSTRACT

We investigate the structural style and evolution of a salt-influenced, extensional fault array in the Egersund Basin (Norwegian North Sea) through analysis of 3D reflection seismic and well data. Analysis of fault geometry/morphology, throw distribution and syn-kinematic strata reveal an intricate but systematic style of displacement and growth, suggesting an evolution of (1) initial syn-sedimentary fault growth contemporaneous with salt mobilization initiated during the Late Triassic, (2) cessation of fault activity and burial of the stagnant fault tips, and (3) subsequent nucleation of new faults in the cover above contemporaneous salt re-mobilization initiated during the Late Cretaceous, with downward propagation and linkage with faults. Stage 3 was apparently largely controlled by salt mobilization in response to basin inversion, as reactivated faults are located where the underlying salt is thick, while the non-reactivated faults are found where salt is depleted. Based on the 3D-throw analyses, we conclude that a combination of basement faulting and salt (re-) mobilization is the driving mechanisms behind fault activation and reactivation. Even though the sub- and supra-salt faults are mainly geometrically decoupled through the salt, a kinematic coupling must have existed as sub-salt faults still affected nucleation and localization of the cover faults.

1. Introduction

The structural style and evolution of normal fault arrays developing in the presence of mechanically weak detachments rich in, for example, halite (salt) or mudstone, are different to and less well understood than, fault arrays forming in the absence of such detachments. These differences arise in part due to the ability of salt and mudstone to accommodate strain and displacement by ductile flow. For example, salt- or mudstone-rich layers can: (i) act as regional detachment horizon or *décollement* (Morley et al., 2003; Jackson and Hudec, 2005); (ii) inhibit the vertical or lateral propagation of faults (e.g. Withjack et al., 1990; Pascoe et al., 1999; Maurin and Niviere, 2000; Withjack and Callaway, 2000; Richardson et al., 2005; Ford et al., 2007; Kane et al., 2010; Marsh et al., 2010); and (iii) cause full or partial geometric and kinematic decoupling of sub- and supra-detachment deformation (e.g. Stewart et al., 1997; Withjack and Callaway, 2000; Ford et al., 2007). Hence, ductile layers may significantly affect the geometry and evolution of extensional fault arrays, resulting in marked temporal and spatial variations in structural style, fault-related folding and displacement distribution (e.g. Rowan et al., 1999; Kane et al., 2010; Marsh et al., 2010; Duffy et al., 2012). The impact of ductile layers on normal fault array evolution becomes even more complex when polyphase extension occurs, because a second phase of extension can lead to: (i) reactivation of sub-detachment, typically 'thick-skinned' faults, and triggering of 'thin-skinned' extension of the supra-detachment cover; and (ii) the growth of salt- and shale-cored structures due to thin-skinned extension of the cover, which can itself cause faulting of the overburden (e.g. 'reactive diapirism'; Vendeville and Jackson, 1992; Jackson and Vendeville, 1994; Van Rensbergen et al., 1999).

Relatively few studies have addressed the structural style and evolution of normal fault arrays forming in response to salt- or mudstone-influenced, polyphase extension (Richardson et al., 2005; Kane et al., 2010; Duffy et al., 2012). The aims of this study are to: (i) highlight the relative roles of sub-salt 'basement' reactivation and salt mobilization, on the distribution and magnitude

* Corresponding author. Uni CIPR, PO Box 7800, N-5020 Bergen, Norway. Tel.: +47 97562768, +47 55583650.
E-mail address: Anette.B.Tvedt@uni.no (A.B.M. Tvedt).

0191-8141/$ – see front matter © 2013 Elsevier Ltd. All rights reserved.
http://dx.doi.org/10.1016/j.jsg.2013.08.002

of supra-salt 'cover' deformation; (ii) assess the impact that salt has on the magnitude of kinematic coupling between supra- and sub-salt faulting; and (iii) determine how mudstone layers influence the growth of normal fault systems in the supra-detachment sequence. To achieve these aims we use high-quality, 3D seismic reflection data (PGS MC3D-EGB2005) from the Egersund Basin, offshore Norway (Figs. 1 and 2), which allow us to constrain, in three-dimensions, the spatial relationship between, geometry and distribution of displacement on basement and cover faults, and thickness changes in coeval growth strata. Borehole data allows us to directly constrain the composition of the faulted sequence, and provide insight into the growth rate and spatial evolution of the studied fault array. Our results provide new insight into the control of polyphase rifting and ductile layers on the temporal and spatial evolution of normal fault arrays.

2. Geological framework

The Egersund Basin trends NW–SE and represents the NW extension of the Norwegian Danish Basin (Fig. 1). The basin initially formed in response to Carboniferous-to-Permian rifting (Sørensen et al., 1992; Ziegler, 1992). A thick succession of continental sediments was deposited in the basin during the Early Permian (Sørensen et al., 1992). During the Late Permian, the Egersund Basin represented a sub-basin of the 'North Permian Basin' (Sørensen et al., 1992; Ziegler, 1992), which formed following the syn- to

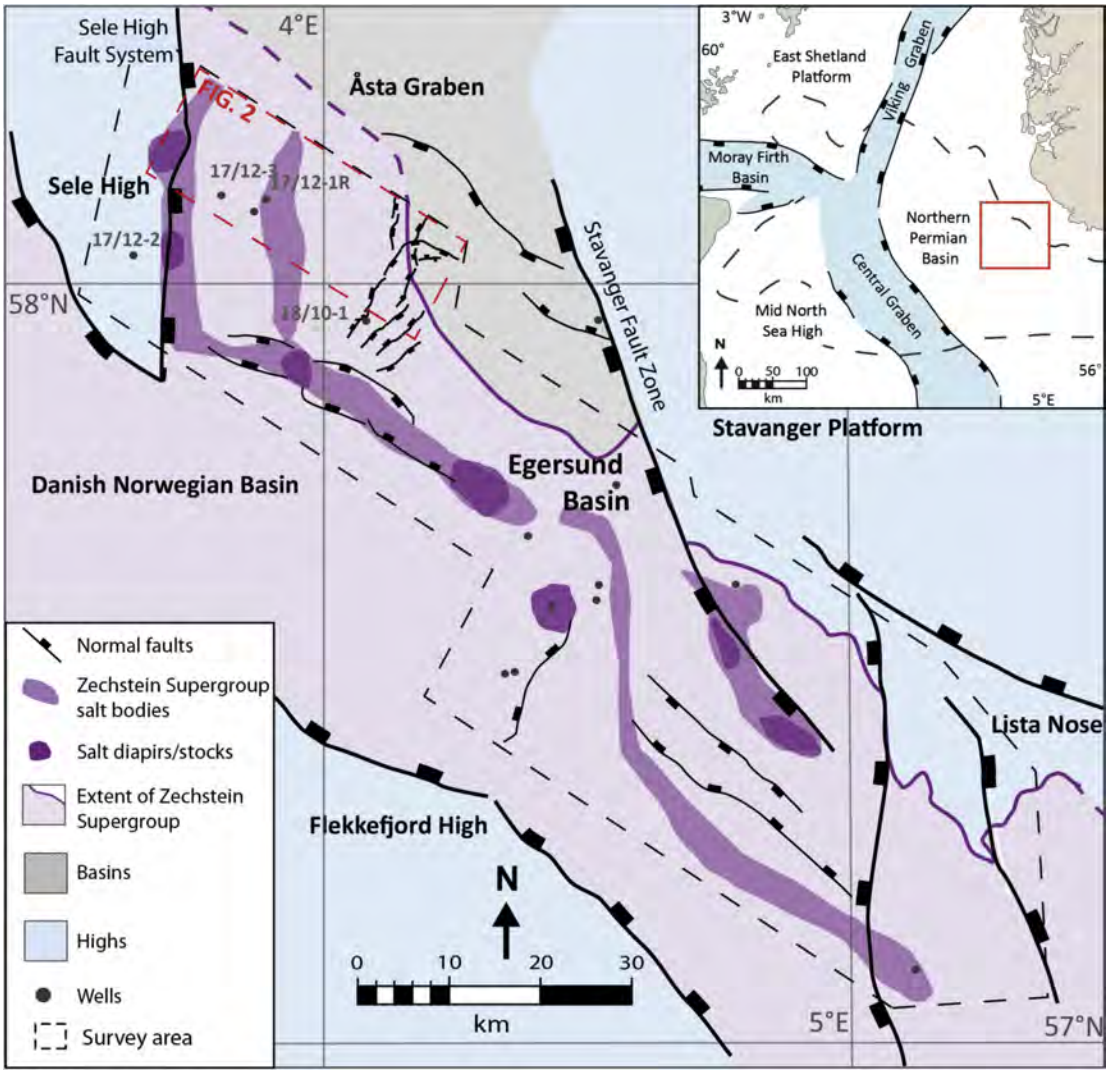

Fig. 1. Location of the Egersund Basin (EGB) in the North Sea north east of the Central Graben (red square in the inset of simplified structural map of the North Sea). Structural maps and extent of ZSG is based on observations in this study with data from Millennium Atlas (Zanella and Coward, 2003) and data from the Norwegian Petroleum Directorate. (For interpretation of the references to colour in this figure legend, the reader is referred to the web version of this article.)

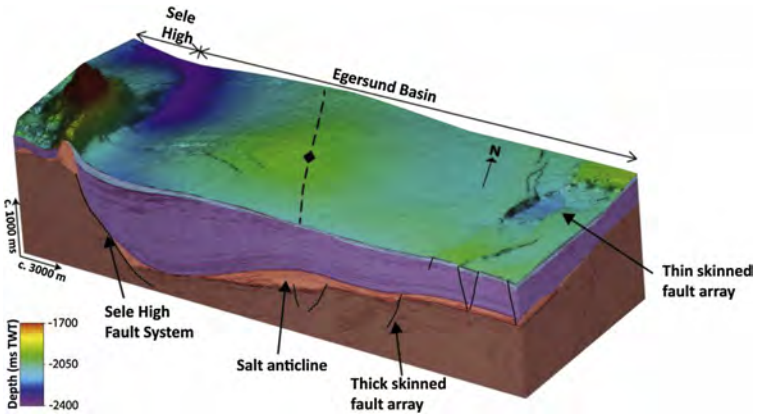

Fig. 2. Block diagram indicating the location of the studied fault array related to the salt anticline to the east. Horizon displayed on the top of the block is the top of the Bryne Formation. The colours on the sides of the block represent the age of the stratigraphy: Brown = Permian, Light red = Zechstein Supergroup, Purple = Triassic and Blue = Jurassic. (For interpretation of the references to colour in this figure legend, the reader is referred to the web version of this article.)

post-orogenic extensional collapse of the Variscan Orogen (Hodgson et al., 1992; Sørensen et al., 1992). Repeated flooding and desiccation of the North Permian Basin resulted in deposition of a thick (1000–1500 m; Sørensen et al., 1992) salt-rich succession (the Zechstein Supergroup; Hodgson et al., 1992; Sørensen et al., 1992; Davison et al., 2000; Glennie et al., 2003). Early Triassic rifting triggered flow and reactive rise of the salt, and formation of a variety of salt structures. The faults investigated in the study area nucleated in the supra-salt cover at this time (Sørensen et al., 1992).

Lower Jurassic deposits are absent in the Egersund Basin (Figs. 2 and 3) due to formation of the Mid-North Sea Dome during the Early Jurassic (Husmo et al., 2003). Subsequent rifting during the Middle Jurassic initiated in response to deflation of the dome (Underhill and Partington, 1993; Husmo et al., 2003), causing reactivation of major NW–SE-striking normal faults that bound the Egersund Basin (Sørensen et al., 1992). Syn-tectonic deposition of the Bryne, Sandnes, Egersund, Tau and Sauda Formations (Fig. 3) documents net-deepening of the basin during the Middle to Late Jurassic (Vollset and Doré, 1984). Extension rates decreased (Møller and Rasmussen, 2003), and a marine transgression occurred during the Early Cretaceous, resulting in deposition of deep-water mudstone and marl (Flekkefjord, Åsgård, Sola, and Rødby Formations) (Fig. 3) (Vollset and Doré, 1984; Isaksen and Tonstad, 1989). Rifting eventually ceased in the Late Early Cretaceous, and a period of basin shortening and inversion, probably related to the onset of the Alpine orogenic event, occurred during the Late Cretaceous, leading to folding, salt re-mobilisation and reverse reactivation of pre-existing, rift-related faults (Ziegler, 1992; Vejbæk and Andersen, 2002; Jackson and Lewis, 2012; Jackson et al., 2013).

3. Data and methodology

3.1. Database

The database for this study comprises a pre-stack time-migrated, three-dimensional reflection seismic survey (PGS MC3D-EGB2005), tied to 13 wells. The study area covers an area of 552 km^2 in the north-western part of the Egersund Basin (Figs. 1 and 2). Crossline and inline spacing are 25 m, and the seismic sections are displayed with reverse polarity, so that an increase in acoustic impedance is presented by a trough (red), while a decrease in acoustic impedance is represented by a peak (black) (SEG European Convention; Brown, 2003). Crosslines are orientated NE-SW and inlines are orientated NW–SE. The vertical seismic resolution in the interval of interest is c. 20–40 m, based on a frequency range of 25–35 Hz and velocity range of 2700–3700 ms^{-1}.

The age of the mapped seismic horizons and the lithology of the stratigraphic intervals they bound, were constrained by formation top data from 13 wells (Fig. 1; Table 1). We mapped 24 faults in the studied fault array, and 15 were subject to quantitative analysis of throw. Fourteen seismic horizons were mapped to constrain the throw distributions on the fault surfaces, and thickness variations in stratigraphy adjacent to the faults. Both fault throw and growth strata thickness patterns provide insights into the growth history of individual fault segments and the array as a whole.

3.2. Methodology

Four methods were used to determine the growth history of the studied fault array: (i) creation of throw-length (*T-x*) plots, which allow the map-view growth history of the faults to be assessed (Walsh and Watterson, 1990; Childs et al., 1995; Gawthorpe and Leeder, 2000); (ii) creation of throw-depth (*T-z*) plots, which provide insights into the potential role of dip linkage on fault growth (Mansfield and Cartwright, 1996; Hongxing and Anderson, 2007), and which allow us to discriminate between periods of syn-sedimentary faulting and blind fault propagation (e.g. Williams et al., 1989; Nicol et al., 1996); (iii) strike-projections of fault throw, which illustrate throw distribution across fault surfaces and provide insights into the growth and linkage history of segmented normal fault systems (Walsh and Watterson, 1991); and (iv) generation of time-thickness (isochron) maps and expansion indices for key stratigraphic intervals, which together illustrate variations in sediment thickness adjacent to and reveal the growth history of, fault systems and arrays (Thorsen, 1963; Rouby et al., 2003; Jackson and Rotevatn, 2013). The use of isochron maps to constrain the growth of normal faults is only valid if sedimentation rate exceeds or is comparable to fault displacement rates (Childs et al., 2003), which we will demonstrate is the case for the Egersund Basin.

Fault throw was constrained by measuring differences between the footwall and hanging wall horizon cut-offs on seismic profiles

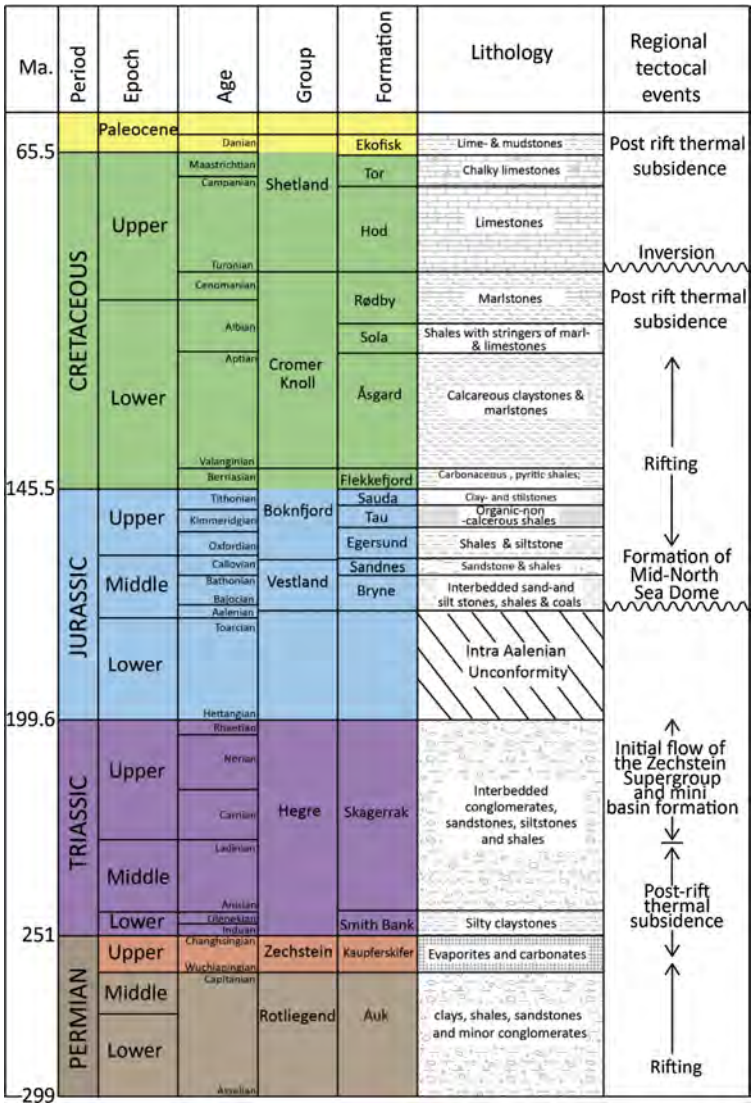

Fig. 3. Stratigraphic framework showing the key seismic horizons, their ages and information about the evolution of the Egersund Basin. Colour coding of the different periods is continued throughout the article. (For interpretation of the references to colour in this figure legend, the reader is referred to the web version of this article.)

(generally inlines) oriented perpendicular to local fault strike. Throw was recorded every 100–600 m, depending on the degree of structural complexity and rapidity of along-strike throw variations. The error of throw measurements in the Middle Jurassic and post-Aptian succession is small and estimated to ±4 ms, based on the generally excellent quality of the seismic data. However, data quality and resolution deteriorates in the Triassic succession as well as in the Tithonian to Aptian interval, where we estimated throw measurement errors to be ±6 ms. Where folds are developed adjacent to the fault surfaces, we record fault throw values that include and exclude the ductile component of deformation.

We use check-shot velocity data from nearby wells (18/10-1, 17/12-1 and 17/12-2; Table 1) to depth convert throw values recorded in time (ms TWT) to metres. This exercise indicates that the patterns and shapes of throw variations on *T-z* plots are the same in both the time and depth domains, so we elect to present all throw values in milliseconds two-way time (ms TWT) (Fig. 4). Well data and seismic facies observations suggest that limited lateral sedimentological heterogeneity exists in the faulted succession, which together with small throw values leads us to believe that the effects of differential compaction across the studied faults is negligible (Mansfield and Cartwright, 1996).

Table 1
Wells within the Egersund Basin (Data from the Norwegian Petroleum Directorate).

Well	TD depth (m RKB)	Oldest penetrated stratigraphic unit
17/12-1R	4298	Zechstein
17/12-2	2334	Devonian (no formation defined)
17/12-3	2730	Skagerrak
18/10-1	2800	Skagerrak
9/2-1	3755	Skagerrak
9/2-2	3548	Skagerrak
9/2-3	3421	Bryne
9/2-4s	3313	Bryne
9/2-5	3354	Bryne
9/2-6s	3642	Bryne
9/2-8s	3345	Zechstein
9/2-11	2836	Bryne
9/3-1	1970	Skagerrak
9/3-2	3151	Skagerrak

4. Description of the salt-influenced fault array

The fault array contains a wide range of normal fault geometries and styles of linkage. For descriptive purposes, the fault array is divided into a *basement-restricted fault array* (i.e. faults that tip-out upward into the salt), *cover-restricted fault array* (i.e. faults that tip-out downward into the salt) and a *basement-involved fault array* (i.e. faults that offset both sub- and supra-salt strata and the salt itself) (Fig. 5).

4.1. Geometry of the basement-restricted fault array

The basement-restricted fault array consists of faults which strike NNW-SSE and mainly dip to the west. A small subpopulation of faults, which are shorter and have less throw, are oriented at a large angle to this trend (Fig. 5a and b). The largest basement fault is 13.8 km long, has a maximum throw of 165 ms (314 m) at top basement level and is divided into four geometric segments. Throw on the basement-restricted faults typically varies between 80 and 140 ms (c. 150–266 m) (Fig. 6).

4.2. Geometry of the cover fault array

The NNE–SSW-trending, cover-restricted fault array is c. 16 km long, c. 6 km wide and consists of a series of WNW- or ESE-dipping, *en-echelon* normal fault segments that step progressively westward toward the north (Figs. 2 and 5c–f). The cover-restricted fault array occurs directly above the basement-related fault array, or along the southern part of the array it is laterally offset from it by up to 8 km. In the north–east of the array, mean fault strike changes from NNE–SSW to WNW–ESE (Fig. 5c–f). In cross-section, the majority of the cover-restricted faults are planar and dip 45–55° on the time-migrated seismic data. In map-view, the faults are straight or slightly curved. Based on the vertical extent (i.e. height) of their constituent fault segments, their location within the study area and their inferred style of growth, the cover-restricted fault array is divided into two geographic domains (northern and southern; Fig. 5d).

4.2.1. Northern Domain

Faults in the Northern Domain (Figs. 5d and 7) are 1 km to at least 3.2 km long, and they generally tip out downward either into a very thin (<30 ms or 55 m) salt layer or within the basement where salt is absent. The faults tip out upward within Triassic or Upper Jurassic strata (Fig. 7a and b). Many fault tips are overlain by low-relief (30 ms or 45 m) monoclines, especially above faults that do not breach the mudstone-rich Upper Jurassic interval (Fig. 7b). *T-z* plots (Fig. 7b) and throw strike-projections (Fig. 7d) for cover-restricted faults in the Northern Domain are typically characterized by an asymmetric throw distribution. For example, maximum throw (56 ms or 90 m) occurs at the centre of fault C1, near the top Triassic (Fig. 7b), gradually decreasing downward (throw gradient = 0.03) toward the lower Triassic, followed by an abrupt decrease in throw and marked increase in throw gradient (throw gradient = 0.30) from this stratigraphic level to the lower fault tip. Above the position of maximum throw, throw decreases relatively rapidly upward (throw gradient = 0.24) to just below the top of the Bryne Formation. Above this point, throw decreases at a lesser rate (throw gradient = 0.06) toward the upper fault tip, which occurs in the lower part of the Sauda Formation (Fig. 7b). Near the lateral tips of fault C1, where less throw occurs, the same gradual downward decrease in throw into the lower part of the Triassic succession is observed. In summary, *T-z* plots for cover-restricted faults in the northern domain contain three main inflection points and are thus characterized by: (i) high throw gradients just above where they terminate downward into the salt; (ii) gentle throw gradients within the Triassic succession; (iii) high throw gradients in the Middle Jurassic; and (iv) low throw gradients in the Lower Jurassic.

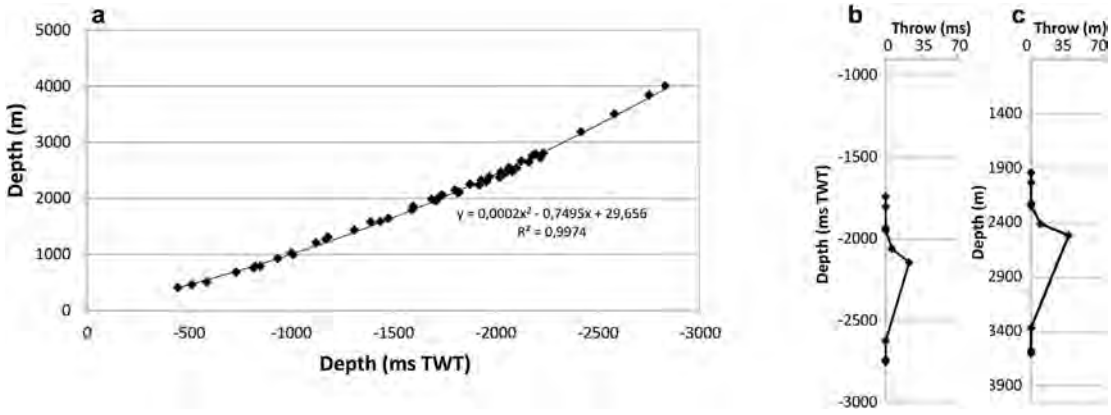

Fig. 4. (a) Graph for depth to travel-time comparison so as to determine the depth conversion formula, using check shots from three nearby wells; (b) Throw-time (ms) plot and (c) Throw – depth (m) differ in shape, but not geometry.

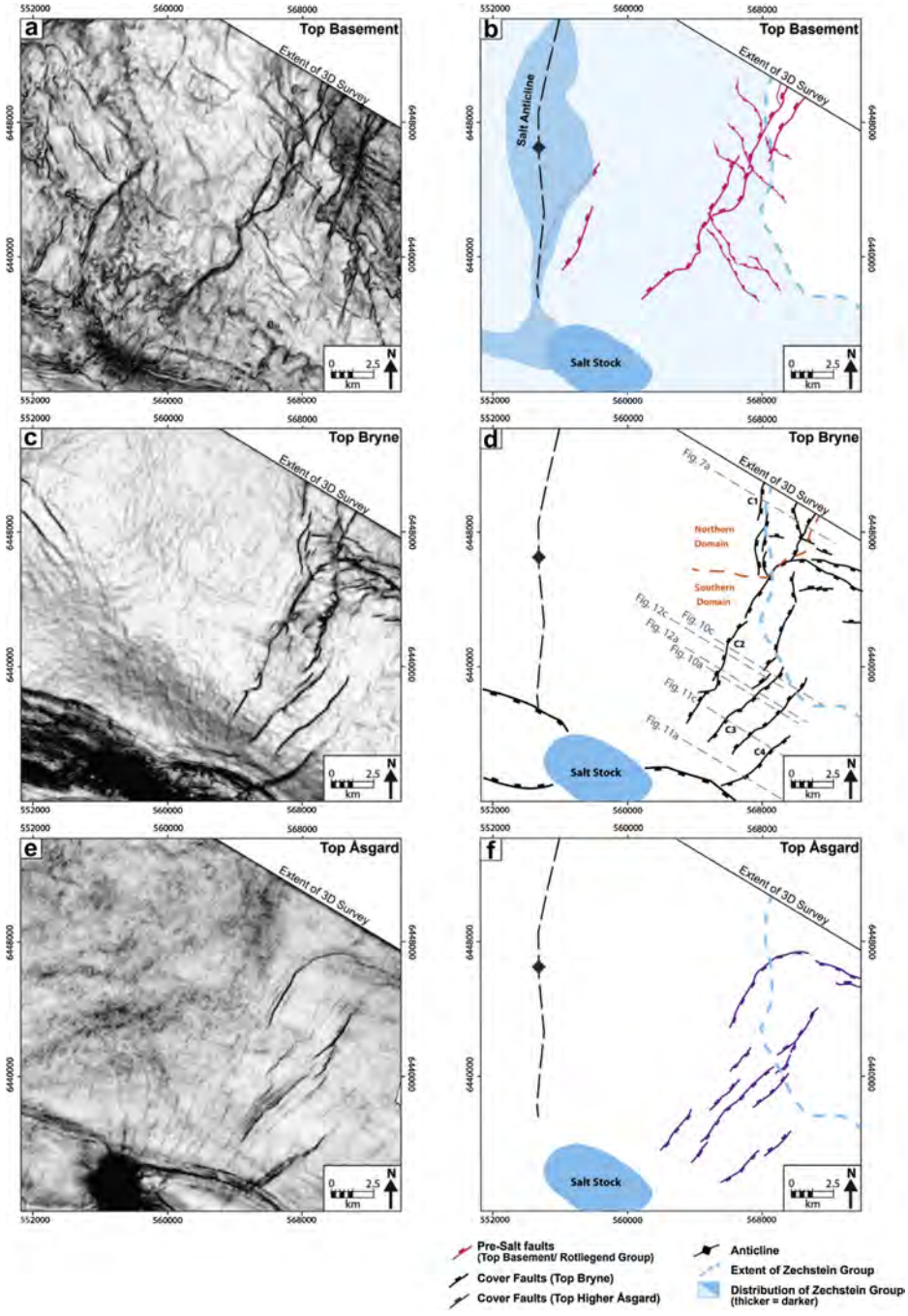

Fig. 5. Simplified maps of fault patterns based on fault interpretations and coherance discontinuities in the horizontal continuity of amplitude of the seismic (variance maps) for: (a) and (b) Basement (pre-Zechstein) fault array and salt distribution. (c) and (d) Cover faults at Middle Jurassic level for the Top Bryne Formation where the cover fault array has approximately its maximum throw. Figure lines for later figures included. (e) and (f) the cover fault array at a Middle Cretaceous level displayed on the Top Higher Åsgaard.

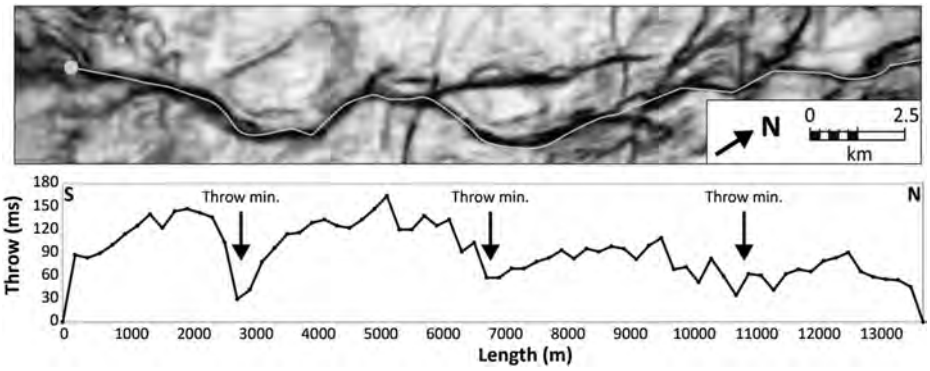

Fig. 6. Example variance map of a measured basement fault with corresponding D-L profile. The measured basement fault can be divided into at 4 hard linked segments based on the 3 throw minima.

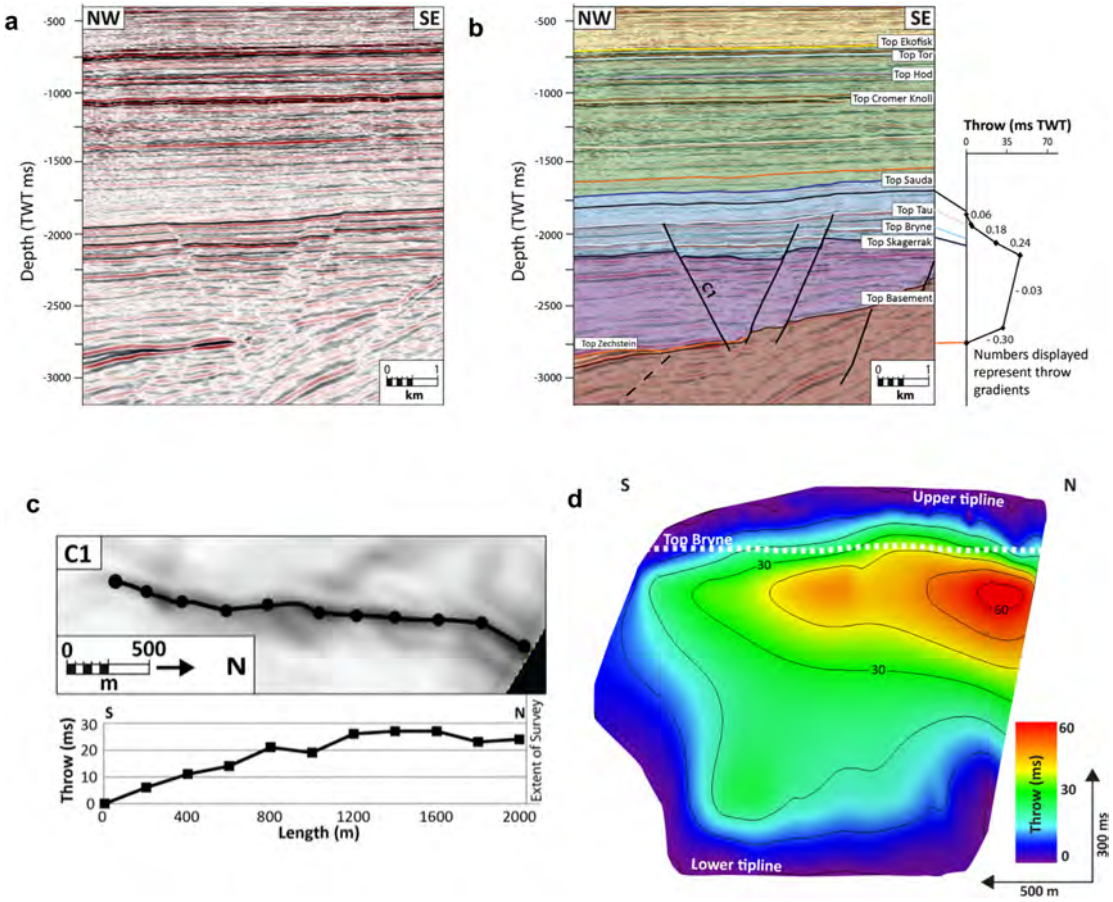

Fig. 7. (a) and (b) Seismic profile illustrating the cover fault C1 to the right, bound between the basement or very thin salt and Upper Jurassic strata. *T-z* plot shows an asymmetric, upward-truncated vertical-throw profile where the maximum throw is at the transition between Upper Triassic and Middle Jurassic. (c) Variance map of fault C1 in the Northern Domain with each selected point for the throw-length profile along the Top Bryne Formation. (d) Throw strike-projections with truncated contours toward the upper tipline.

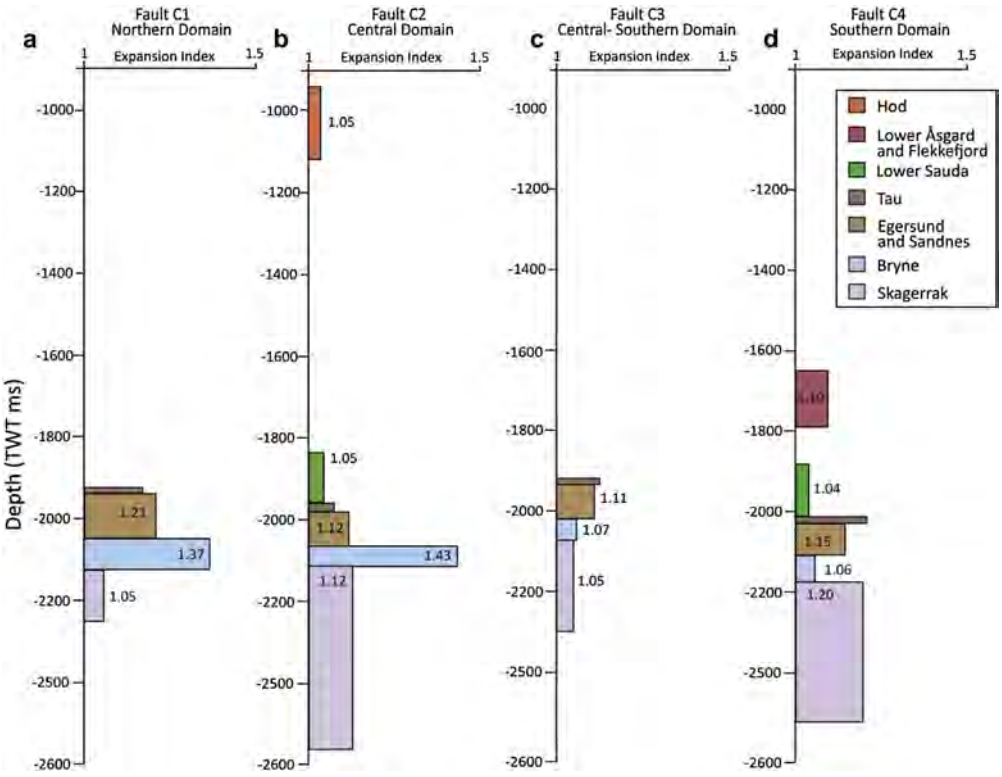

Fig. 8. Expansion indices showing growth in the hanging wall of faults; (a) C1 the Northern Domain with increasing fault growth from the deposition of the Skagerrak, Bryne, Sandnes, Egersund and Tau Formations. (b) C2 in the Southern Domain showing fault growth during deposition of the Skagerrak, Bryne, Egersund, Tau and Sauda Formations and during deposition of the Hod Formation. (c) C3 in the southern domain show fault growth during deposition of Skagerrak, Bryne, Egersund and Tau Formations. (d) C4 in the southern domain show fault growth during deposition of Skagerrak, Bryne, Egersund, Tau and the lower Åsgard and Flekkefjord Formations.

Expansion indexes indicate increased hanging wall thickness for the Skagerrak, Bryne Egersund Sandnes and Tau Formations (Figs. 8a and 9a–b).

4.2.2. Southern Domain

Faults in the Southern Domain strike NE-SW, dip NW or SE and are up to 6.2 km long (Fig. 5d). The majority of these faults tip out upward in Lower Cretaceous strata and downward into the salt.

T-z plots taken at the point of maximum throw, and strike-projections of throw on the fault surfaces indicates that, like the faults in the northern domain, faults in the Southern Domain are characterized by asymmetric throw distributions (Figs. 10–12). Several faults in the southernmost part of the Southern Domain bifurcate along strike, such that a single fault surface passes along-strike into two, laterally separate segments (e.g. C3 and C4; Figs. 1, 10 and 13a). Where two segments are developed, they are typically separated across and tip out into the mudstone-dominated Upper Jurassic interval. For example, seismic sections and *T-z* profiles (Fig. 10b) indicate that where throw on the structure is greatest (70 ms or 109 m), fault C3 consists of a single fault surface with throw distributed asymmetrically on the lower portion similar to northern domain faults, whereas the upper portion of the fault has more symmetrically distributed throw laterally and an overall c-shaped profile in the slip direction. Two throw maxima are observed on the fault: a lower one near the top of the Bryne Formation (70 ms and 109 m), and an upper one near the top of the Åsgard Formation (36 ms or 47 m) (Fig. 10b). Along strike to the north, C3 is represented by two discrete segments, with the upper and lower segments being stratigraphically restricted to the Lower Cretaceous and Triassic-to-Middle Jurassic intervals, respectively (Figs. 10d and 13a). In this location, mudstone-dominated strata of the Egersund, Tau and the Sauda Formations are undeformed, and maximum throw on the lower and upper segment occurs near the top of the Bryne (17 ms and 27 m) and Åsgard (16 ms or 21 m) Formations, respectively (Fig. 10d). A strike-projection of throw on fault C3 confirms that the upper and lower segments are only locally linked for about a 1 km long portion located near the centre of its 7.5 km length (Fig. 10f). Furthermore, Fig. 10f indicates that the lower segment has a strongly asymmetric throw distribution, whereas the upper segment is characterized by relatively symmetric, broadly elliptical throw contours. Expansion indices and isochron maps indicate increased hanging wall thickness for the Skagerrak, Bryne, Egersund and Tau Formations (Figs. 8c and 9a–c).

Fault C4 has the same general geometry as fault C3, and is a single fault where throw is greatest, and two physically separate segments laterally toward the fault tips (C4 in Fig. 5d; Fig. 11). However, *T-z* plots indicate that the point of maximum throw (127 ms or 227 m) on the lower segment is observed within the Triassic rather than near the top of the Middle Jurassic. Below this point, throw decreases gradually and gently downward

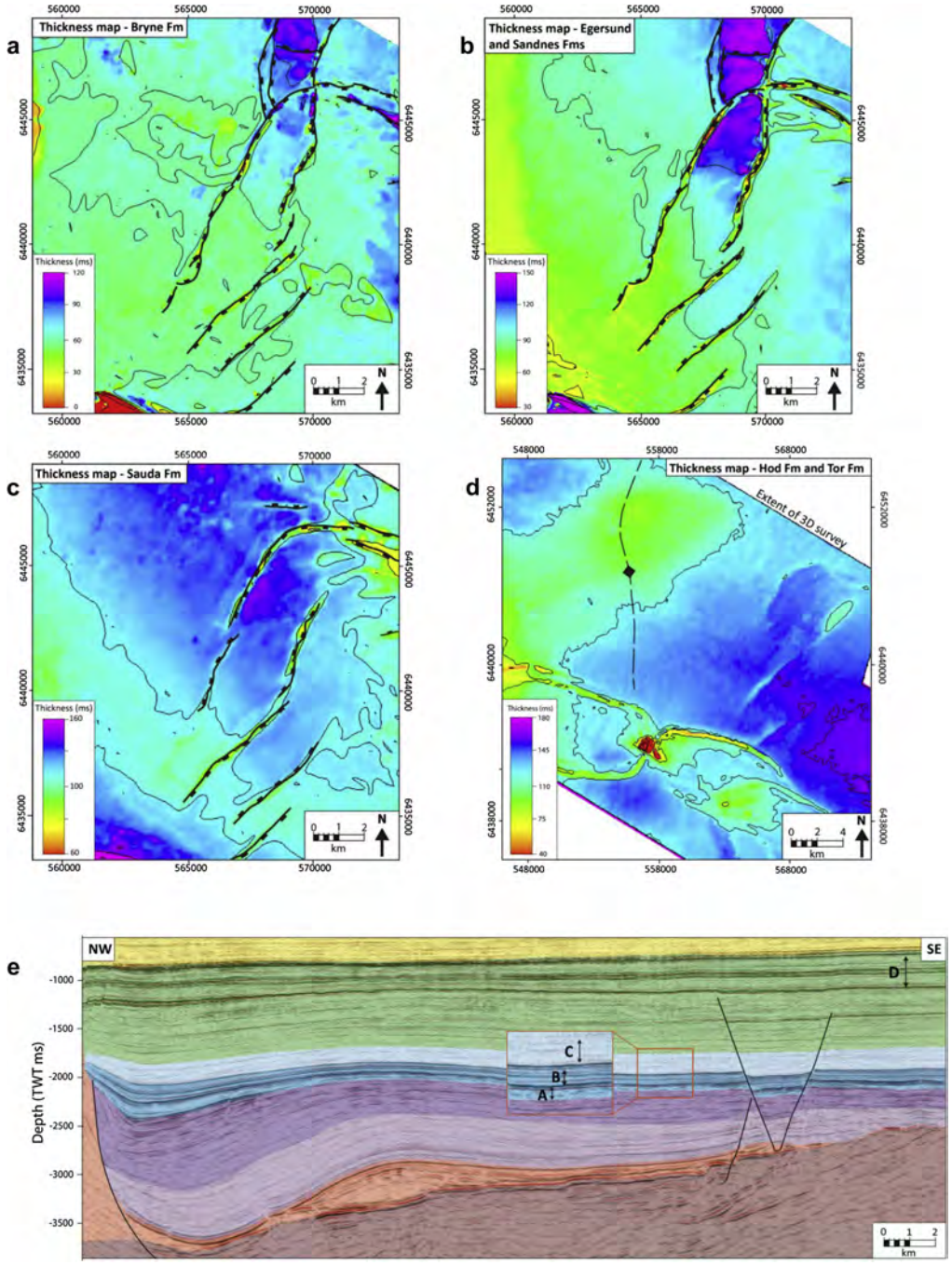

Fig. 9. Isochron thickness maps illustrating sediment thicknesses and depocentre migration of the: (a) Bryne Formation (Upper Triassic to Middle Jurassic) with increased hanging wall thickness in the graben toward the north, indicative of syn-sedimentary faulting during this time. (b) Sandnes and Egersund Formations (Middle -Upper Jurassic) where the depocentre migrated southward. (c) Lower part of Sauda Formation (Upper Jurassic) where the main depocentre migrated further south. (d) Tor and Hod Formations (Upper Cretaceous) with decreasing sediment thickness across the salt anticline (note the change of scale on this map). (e) Each interval used for time thickness maps is indicated by letters on figure showing thickness variations of sedimentary sequences. Upper Triassic and Middle Jurassic sediments (highlighted purple and blue colours) increase in thickness toward the NW indicating the initiation of the formation of a salt weld between the salt diapir and the salt anticline during this time. There is also a slight decrease in thickness from the east toward the top of the salt anticline of the Upper Triassic sediments which may indicate build-up of the salt anticline. Intra Aalenian unconformity is thought to have caused some of the thinning of the Skagerrak Formation across the salt anticline. (For interpretation of the references to colour in this figure legend, the reader is referred to the web version of this article.)

(throw gradient = 0.10) within the lower part of the Triassic, before abruptly and rapidly (throw gradient = 0.76) decreasing just above the salt. In this location, the top of the salt is offset by 100 ms (186 m), whereas the base of the salt (i.e. top basement) is not offset, even though the salt is relatively thin (<200 ms or 370 m) in this area (Fig. 11a–d and f). Above the point of maximum throw, throw decreases gradually upward toward the top of the Sauda Formation, thereby defining an overall asymmetric profile to the lower segment of C4. In contrast, the upper segment of fault C4 is characterized by a more symmetric distribution of throw and elongated, elliptical throw contours, which are centred on the point of maximum throw (32 ms or 42 m) in the upper part of the Åsgard Formation (Fig. 11f). Expansion indices and isochron thickness maps indicate increased hanging wall thickness for the Skagerrak, Bryne, Egersund, Tau and the lower Åsgard and Flekkefjord Formations (Figs. 8d and 9a–c).

The Tau and Egersund Formations are typically folded into low-relief (up to 50 ms or 75 m), 100–400 m wide synclines in the hangingwalls of faults in the Southern Domain (Figs. 10a–d, 11a–b and 12a–d). *T-z* profiles that include this ductile component of the deformation show that the large amount of folding occurs in the mudstone-dominated Upper Jurassic unit (Fig. 11b and d). The relief of the synclines increases with increasing fault throw (e.g. Tau Formation in Fig. 11b and d). Where the faults in the Southern Domain bifurcate along strike, these mudstone-dominated Upper Jurassic layers appear as low relief (22 ms or 33 m) monoclines above the upper tip-line of the lower segment of the fault (Fig. 10d).

4.3. Basement-involved faults

By definition, cover-restricted faults do not offset basement. However, cover fault C2, which is located in the western part of the Southern Domain, represents a notable exception because, along its northern portion, it is physically linked to a basement-involved fault (Figs. 12, and 13b). Where C2 is decoupled from the basement-involved fault, *T-z* profiles display an asymmetrical lower part located within Triassic-Upper Jurassic strata, and a slightly offset upper part within Upper Jurassic-Cretaceous strata (Fig. 12a–b). Two throw maxima are observed: a lower one at the top of the Skagerrak Formation (48 ms or 76 m) and an upper one at the top of the Åsgård Formation (10 ms or 14 m). Along strike to the north, where the cover-restricted and basement-restricted faults are physically linked and form a through-going fault, *T-z* profiles can be divided into three segments, where a lower asymmetric portion has throw maximum at top Basement (125 ms or 237 m) (Fig. 12c–d) with a rapid upward decreasing throw gradient (0.79) into the salt, an asymmetric middle portion and a symmetric upper part, which are similar to those observed along strike to the south. Strike-projections of throw display tightly spaced contours toward the lower fault tip. Tightly spaced contours are also observed toward the top of the Bryne Formation (Fig. 12f), whereas the uppermost portion of the fault displays more elliptical contours that are centred on maximum throw at the top of the Åsgård Formation. Expansion indices and isochron thickness maps indicates increased hanging wall thickness for the Skagerrak, Bryne, Egersund, Tau, Sauda and Hod Formations (Figs. 8b and 9a–d).

5. Growth of the thin-skinned fault array

Based on their stratigraphic occurrence (i.e. cover- or basement-restricted, or basement-involved) and growth histories, we define three type of faults: 1) cover-restricted growth faults formed by radial propagation of a single fault surface, 2) cover-restricted growth faults formed in response to dip-linkage of segments and 3) dip-segmented, basement-involved faults formed in response to upward propagation of a sub-salt fault into the cover.

5.1. Cover-restricted growth faults formed by radial propagation

Cover-restricted growth faults are mainly developed in the Northern Domain (Fig. 5d). Maximum throw is observed at the top of the Triassic succession, suggesting that the fault nucleated at this structural level. This interpretation is supported by the observation that Middle Jurassic strata thicken abruptly across these faults (Figs. 8 and 9a), which we also infer to mean that the faults nucleated in the very shallow subsurface and/or rapidly propagated upward to the free surface (Baudon and Cartwright, 2008a; Jackson and Rotevatn, 2013). Furthermore, high throw gradients near the upper tips of these faults are characteristic of syn-sedimentary growth faults (Fig. 14) (e.g. Nicol et al., 1996; Baudon and Cartwright, 2008a). The elliptical throw contours, which are centred on the position of maximum throw, and D-L profiles strongly suggest that the fault grew via radial propagation of its tips rather than via segment linkage (e.g. Watterson, 1986; Walsh and Watterson, 1988; Baudon and Cartwright, 2008a). The absence of Lower Jurassic strata make it is difficult to determine whether faulting also occurred during the Early Jurassic. Irrespective of the Early Jurassic history of these faults, the observation that the latest Middle Jurassic and Upper Jurassic succession (Sandnes, Egersund and Tau Formations) thicken across the faults, and that the upper tips are associated with high throw gradients, indicate that these faults were active in the Late Jurassic (Early Tithonian) (Figs. 7, 8a and 9a–b).

5.2. Cover-restricted growth faults formed by dip linkage of blind faults

Most faults in the Southern Domain of the cover fault array are longer and taller than faults in the Northern Domain, implying that they accommodated strain over a greater rock volume than their northern counterparts. Faults in the Southern Domain (Fig. 5d) are characterized by either a single, continuous fault surface that offset Triassic, Jurassic and Cretaceous strata (Figs. 10–12), or a fault surface that bifurcates along strike (Figs. 1, 10 and 13a). This variability in structural style, in combination with their more complex throws distributions, suggests that faults in the Southern Domain have a more complex growth history than those in the north. The asymmetric throw distribution of the lower fault segments of cover faults C2 and C3 show rapid upward decrease in throw from the point of maximum throw. Based on this observation, and expansion indices (Fig. 8b and c) and isochron maps (Fig. 9), we interpret that faults exemplified by C2 and C3 were syn-sedimentary growth faults that were active from the Triassic to Late Jurassic. Fault C4 has a slightly different throw profile, characterized by a gradual upward decrease from the point of maximum throw, which is indicative of a fault that propagated blind and did not breach the free surface. However, expansion indices (Fig. 8d) indicate that the fault breached the surface during the middle Triassic, and remained as surface-breaching structure until it was finally buried in the Kimmeridgian. The low throw gradients in the Triassic could possibly be explained by high sedimentation rates in the south.

C2, C3 and C4 all show elliptical throw contours centred on a second throw maximum located on the upper part of the fault. We suggest that this throw distribution results from a second phase of fault growth related to post-burial reactivation in the Southern Domain, which occurred by either 1) upward,

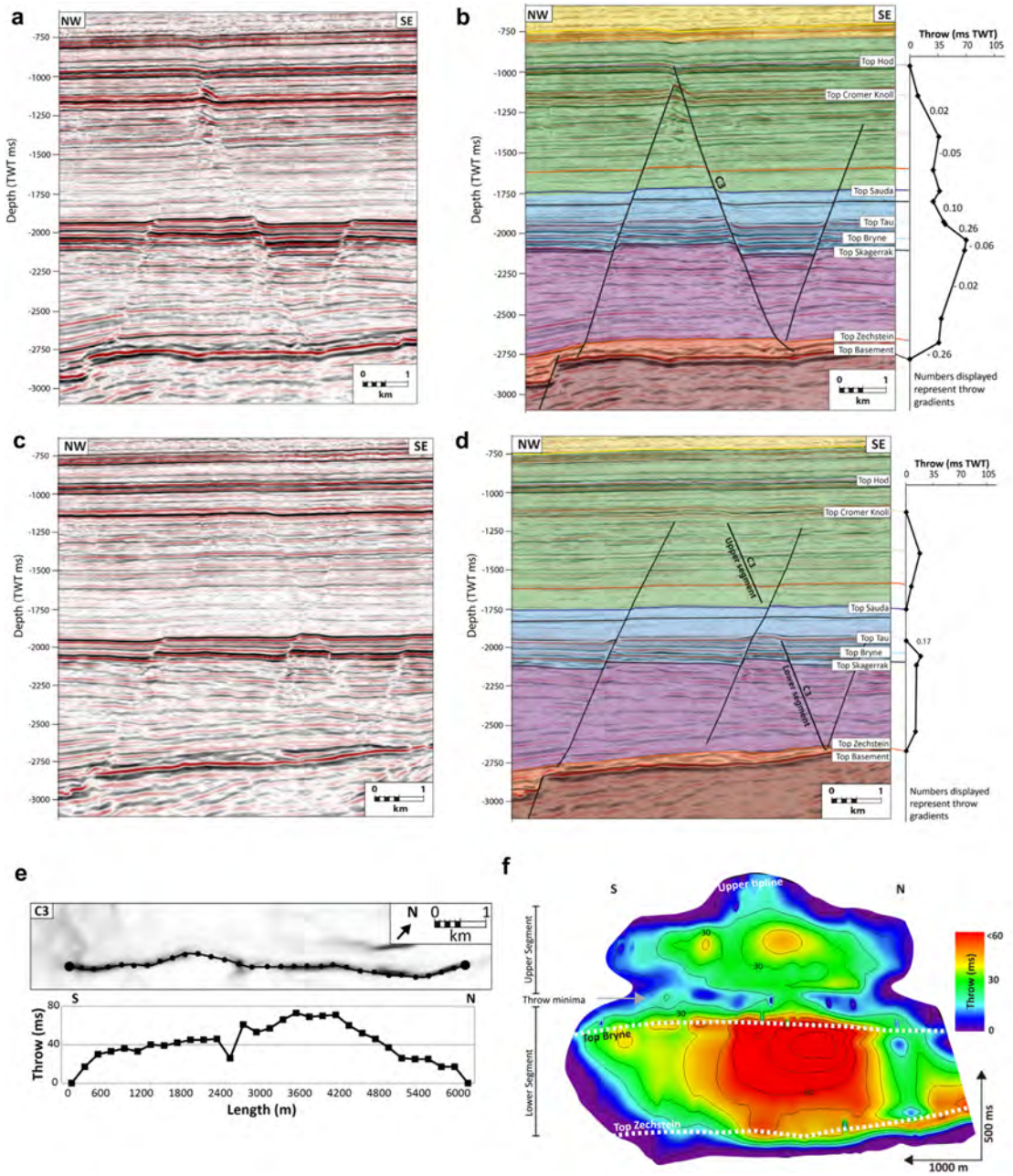

Fig. 10. (a) Seismic profile with cover fault C3 (C3) in the Southern Domain, where (b) is with interpreted horizons and faults. *T-z* plots indicate the asymmetric throw distribution across the location of throw maximum. (c) and (d) Seismic profile illustrating fault C3 north of profile in (a) and (b). Cover Fault C3 has an upper and lower segment as indicated on the *T-z* curve. (e) Variance map of fault C3 with corresponding throw length profile along the top of the Bryne Formation showing gradual decrease in throw toward the northern and southern fault tips. (f) Throw strike-projections on the fault surface illustrating a concentric shape of throw distribution on the upper part of the fault segment, and an asymmetrical shape on the lower part of the fault segment.

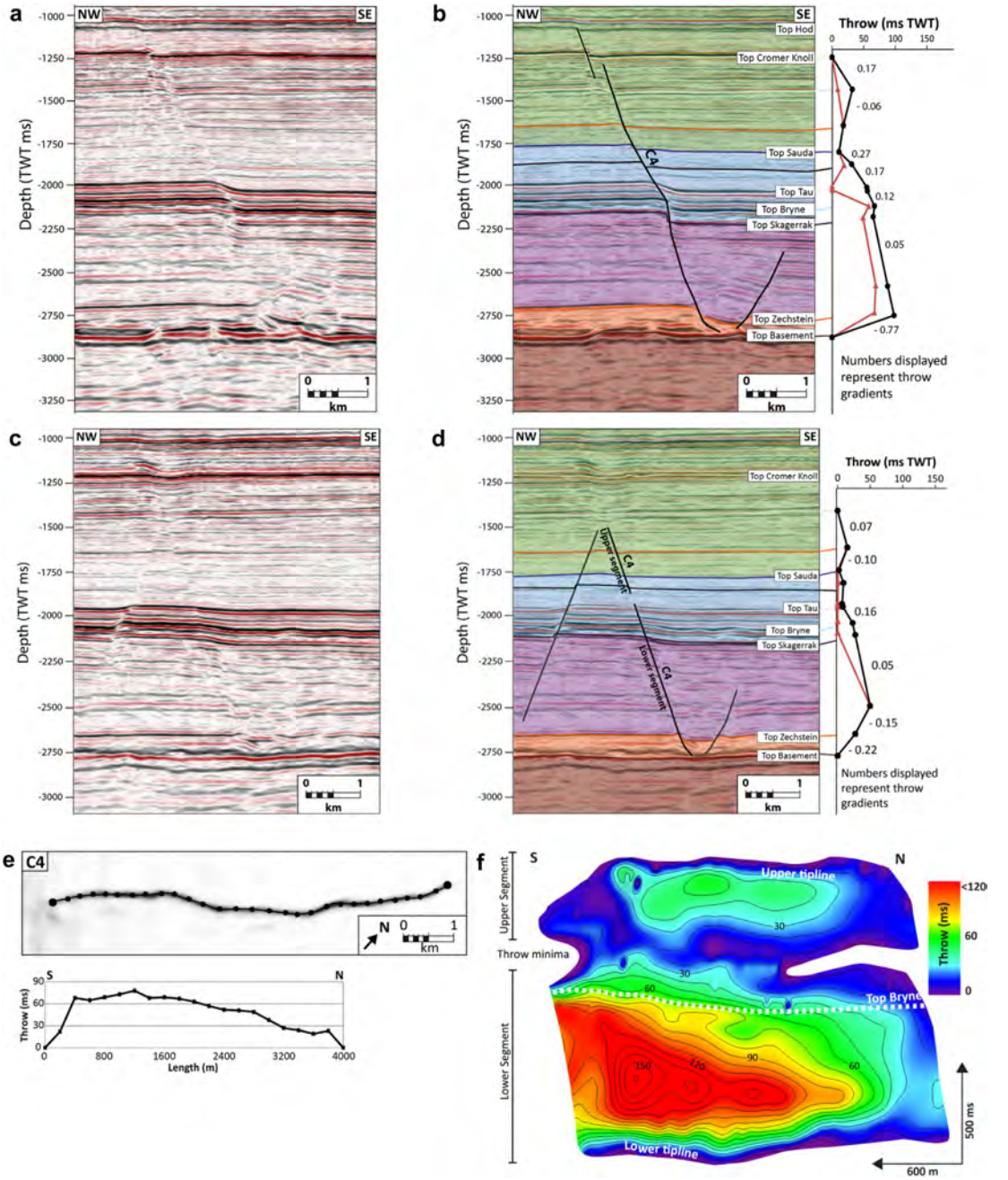

Fig. 11. (a) Seismic profile with cover fault C4 in the Southern Domain, where (b) is with interpreted horizons and faults. (c) and (d) Showing fault segments which split along strike into an upper and lower segment. *T-z* plots perpendicular to strike of the fault plane (red line indicating where drag is not included in the picks, while black line indicates where throw is recorded at inflection points of the drag folds. (e) Variance map of Cover Fault C4 with corresponding throw length profile showing gradual decrease in throw toward the northern fault tip, while more rapid decreasing throw toward the southern fault tip. (f) Throw strike-projections on the fault plane showing the asymmetrical throw distribution. (For interpretation of the references to colour in this figure legend, the reader is referred to the web version of this article.)

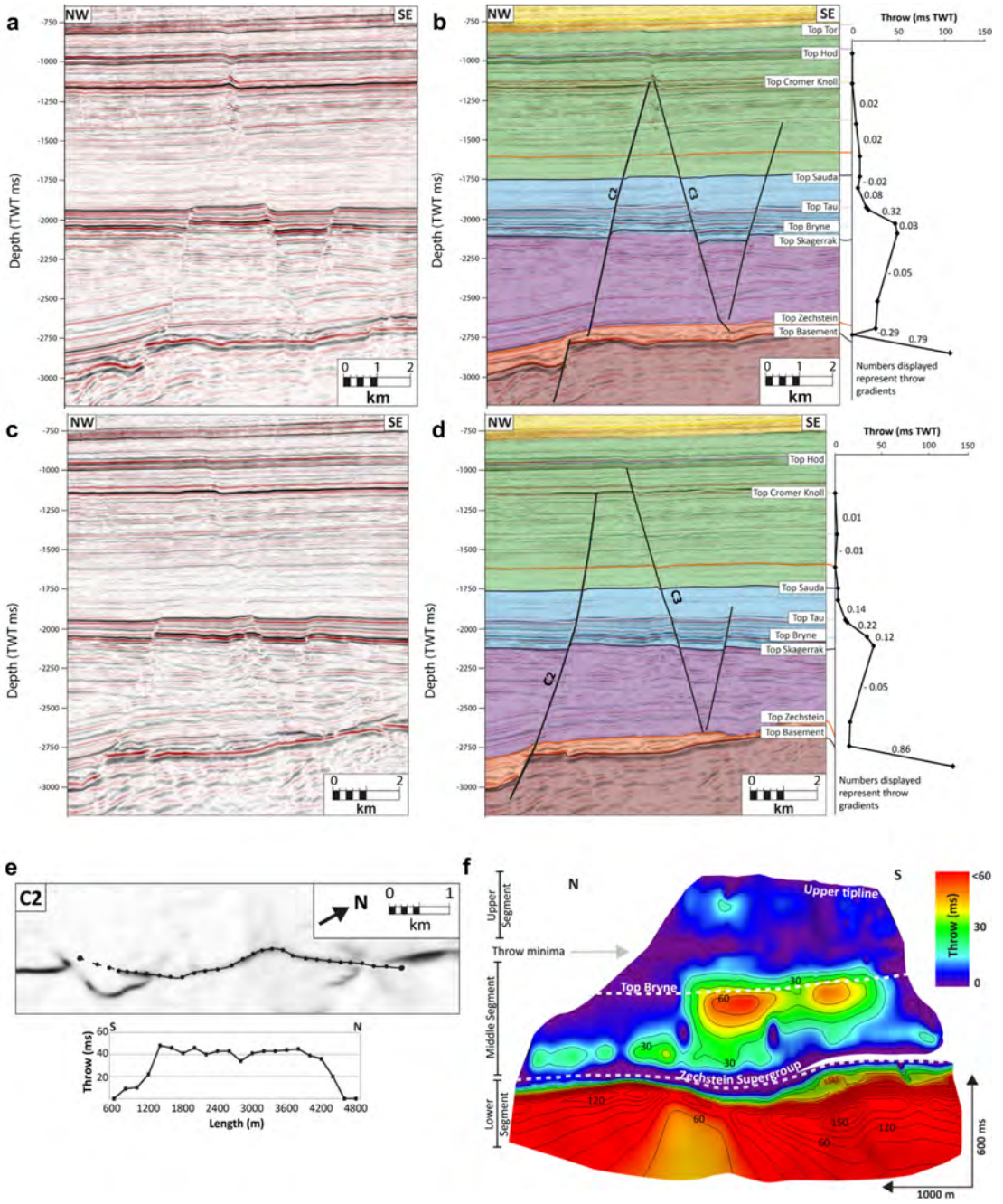

Fig. 12. (a) and (b) Seismic profile perpendicular to strike of the Cover Fault C2 in the Southern Domain. Here the fault offsets the basement, while in figure (c) and (d) a flat-ramp structure decoupling the basement fault from C2,as shown by the *T-z* plots in (b) and (d). (e) Variance map of fault C2 with corresponding throw-length profile along the Top Bryne Formation showing one throw minima at 2900 m, which can be an indication of early linkage of two individual fault segments. This linkage is also indicated on (f) the throw strike-projection on the fault surfaces with two bulls' eyes at level of Top Bryne. Throw strike-projections also illustrate the coupled and decoupled relationship between the lower and middle segment through the salt.

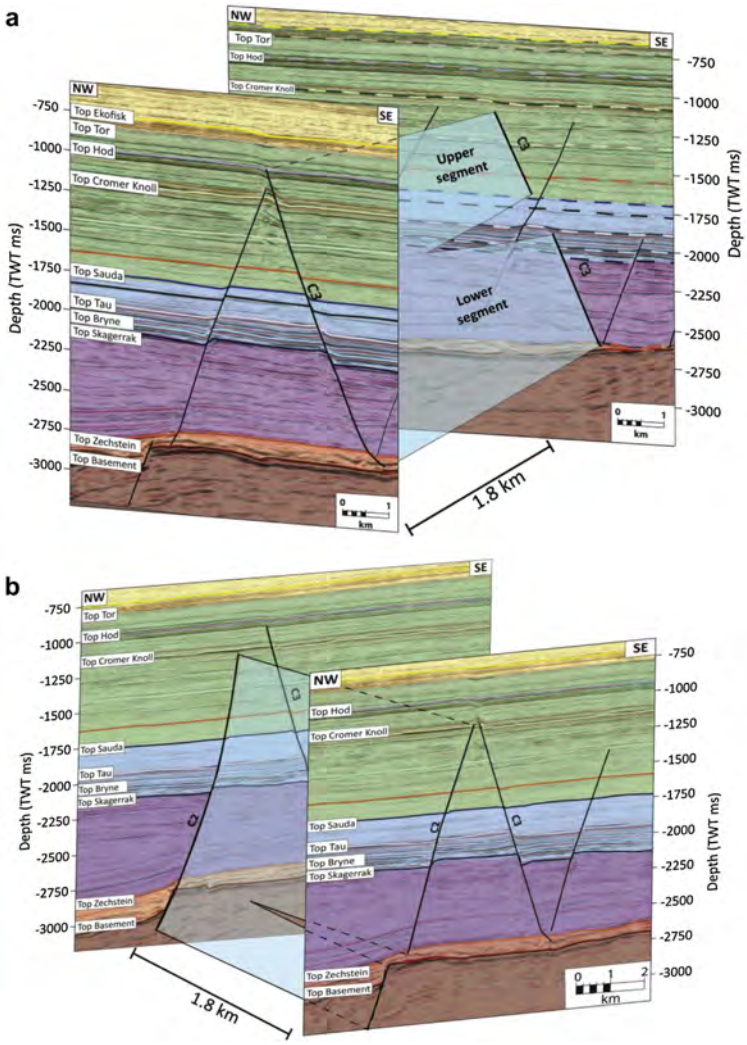

Fig. 13. (a) Illustration of bifurcation of cover fault C3 along strike, where a single fault surface passes along-strike into two, laterally offset segments. (b) Illustration of the interaction between the basement and cover fault C2.

blind propagation of pre-existing, buried faults (i.e. the 'classic' model for fault reactivation; Richard and Krantz, 1991) or 2) by nucleation of a newly formed fault segment in the 'cover', in Lower Cretaceous strata, which propagated downward (and upward) before linking with the deeper segment (Fig. 14) (Baudon and Cartwright, 2008b). We suggest the latter model is applicable for faults in the Southern Domain, based on the observation that two throw maxima are developed. One is below and one above the Jurassic mudstone-dominated detachment, which are separated by a zone of little or no throw (Figs. 14c and d and 15). We interpret that folding adjacent to this style of fault documents upward propagation and fault-related folding ahead of the upward-propagating, lower segment; eventual linkage of the upper and lower segment leads to breaching of the fold and its preservation in the hanging wall of the now-linked structure (Mansfield and Cartwright, 2001; Rykkelid and Fossen, 2002).

6. Trigger for nucleation and growth of the cover-restricted fault array

A key question is "What caused the nucleation and growth of the cover-restricted fault array?" The north-western part of the Egersund Basin is defined by a west-dipping half graben, which is bound by the east-dipping Sele High Fault System. Sub-salt, Lower Permian (and older) strata, and the salt-basement contact, dip westward toward the basin-bounding fault (Fig. 16), implying that the thin-skinned fault array could have simply formed as a gravity-

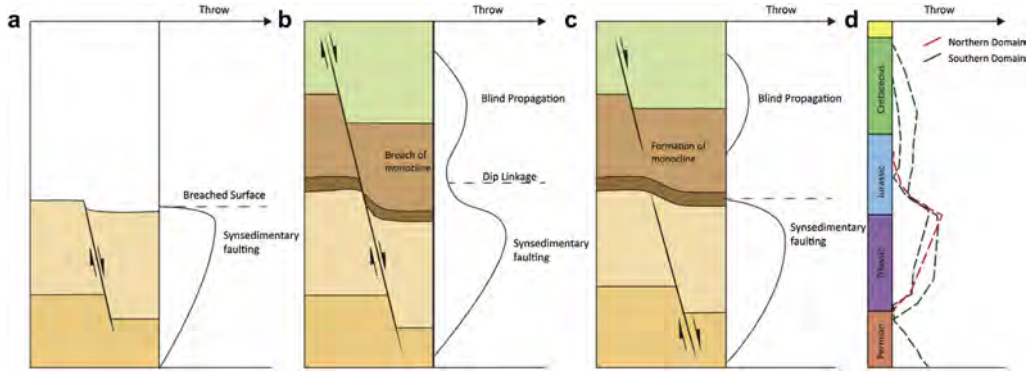

Fig. 14. Simplified illustrations of a vertical throw distribution plots for (a) a syn-sedimentary fault, such as the faults in the northern domain; (b) for a fault which first was syn-sedimentary with a blind fault nucleating in the overburden and propagating to interact with the syn-sedimentary fault; and (c) syn-sedimentary fault with a blind fault nucleating in the overburden. The blind propagation of faults forms a monocline with the shale which acts more ductilly. As the two faults propagate, the monocline is breached resulting in coupled deformation as in (b). (d) Simplified vertical-throw profiles from this study for comparison.

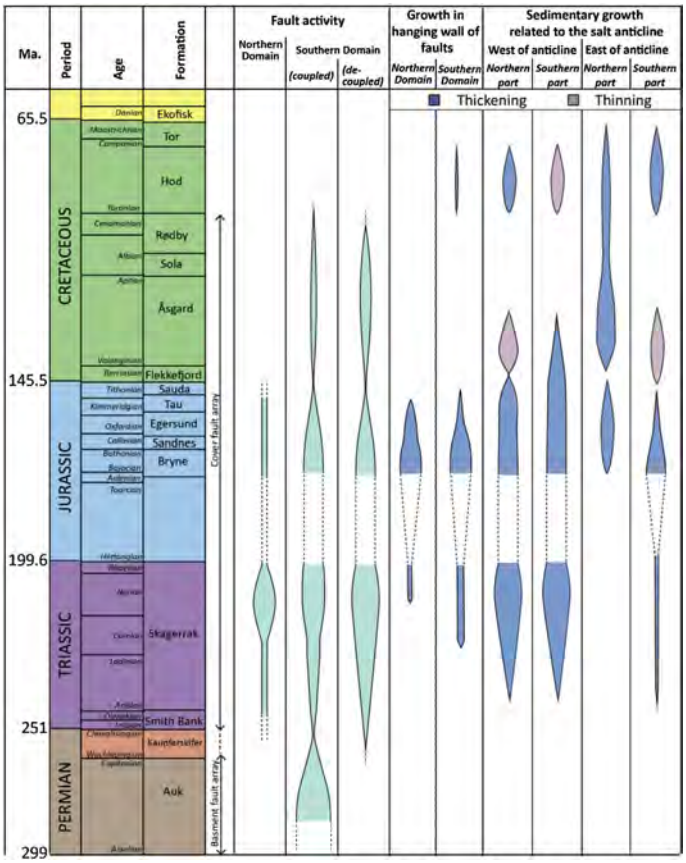

Fig. 15. Summary of analyses for this study. Fault activity is illustrated by wider shaded area for greater throw. Hanging wall growth of faults illustrating the thickening of different formations in the hanging wall, and sedimentary growth on either side of the salt anticline are based on the thickness maps and expansion indices (see Figs. 8, 9 and 17).

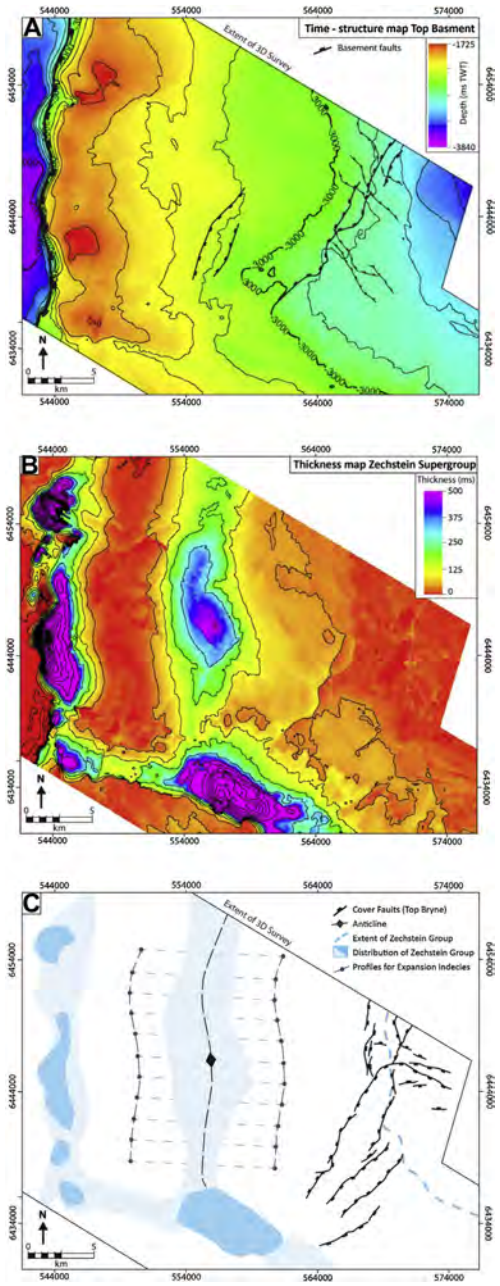

Fig. 16. (a) Time structure map of Top Basement with basement fault array on top and the Sele High Fault System to the west. (b) Isochron thickness map of the ZSG. (c) The salt anticline is close to parallel to the salt wall with diapirs to the west and the studied fault array in the east. The lines on either side of the salt anticline represent profiles used for expansion indices in Fig. 17.

driven system, triggered by basin margin faulting and associated basement tilting. This interpretation would be consistent with the mean NNE–SSW trend of the thin-skinned fault array. However, salt mobilization, in the absence of thick-skinned tectonics, can also occur. To assess whether the studied fault array formed in response to thick-skinned extension and 'passive' gravity-gliding above the salt or active growth of a salt structure, which may or may not have been linked to basement-involved tectonics, we need to assess the pattern of the salt mobilization.

6.1. Timing of salt mobilization

Several salt structures are developed in the north-western part of the Egersund Basin. One of these structures is a broadly ENE–WSW-trending salt anticline. This anticline displays relief of 500 ms (1019 m) and it is flanked to the west by an apparent weld, where the salt would be very thin or absent (Figs. 2, 9e and 16b) (Wagner III and Jackson, 2011). Because it is located only 10 km to the west of, and has the same strike length as and trends sub-parallel to the fault array, we speculate that salt flow related to the growth of this anticline was responsible for the nucleation and growth of cover-restricted fault array (Figs. 5 and 16b and c). We therefore use seismic-stratigraphic observations from seismic profiles, supra-salt isochron maps and isochron thinning ratios (*sensu* Higgins et al., 2009; see also Jackson et al., 2013) to assess the timing of formation of this salt anticline, and its temporal relationship to the cover-restricted fault array (Figs. 9, 16 and 17). Isochron thinning ratios illustrate the ratio between the sediment thickness above the salt anticline and the thickness of the same unit 6 km to the west and east of the salt anticline. The profile to the west of the anticline is located above the salt weld and the one to the east is located between the anticline and the fault array (Figs. 16b–c and 17).

Our analysis indicates that the Lower Triassic interval is broadly tabular and concordant with the folded upper surface of the salt anticline, whereas the upper part of the Skagerrak Formation (Carnian-to-Rhaetian age strata), the Bryne, Egersund, Sandnes and Tau Formations, and the lower part of Sauda Formation (i.e. middle Aalenian–to-middle Tithonian age strata) thin across the salt anticline (Figs. 9e and 17). Major thickening of the Carnian-to-Rhaetian interval of the Skagerrak Formation is only observed down the western flank of the anticline, implying that the structure was primarily growing in response to salt withdrawal from the west, below the subsiding minibasin in the region of the future weld (Fig. 17a). It is important to note that some thinning may have been caused by erosion along the Intra Aalenian Unconformity (Husmo et al., 2003), but from seismic profiles and growth analysis it is clear that some of the thickening is related to true syn-sedimentary structural growth (Fig. 9e). From the Bajocian to the Bathonian, further growth of the anticline is demonstrated by thickness variations in the Bryne Formation. However, in contrast to the Triassic times, stratal thickening is asymmetric along strike of the western limb, and most pronounced along the southern end of the structure, implying preferential growth of the salt anticline in this location at this time. Furthermore, thinning of Bajocian-to-Bathonian strata onto the eastern flank of the anticline is observed at this time, implying that: (i) salt was now being withdrawn from east of the anticline; or (ii) that structures along the newly initiated, cover-restricted fault array were responsible for generating accommodation and thicker successions to the east of the anticline. After a period of relatively dramatic growth in the Triassic and Middle Jurassic (i.e. expansion indices of up to 4.5), growth of the salt anticline during the Late Jurassic and Cretaceous appears to have been more moderate (i.e. expansion indices <1.5). Almost no growth occurred in the Albian to Cenomanian, before a

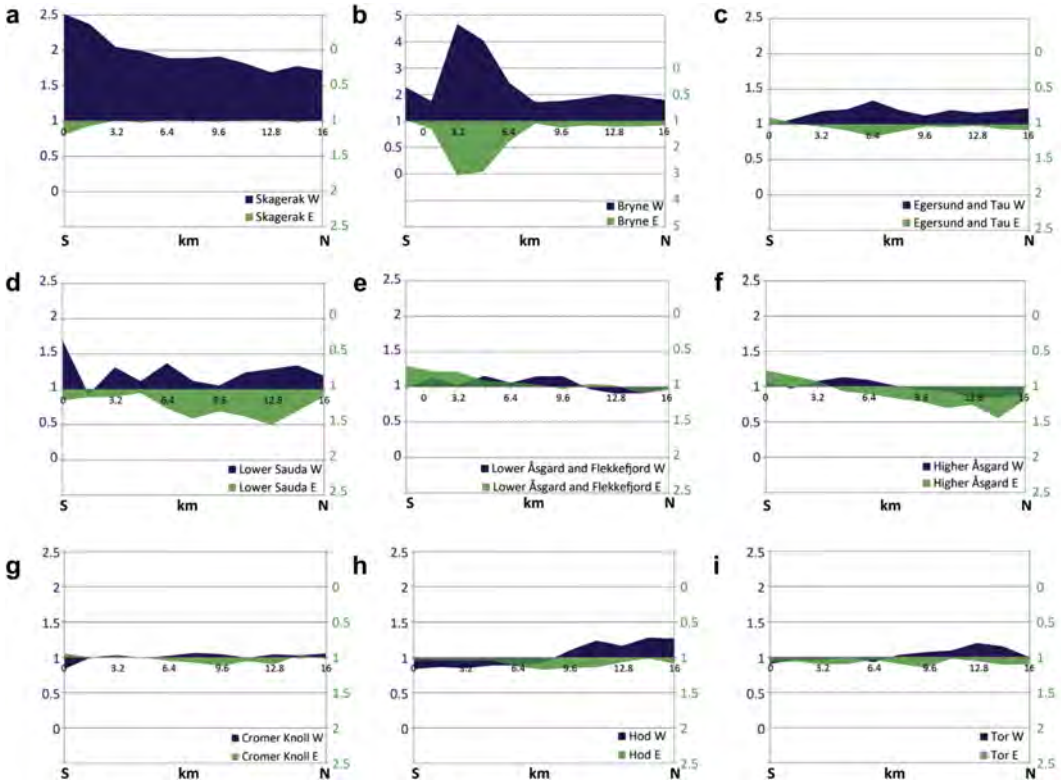

Fig. 17. Profiles of expansion indices for the sedimentary formations on the western (Dark purple) and eastern side (green) of the salt anticline (for profile locations see Fig. 16c); (a) The upper part of the Skagerrak Formation; (b) the Egersund Formation (note the change in axis values on this specific profile); (c) the Egersund and Tau Formations; (d) the Sauda Formation; (e) the Lower part of Åsgard and the Flekkefjord Formation; (f) the higher part of the Åsgard Formation; (g) the Cromer Knoll Group; (h) the Hod Formation; and (i) the Tor Formation. The axes to the left give the expansion index value for the western side of the salt anticline, while the ones to the right are for the eastern side of the salt anticline. Note that the axis values are the same on every figure with the exception of (b). (For interpretation of the references to colour in this figure legend, the reader is referred to the web version of this article.)

second period of anticline growth occurred during the Turonian to Campanian, which was principally associated with growth in the north while thinning in the south on the western side of the salt anticline (Figs. 9d and 17h). The same pattern can also be recognized in strata of Maastrichtian age (i.e. Tod Formation), along the smaller thickness variations imply slower rates of growth (Fig. 17i).

6.2. Controls on salt mobilization

These analyses indicate that salt flow and growth of the anticline was pulsed, and can be divided into two stages. The first stage occurred in the Late Triassic (Carnian times) (Hospers et al., 1988; Sørensen et al., 1992; Goldsmith et al., 2003). Hospers et al. (1988) claimed that a large amount of salt structures developed independent of faulting and were randomly distributed in the flat-bottomed, deep part of the Norwegian–Danish Basin. In contrast, Koyi and Petersen (1993) argued that the salt structures were largely controlled by basement faults. We suggest that in the Triassic, activity on the Sele High Fault System caused basement tilting and salt flow, possibly due to the withdrawal of salt from the western side of the anticline to feed a salt wall that developed in the immediate hanging wall of the Sele High Fault System (Fig. 18a–c). The second stage of salt mobilization occurred during the Late Cretaceous (Figs. 9d, 17h–i and 18e–f), possibly in response to basin shortening and inversion (Jackson et al., 2013). Diapir rejuvenation and 'active' diapirism has also been suggested for the large salt diapirs in Central Graben, North Sea (Davison et al., 2000).

7. Discussion

7.1. What triggered nucleation and growth of the cover-restricted fault array?

A clear spatial relationship exists between the cover- and basement-restricted fault arrays. Previous studies have shown that cover-restricted fault arrays are more likely to develop nearby and strike sub-parallel to, basement-restricted faults, because flexure, tilting and gravity gliding of the cover above basement faults can lead to fault nucleation and growth (Vendeville et al., 1995; Erratt et al., 1999; Withjack and Callaway, 2000). We propose that Triassic activity on the Sele High Fault System triggered westward gliding and mobilization of salt, and formation of the cover-restricted fault array due to thin-skinned extension of the Triassic cover (Fig. 18a–d). Based on the spatial relationship between the cover- and basement-restricted fault arrays, we propose that flexure of the cover across a series of sub-salt steps associated with

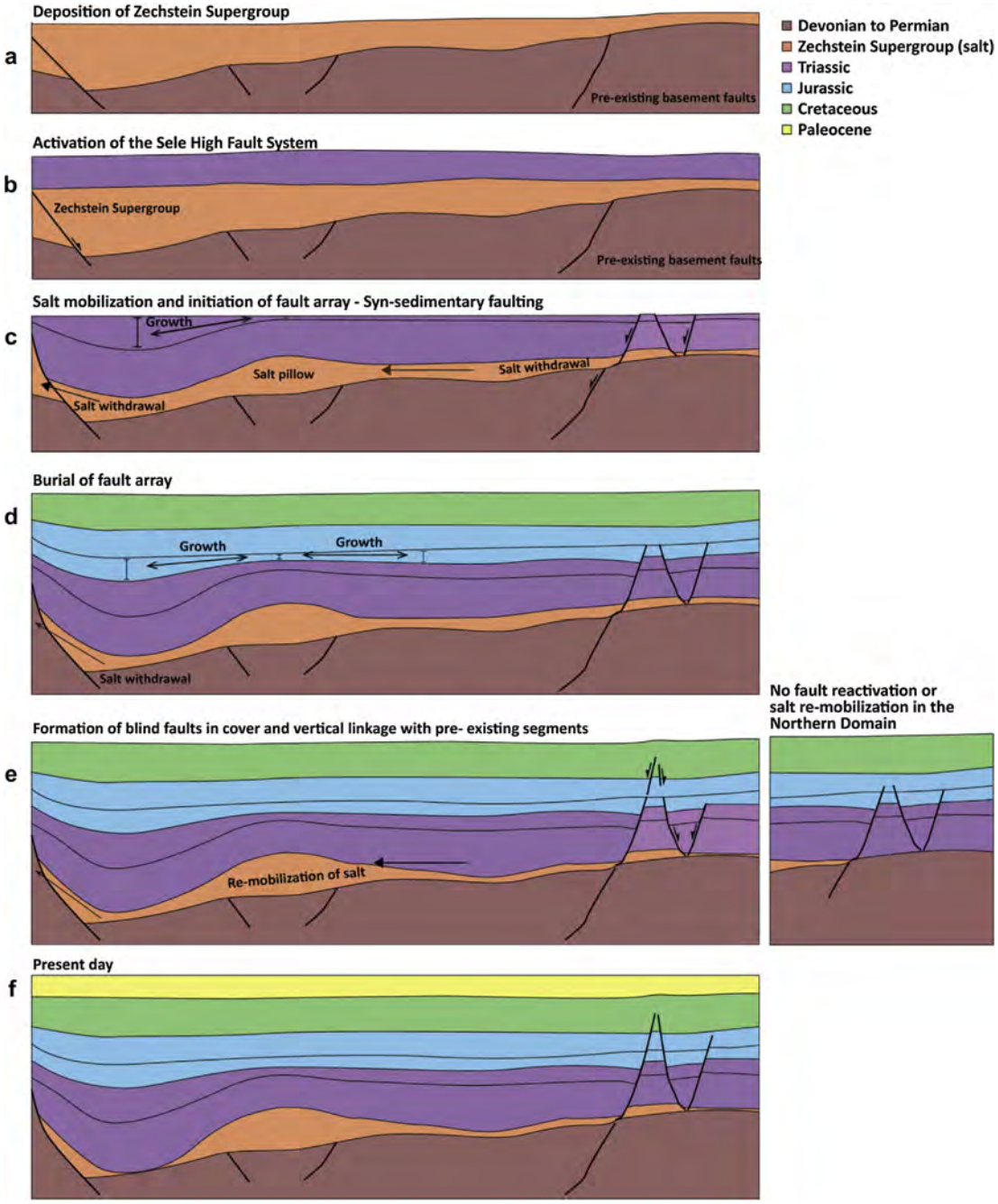

Fig. 18. Simplified sketch of the evolution of the fault array. (a) to (c) Late Triassic cover faults developed from pre-existing basement-bounding faults and contemporaneous salt mobilization during the Middle to late Triassic. This resulted in formation of the cover fault array in the Late Triassic. (d) The faulting continued into the Upper Jurassic when the tectonic activity ceased and the cover fault array was buried. (e) Late Cretaceous inversion triggered re-mobilization of salt which led to nucleation of blind faults in the cover, which again reactivated some faults within the fault array (f). To the North where the Zechstein Group was already depleted by the Middle Jurassic, no reactivation occurred (e).

basement-restricted faults controlled the initiation and localisation of the cover-restricted fault array. The Sele High Fault System acted as a downdip buttress, which resulted in the formation of a salt-cored buckle fold that was principally fed by salt derived from its western margin. Death of the fault array probably occurred in response to the development of the salt weld, and the cessation of salt flow and cover gravity gliding.

We speculate that mild reactivation of the cover-restricted fault array in the Southern Domain was triggered by Late Cretaceous (Turonian) basin inversion (Jackson et al., 2013), which cause shortening and amplification of the salt anticline, which may have resulted in local extension of the cover updip to the east. The location of basement-restricted faults and salt thickness controlled the location and style of cover-restricted fault growth at this time. For example, in the northern part of the fault array, where the salt is relatively thin, the cover-restricted faults were *not* reactivated (Fig. 18e). In the southern part of the fault array, where the salt is relatively thick, cover faults *were* reactivated, and new faults formed in the Cretaceous overburden (Fig. 18e and f). Furthermore, salt thickness has a clear relationship to the magnitude of lateral offset between basement and cover faults; i.e. cover faults in the north are co-linear in cross-section with basement faults, whereas in the south, lateral offset between these two fault populations scales roughly with the thickness of the salt. These observations are in general agreement with the predictions of scaled physical models by Withjack and Callaway (2000), who indicated a close relationship between the style and distribution of supra-salt deformation and the thickness of salt, where the lateral offset between basement faults and cover faults increases with increasing salt thickness.

7.2. Growth of normal faults in mechanically layered sequences

The growth of the fault array was influenced by mechanically layered nature of the host rock. For example, salt locally controlled the degree and style of coupling between sub- and supra-salt deformation, and thick mudstone-dominated units in the cover controlled the growth and final structural style of several structures in the cover-restricted fault systems. The fact that through-going, basement-involved faults bifurcate and pass along strike into physically separate, laterally distinct segments, which are decoupled by salt, implies that in the latter location, the segments are *kinematically coupled* despite being *geometrically decoupled*. This relationship suggests that kinematic coherency between sub- and supra-salt segments is maintained by sub-seismic, distributed, ductile strains within the salt (Childs et al., 1996; Schöpfer et al., 2006). A similar interpretation can be applied to the relationship between cover-restricted faults that bifurcate along strike. In this case, thick mudstones, rather than salt, deform by ductile flow and serve to maintain kinematic coherency between the sub- and supra-mudstone segments. This model of segmented fault growth by fault formation in 'strong', brittle layers and, at least at low strains, ductile flow in 'weak' layers is consistent with the results of discrete element models (DEM) of Schöpfer et al. (2006).

8. Conclusions

This study has provided a detailed analysis of the geometry and throw distribution of a thin-skinned fault array located immediately south–east of a low-relief salt anticline. We conclude that the supra-salt fault array evolved in stages of (i) syn-depositional growth faulting at the free surface due to salt mobilization triggered by Triassic extension along major basin-bounding basement faults; (ii) tectonic quiescence and burial of the fault tips Upper Jurassic to Turonian times; and (iii) salt re-mobilization triggered by basin inversion initiated in the Turonian, leading to blind reactivation in parts of the fault array (Figs. 15 and 18).

The driving mechanism behind fault activation and reactivation, and thus the overall evolution of the fault array is a combination between basement faulting and salt (re-)mobilization in response to regional tectonic events. In the final part of the evolution of the fault array, reactivation appears to have been largely controlled by salt mobilization in response to basin inversion without reactivation of the *basement-involved fault array*, because faults that show blind reactivation at this stage are located where the underlying salt is thick, while the non-reactivated faults are found where salt is near depleted. Hence, reactivation only occurred where salt mobilization was able to affect the fault array. The fault array provides an example of sub- and supra-salt faults that are geometrically un-linked through the salt along most of its extent, but locally physically linked where strains were sufficiently large to discretely breach the ZSG. However, despite the large extent of geometric decoupling across the ZSG, deformation was kinematically coupled, in the sense that the basement faults still affected the nucleation and localization of the cover faults.

Acknowledgements

We thank Brent Couzens-Schultz, an anonymous reviewer and Editor William M. Dunne for their thorough reviews, which greatly improved this article. We also thank PGS for access to seismic data and also granting permission to publish. In particular, we thank Richard Lamb at PGS for his assistance in securing relevant permissions to access and publish images from these data. We also thank Schlumberger for providing access to Petrel software and Badleys Geosciences for their TrapTester modelling software.

References

Baudon, C., Cartwright, J., 2008a. Early stage evolution of growth faults: 3D seismic insights from the Levant Basin, Eastern Mediterranean. Journal of Structural Geology 30, 888–898.

Baudon, C., Cartwright, J., 2008b. The kinematics of reactivation of normal faults using high resolution throw mapping. Journal of Structural Geology 30, 1072–1084.

Brown, A.R., 2003. Interpretation of Three-dimensional Seismic Data, sixth ed., vol. 42. American Association of Petroleum Geologists Memoir, p. 541.

Childs, C., Nicol, A., Walsh, J.J., Watterson, J., 1996. Growth of vertically segmented normal faults. Journal of Structural Geology 18, 1389–1397.

Childs, C., Nicol, A., Walsh, J.J., Watterson, J., 2003. The growth and propagation of synsedimentary faults. Journal of Structural Geology 25, 633–648.

Childs, C., Watterson, J., Walsh, J.J., 1995. Fault overlap zones within developing normal fault systems. Journal of the Geological Society 152, 535–549.

Davison, I., Alsop, I., Birch, P., Elders, C., Evans, N., Nicholson, H., Rorison, P., Wade, D., Woodward, J., Young, M., 2000. Geometry and late-stage structural evolution of Central Graben salt diapirs, North Sea. Marine and Petroleum Geology 17, 499–522.

Duffy, O.B., Gawthorpe, R.L., Docherty, M., Brocklehurst, S.H., 2012. Mobile evaporite controls on the structural style and evolution of rift basins: Danish Central Graben, North Sea. Basin Research 25, 310–330.

Erratt, D., Thomas, G.M., Wall, G.R.T., 1999. The evolution of the Central north sea rift. In: Geological Society, London, Petroleum Geology Conference Series, vol. 5, pp. 63–82.

Ford, M., Le Carlier de Veslud, C., Bourgeois, O., 2007. Kinematic and geometric analysis of fault-related folds in a rift setting: the Dannemarie basin, Upper Rhine Graben, France. Journal of Structural Geology 29, 1811–1830.

Gawthorpe, R.L., Leeder, M.R., 2000. Tectono-sedimentary evolution of active extensional basins. Basin Research 12, 195–218.

Glennie, K.W., Higham, J., Stemmerik, L., 2003. Permian. In: Evans, D., Graham, C., Armour, A., Bathurst, P. (Eds.), The Millennium Atlas: Petroleum Geology of the Central and Northern North Sea. The Geological Society of London, London.

Goldsmith, P., Hudson, G., Van Veen, P., 2003. Triassic. In: Evans, D., Graham, C., Armour, A., Bathurst, P. (Eds.), The Millennium Atlas: Petroleum Geology of the Central and Northern North Sea. The Geological Society of London, London.

Higgins, S., Clarke, B., Davies, R.J., Cartwright, J., 2009. Internal geometry and growth history of a thrust-related anticline in a deep water fold belt. Journal of Structural Geology 31, 1597–1611.

Hodgson, N.A., Farnsworth, J., Fraser, A.J., 1992. Salt-related tectonics, sedimentation and hydrocarbon plays in the Central Graben, North Sea, UKCS. In: Geological Society, London, Special Publications, vol. 67, pp. 31–63.
Hongxing, G., Anderson, J.K., 2007. Fault throw profile and kinematics of normal fault-conceptual models and geologic examples. Geological Journal of China Universities 13, 75–88.
Hospers, J., Rathore, J.S., Jianhua, F., Finnstrøm, E.G., Holthe, J., 1988. Salt tectonics in the Norwegian–Danish basin. Tectonophysics 149, 35–60.
Husmo, T., Hamar, G., Høiland, O., Johannessen, E.P., Rømuld, A., Spencer, A., Titterton, R., 2003. Lower and middle Jurassic. In: Evans, D., Graham, C., Armour, A., Bathurst, P. (Eds.), The Millennium Atlas: Petroleum Geology of the Central and Northern North Sea. The Geological Society of London, London.
Isaksen, D., Tonstad, K., 1989. A Revised Cretaceous and Tertiary Lithostratigraphic Nomenclature for the Norwegian North Sea. Oljedirektoratet, Stavanger.
Jackson, C.-L., Chua, S.-T., Bell, R., Magee, C., 2013. Structural style and early stage growth of inversion structures: 3D seismic insights from the Egersund Basin, offshore Norway. Journal of Structural Geology 46, 167–185.
Jackson, C.A.L., Rotevatn, A., 2013. 3D seismic analysis of the structure and evolution of a salt-influenced normal fault zone: a test of competing fault growth models. Journal of Structural Geology. ISSN:0191-8141.
Jackson, C.A.L., Lewis, M.M., 2012. Origin of an anhydrite sheath encircling a salt diapir and implications for the seismic imaging of steep-sided salt structures, Egersund Basin, Northern North Sea. Journal of the Geological Society 169, 593–599.
Jackson, M.P.A., Hudec, M.R., 2005. Stratigraphic record of translation down ramps in a passive-margin salt detachment. Journal of Structural Geology 27, 889–911.
Jackson, M.P.A., Vendeville, B.C., 1994. Regional extension as a geologic trigger for diapirism. Geological Society of America Bulletin 106, 57–73.
Kane, K.E., Jackson, C.A.L., Larsen, E., 2010. Normal fault growth and fault-related folding in a salt-influenced rift basin: south Viking Graben, offshore Norway. Journal of Structural Geology 32, 490–506.
Koyi, H., Petersen, K., 1993. Influence of basement faults on the development of salt structures in the Danish Basin. Marine and Petroleum Geology 10, 82–94.
Mansfield, C., Cartwright, J., 2001. Fault growth by linkage: observations and implications from analogue models. Journal of Structural Geology 23, 745–763.
Mansfield, C.S., Cartwright, J.A., 1996. High resolution fault displacement mapping from three-dimensional seismic data: evidence for dip linkage during fault growth. Journal of Structural Geology 18, 249–263.
Marsh, N., Imber, J., Holdsworth, R.E., Brockbank, P., Ringrose, P., 2010. The structural evolution of the Halten Terrace, offshore Mid-Norway: extensional fault growth and strain localisation in a multi-layer brittle-ductile system. Basin Research 22, 195–214.
Maurin, J.-C., Niviere, B., 2000. Extentional forced folding and decollement of the pre-rift series along the Rhine graben and their influence on the geometry of the syn-rift sequences. In: Special Publication – Geological Society of London, vol. 169, pp. 73–86.
Morley, C., Back, S., Van Rensbergen, P., Crevello, P., Lambiase, J., 2003. Characteristics of repeated, detached, Miocene–Pliocene tectonic inversion events, in a large delta province on an active margin, Brunei Darussalam, Borneo. Journal of Structural Geology 25, 1147–1169.
Møller, J.J., Rasmussen, E.S., 2003. Middle Jurassic–Early Cretaceous rifting of the Danish Central graben. Geological Survey of Denmark and Greenland Bulletin 1, 247–264.
Nicol, A., Watterson, J., Walsh, J.J., Childs, C., 1996. The shapes, major axis orientations and displacement patterns of fault surfaces. Journal of Structural Geology 18, 235–248.
Pascoe, R., Hooper, R., Storhaug, K., Harper, H., 1999. Evolution of extensional styles at the southern termination of the Nordland Ridge, Mid-Norway: a response to variations in coupling above Triassic salt. In: Geological Society, London, Petroleum Geology Conference Series. Geological Society of London.
Richard, P., Krantz, R.W., 1991. Experiments on fault reactivation in strike-slip mode. Tectonophysics 188, 117–131.
Richardson, N.J., Underhill, J.R., Lewis, G., 2005. The role of evaporite mobility in modifying subsidence patterns during normal fault growth and linkage, Halten Terrace, Mid-Norway. Basin Research 17, 203–223.
Rouby, D., Guillocheau, F., Robin, C., Bouroullec, R., Raillard, S., Castelltort, S., Nalpas, T., 2003. Rates of deformation of an extensional growth fault/raft system (offshore Congo, West African margin) from combined accommodation measurements and 3-D restoration. Basin Research 15, 183–200.
Rowan, M.G., Jackson, M.P.A., Trudgill, B.D., 1999. Salt-related fault families and fault welds in the northern Gulf of Mexico. Aapg Bulletin 83, 1454–1484.
Rykkelid, E., Fossen, H., 2002. Layer rotation around vertical fault overlap zones: observations from seismic data, field examples, and physical experiments. Marine and Petroleum Geology 19, 181–192.
Schöpfer, M.P., Childs, C., Walsh, J.J., 2006. Localisation of normal faults in multilayer sequences. Journal of Structural Geology 28, 816–833.
Stewart, S.A., Ruffell, A.H., Harvey, M.J., 1997. Relationship between basement-linked and gravity-driven fault systems in the UKCS salt basins. Marine and Petroleum Geology 14, 581–604.
Sørensen, S., Morizot, H., Skottheim, S., 1992. A tectonostratigraphic analysis of the Southeast Norwegian North Sea basin. In: Special Publication – Norwegian Petroleum Society, NPF, vol. 1, pp. 19–42.
Thorsen, C.E., 1963. Age of growth faulting in southeast Louisiana. Gulf Coast Association of Geological Societies 13, 103–110.
Underhill, J.R., Partington, M.A., 1993. Jurassic thermal doming and deflation in the North Sea: implications of the sequence stratigraphic evidence. In: Geological Society, London, Petroleum Geology Conference Series, vol. 4, pp. 337–345.
Van Rensbergen, P., Morley, C., Ang, D., Hoan, T., Lam, N., 1999. Structural evolution of shale diapirs from reactive rise to mud volcanism: 3D seismic data from the Baram delta, offshore Brunei Darussalam. Journal of the Geological Society 156, 633–650.
Vejbæk, O., Andersen, C., 2002. Post mid-Cretaceous inversion tectonics in the Danish Central Graben—regionally synchronous tectonic events. Bulletin of the Geological Society of Denmark 49, 129–144.
Vendeville, B., Ge, H., Jackson, M., 1995. Scale models of salt tectonics during basement-involved extension. Petroleum Geoscience 1, 179–183.
Vendeville, B.C., Jackson, M.P.A., 1992. The fall of diapirs during thin-skinned extension. Marine and Petroleum Geology 9, 354–371.
Vollset, J., Doré, A.G., 1984. A Revised Triassic and Jurassic Lithostratigraphic Nomenclature for the Norwegian North Sea. Oljedirektoratet, Stavanger.
Wagner III, B.H., Jackson, M., 2011. Viscous flow during salt welding. Tectonophysics 510, 309–326.
Walsh, J.J., Watterson, J., 1988. Analysis of the relationship between displacements and dimensions of faults. Journal of Structural Geology 10, 239–247.
Walsh, J.J., Watterson, J., 1990. New methods of fault projection for coalmine planning. Proceedings of the Yorkshire Geological and Polytechnic Society 48, 209–219.
Walsh, J.J., Watterson, J., 1991. Geometric and kinematic coherence and scale effects in normal fault systems. In: Geological Society, London, Special Publications, vol. 56, pp. 193–203.
Watterson, J., 1986. Fault dimensions, displacements and growth. Pure and Applied Geophysics 124, 365–373.
Williams, G., Powell, C., Cooper, M., 1989. Geometry and kinematics of inversion tectonics. In: Geological Society, London, Special Publications, vol. 44, pp. 3–15.
Withjack, M.O., Callaway, S., 2000. Active normal faulting beneath a salt layer: an experimental study of deformation patterns in the cover sequence. Aapg Bulletin 84, 627–651.
Withjack, M.O., Olson, J., Peterson, E., 1990. Experimental models of extensional forced folds (1). Aapg Bulletin 74, 1038–1054.
Zanella, E., Coward, M., 2003. Structural framework. In: Evans, D., Graham, C., Armour, A., Bathurst, P. (Eds.), The Millennium Atlas: Petroleum Geology of the Central and Northern North Sea. The Geological Society of London, London.
Ziegler, P.A., 1992. North Sea rift system. Tectonophysics 208, 55–75.

Paper IV: Supra-salt normal fault growth during the rise and fall of a salt diapir: insights from 3D seismic reflection data

Anette B.M. Tvedt, Atle Rotevatn, Christopher A.-L. Jackson,

Submitted to Journal of Structural Geology

IV

Abstract

Normal faulting and the deep subsurface flow of salt are the fundamental processes controlling the tectonic development of many salt-rich sedimentary basins. However, our detailed understanding of the spatial and temporal relationship between normal faulting and salt movement is poor due to a lack of natural examples constraining their geometric and kinematic relationship in three-dimensions. We use 3D seismic reflection and borehole data from the Egersund Basin, offshore Norway to determine the structure and growth of a normal fault array formed during the birth, growth and death of an array of salt structures. We show that the fault array and salt structures developed in response to; (i) Late Triassic-to-Middle Jurassic thick-skinned extension and reactive diapirism; (ii) Early Cretaceous extensional collapse of the walls; and (iii) Jurassic-to-Neogene active and passive diapirism, which was at least partly coeval with and occurred along-strike from areas of reactive diapirism and wall collapse. Our study supports physical model predictions, showcasing a three-dimensional example of how protracted, multiphase salt diapirism can influence the structure and growth of normal fault arrays.

1. Introduction

Supra-salt normal fault arrays can form in response to halokinesis and/or regional extension. During regional extension, which may be triggered by thick-skinned extension, or thin-skinned gravity gliding or spreading, reactive diapirs form due to upwelling of salt into space created by extensional thinning of overburden (Fig. 1) (Vendeville and Jackson, 1992b; Jackson and Vendeville, 1994; Mauduit and Brun, 1998; Rowan et al., 1999; Hudec and Jackson, 2007). Even after regional overburden extension has ceased, supra-salt faults can continue to grow in response to more local stretching caused by active or passive diapirism (Fig. 1; Vendeville and Jackson, 1992b; Schultz-Ela et al., 1993; Rowan et al., 2003; Dooley et al., 2009). Faults triggering reactive diapirism normally strike sub-parallel to elongated salt walls, with progressively younger faults developing towards the crest of the salt wall as it rises; in contrast, faults formed during passive or active diapirism are arranged in radial or concentric arrays flanking the rising diapir (Vendeville and Jackson, 1992b; Davison et al., 2000a). Salt diapirs may also collapse in response to ongoing thin-skinned extension, principally due to widening of diapirs at a time when the amount of extension outpaces salt flow into the diapir, which may be linked to the development of salt welds (Vendeville and Jackson, 1992a; Rowan et al., 1999). As demonstrated by physical models, it is thus plausible that a single diapir may simultaneously rise and fall due to the along-strike flow of salt within the body, leading to arching-related, radial and concentric faults where the diapir is active or passive, and wall-parallel faults where the wall is rising or collapsing (Fig. 1d; Vendeville and Jackson, 1992a; Vendeville and Jackson, 1992b; Ge et al., 1995; Guglielmo et al., 1997). The link between overburden deformation and salt mobilisation is important, helping us understand the kinematics and dynamics of salt mobilisation and, more generally, the structural evolution of salt-bearing sedimentary basins.

To the best of our knowledge, the three-dimensional geometry and kinematic evolution of a supra-salt fault array during the multiphase growth and demise of a salt diapir has never been documented using data from a natural example, thus the predictions of

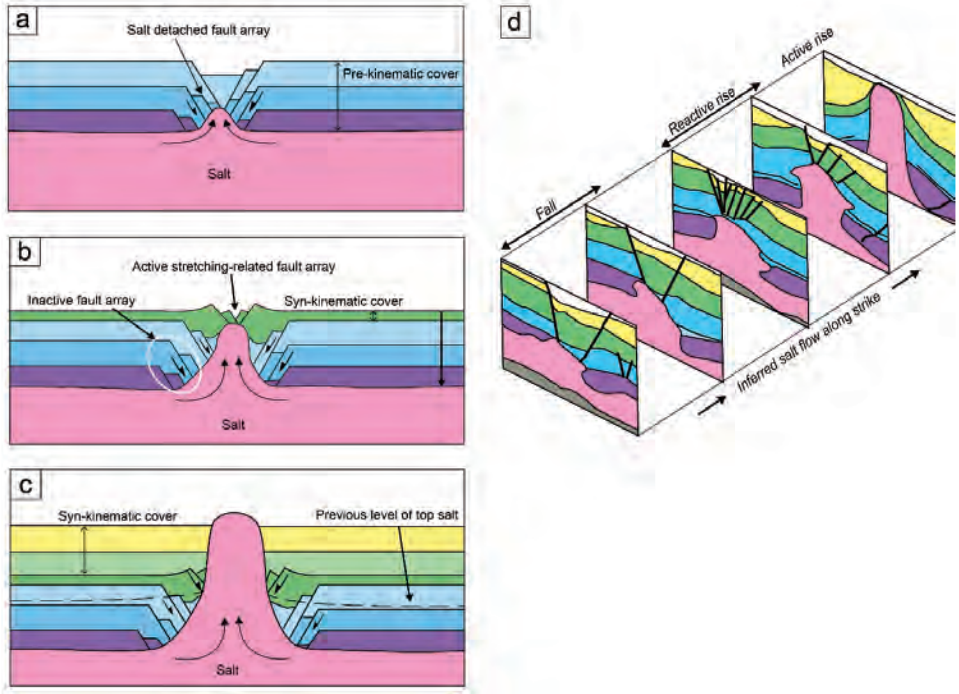

Fig. 1. Conceptual figure showing diapir piercement during regional extension. The growth of diapirs may go through some or all of these stages; (a) reactive diapirism; (b) active diapirism, where the supra-salt cover load pressurizes the salt; and (c) passive diapirism where sediment downbuilding occurs while the diapir continues to grow. These processes can occur simultaneously along strike (d). Modified from Vendeville and Jackson (1992b) and Hudec and Jackson (2007).

physical models remain untested. Motivated by this, we here use high-quality 3D reflection seismic and borehole data from the Egersund Basin, offshore Norway to illustrate how supra-salt normal fault arrays may evolve during multiphase salt diapirism (Fig. 2). We investigate the growth history of individual fault segments and the fault array as a whole, before turning our attention to how this triggers and is triggered by, multiphase salt mobilisation. Because there are no explicit, focused studies on how faulting and salt flow are linked with emphasis on along-strike variability, we investigate the effect that lateral migration of salt along the walls and into flanking stocks has on the evolution of overlying fault arrays. The natural example documented here tests the predictions of physical models replicating the rise and

collapse of salt diapirs. We show that along-strike salt flow within mature salt diapirs has an important control on the nature and timing of overburden deformation (Vendeville and Jackson, 1992b; Vendeville and Jackson, 1992a; Ge et al., 1995; Guglielmo et al., 1997; Guglielmo et al., 1999).

2. Geological Setting

The studied fault array lies in the Egersund Basin, which is located in the southern part of the Norwegian North Sea, c. 115 km offshore SW Norway. The NW-trending basin is bounded by the Sele High to the W, the Stavanger Platform to the NE, the Lista Nose to the SE and the Flekkefjord High to the S (Fig. 2).

Initial opening and subsidence of the Egersund Basin occurred in response to Late Carboniferous to Permian transtension, resulting in the formation of a series of normal faults, including the Sele High Fault System, and the creation of the North Permian Basin (Sørensen et al., 1992; Ziegler, 1992). During the Early Permian, a thick succession of continental sediments was deposited (Sørensen et al., 1992; Glennie, 1998). During the Late Permian, a marine transgression occurred, leading to the deposition of a thick succession of evaporites (the Zechstein Supergroup; Hodgson et al., 1992; Sørensen et al., 1992; Davison et al., 2000b; Glennie et al., 2003). The Zechstein Supergroup is absent or very thin on the structural highs surrounding the Egersund Basin (Jackson and Lewis, 2013; 2016), whereas it is relatively thick in the basin centre (1000-1500 m; Sørensen et al., 1992). During the Triassic, the Sele High Fault System was reactivated, causing tilting of the Zechstein salt layer, and gravity-gliding, stretching and normal faulting of the overburden (Fig. 2b) (Sørensen et al., 1992; Tvedt et al., 2013; Mannie et al., 2014; Jackson and Lewis, 2016). Small salt rollers that developed between overburden rafts later evolved into salt diapirs, the growth and demise of which was intimately related to the supra-salt fault array we study here (see section 6).

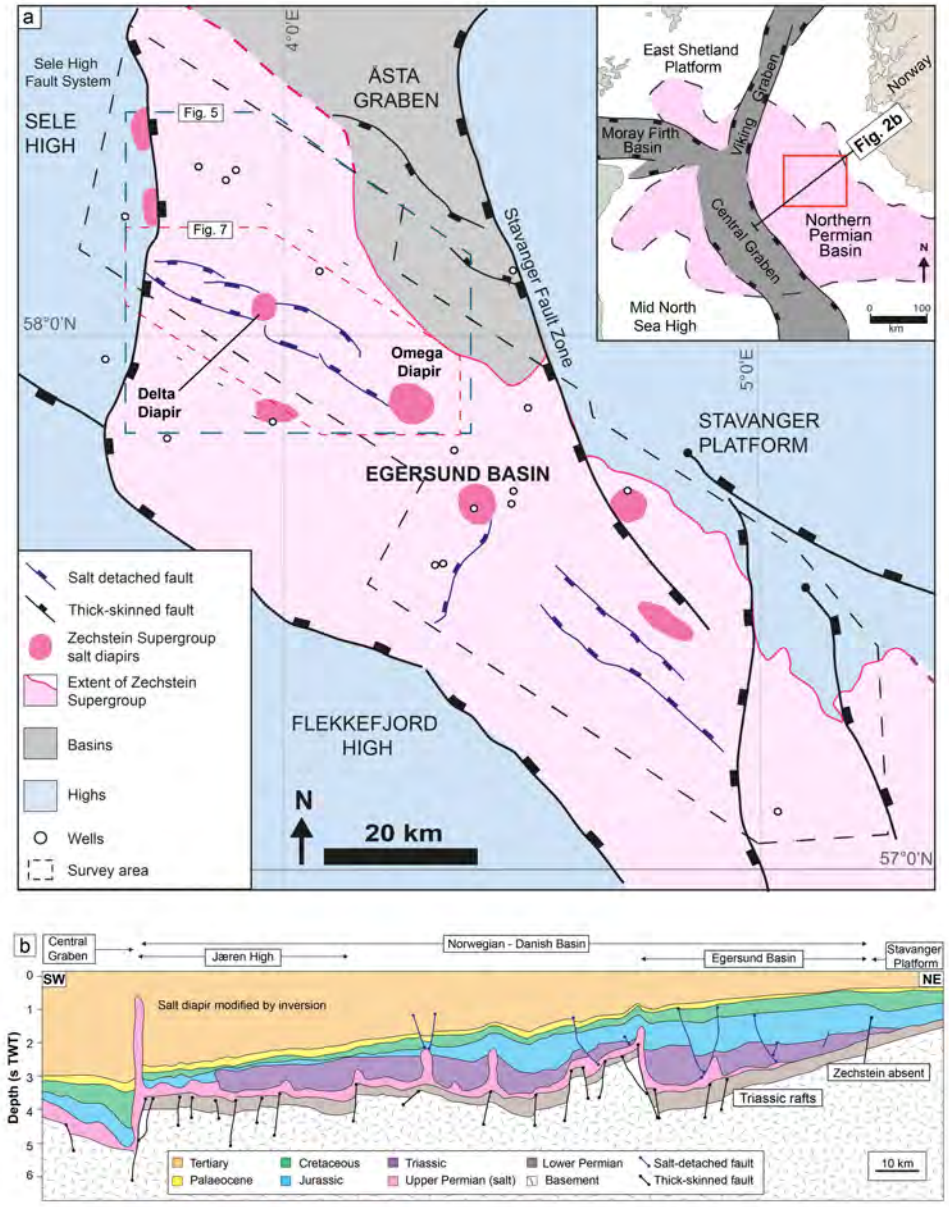

Fig. 2. Location of the Egersund Basin in the North Sea, NE of the Central Graben (red square in the inlet of simplified structural map of the North Sea with the main structural imprints). Extent of Zechstein Supergroup is based on own observations, combined with data from Evans et al. (2003), Jackson and Lewis (2013). Structural maps based on Zanella and Coward (2003), Jackson and Lewis (2013), data from the Norwegian Petroleum Directorate and own observations.

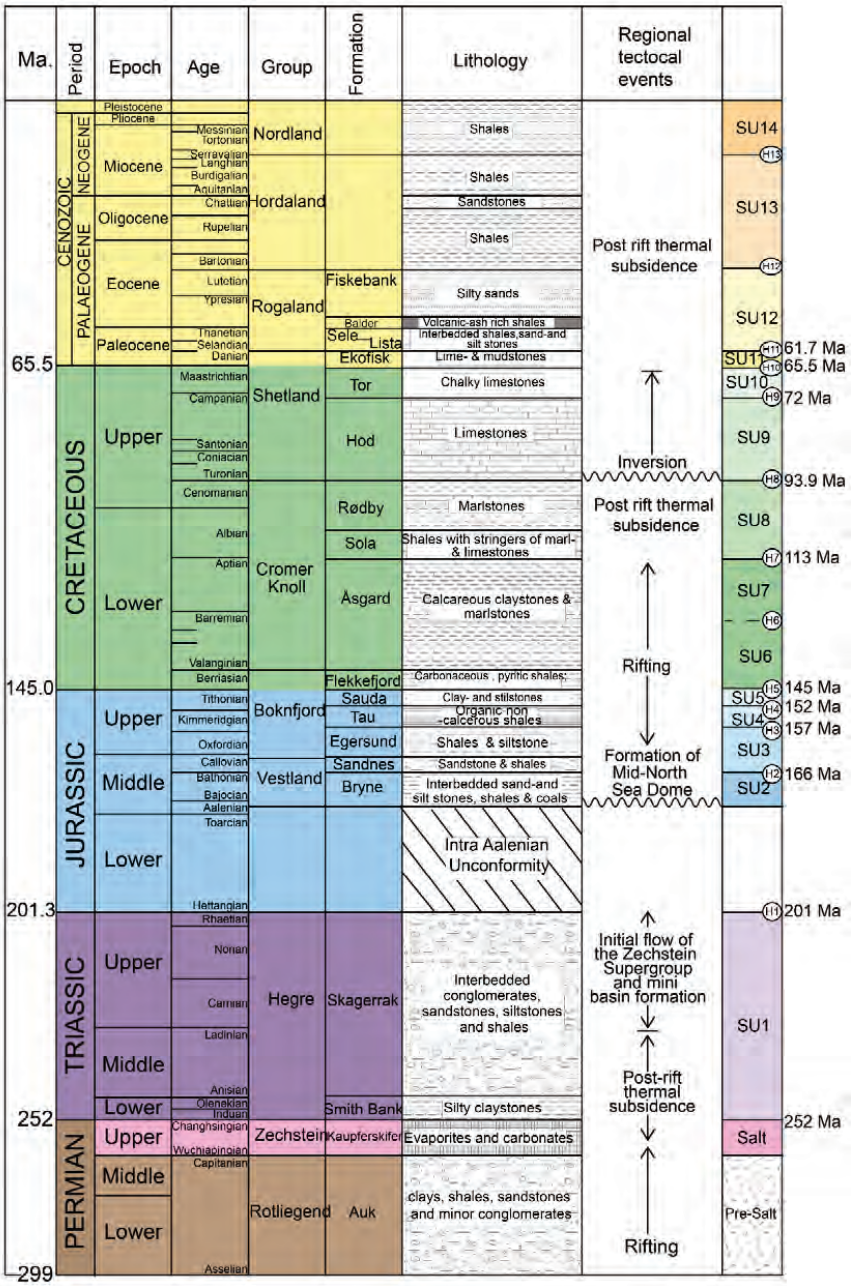

Fig. 3. Stratigraphic framework showing the key (and interpreted) seismic horizons, their representative ages and the tectonostratigraphic evolution of the Egersund Basin. Colour coding of the different periods is continued throughout the article. The data used for the lithologies and tectonostratigraphic framework are compiled from Sørensen et al. (1992), Vollset and Doré (1984), Tvedt et al. (2013), Norwegian Petroleum Directorate and well data.

During the Early Jurassic, plume-related crustal up-warping led to the establishment of the Mid-North Sea Dome, resulting in widespread erosion focused on the North Sea Rift triple junction (Underhill and Partington, 1993). Lower Jurassic deposits are therefore only locally preserved in the study area and, more commonly, are represented by the intra-Aalenian unconformity (Husmo et al., 2003). As the Mid-North Sea dome deflated in the Middle Jurassic, a new episode of rifting initiated, and basin-bounding faults, such as the NW-trending Sele High Fault System, were reactivated (Fig. 2a) (Sørensen et al., 1992; Underhill and Partington, 1993; Husmo et al., 2003). Reactivation triggered renewed salt mobilisation and associated fault growth during the Middle-Late Jurassic (Tvedt et al., 2013; Mannie et al., 2014). During the Late Jurassic fault slip and overall subsidence rates were high (Fig. 3) (Vollset and Doré, 1984). Rifting ceased in the Early Cretaceous (Møller and Rasmussen, 2003) and, during the Late Cretaceous (Turonian - Maastrichtian), inversion occurred in response to Alpine-related crustal shortening (Ziegler, 1992; Vejbæk and Andersen, 2002). Inversion caused rejuvenation of pre-existing salt structures, expressed by diapir squeezing and active diapirism (Wilson et al., 2013), a process that continued until the Miocene (Sørensen et al., 1992).

3. Database and Methods

3.1. Database

The database for this study comprises two pre-stack time-migrated, three-dimensional reflection seismic datasets (PGS MS_ST98M3 and PGS MC3D EGB2005), which are tied to 15 wells (e.g. Figs. 2 and 4). The seismic data cover a total area of 3600 km^2; we here focus on a c. 250 km^2 portion of the north-western Egersund Basin, where salt structures and their genetically related normal fault arrays are well-imaged (Fig. 2).

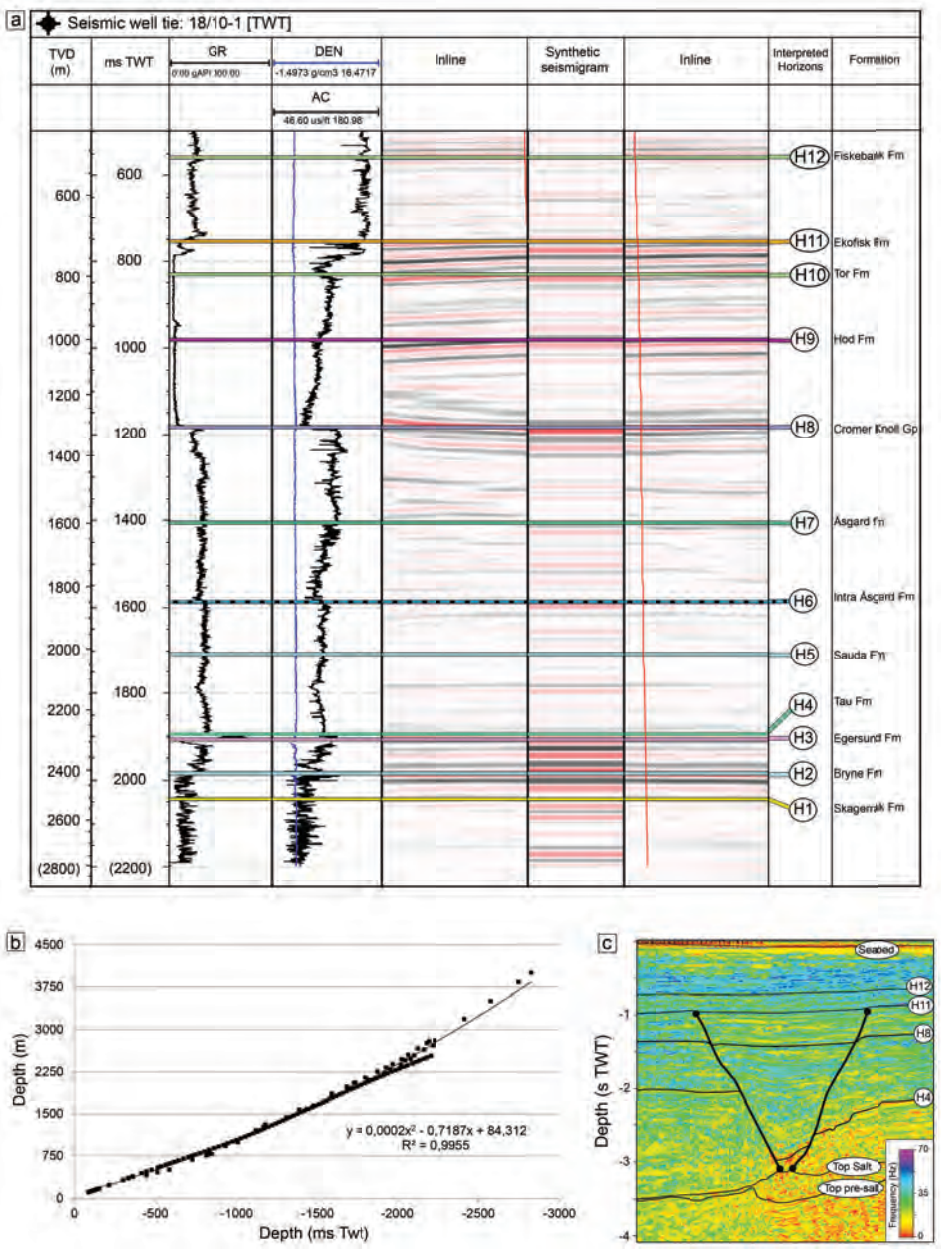

Fig. 4. (a) Seismic well tie of well 18/10-1. (b) Checkshots from three wells in close proximity to the studied fault array are used to construct a depth conversion formula. (c) Frequency map to show the frequency variations in the interval of interest.

Table 1: Wells within the Egersund Basin (Data from the Norwegian Petroleum Directorate).

Well	TD depth (m RKB)	Oldest penetrated stratigraphic unit
17/12-1R	4298	Zechstein
17/12-2	2334	Devonian (no formation defined)
17/12-3	2730	Skagerrak
18/10-1	2800	Skagerrak
8/3-2	2657	Skagerrak
9/2-1	3755	Skagerrak
9/2-2	3548	Skagerrak
9/2-3	3421	Bryne
9/2-4s	3313	Bryne
9/2-5	3354	Bryne
9/2-6s	3642	Bryne
9/2-8s	3345	Zechstein
9/2-11	2836	Bryne
9/3-1	1970	Skagerrak
9/3-2	3151	Skagerrak

Line sampling is 25 m and the seismic sections are displayed with normal polarity (SEG European Convention; Brown, 2003), whereby an increase in acoustic impedance is represented by a peak (black), and a decrease by a trough (red). Inlines are orientated N-S and crosslines are orientated E-W. The dominant frequency in the interval of interest is c. 25–45 Hz and acoustic velocities range between 2700 and 3700 ms^{-1}, yielding a vertical seismic resolution of c. 15-43 m in the interval of interest (Fig. 4c). This resolution is sufficient to allow detailed mapping of the salt structures and their genetically related normal fault arrays, and pre-, syn- and post-kinematic strata documenting their growth (see below).

We have mapped 16 seismic horizons, the ages of which are age-constrained by 15 wells located within the seismic survey area (Figs. 3 and 4a, Table 1). Mapping of these horizons allows us to constrain how throw is distributed on the salt-related faults and to determine their kinematics (see section 3.2). We mapped 22 faults; seven of the largest, best-imaged faults that accommodated the majority of the extensional strain, were selected for detailed kinematic analysis. The faults have been mapped on seismic profiles orientated perpendicular to local fault strike. Attribute maps (e.g. variance

maps showing coherence discontinuities in the horizontal continuity of amplitude of the seismic; Bahorich and Farmer, 1995; Cartwright, 2007) are used to aid fault interpretation.

3.2. Methodology

In this study we use three different techniques to document the structural style and assess the growth of the supra-salt fault array. First, we use throw-distance analysis (T-x) and throw backstripping to detect zones of linkage between fault segments and to elucidate the lateral growth of faults (Walsh and Watterson, 1990; Childs et al., 1995; Gawthorpe and Leeder, 2000; Gupta and Scholz, 2000; Kim and Sanderson, 2005; Giba et al., 2012). As we demonstrate in section 5, the faults established their near-full lengths early in their growth history, before progressively accumulating displacement without further significant lateral tip propagation (cf. Walsh et al., 2002; Giba et al., 2012); we therefore elect to use the 'vertical throw subtraction method' (Chapman and Meneilly, 1991; Childs et al., 1993) rather than the 'T-max method' (Rowan et al., 1998; Dutton and Trudgill, 2009) for throw backstripping. Second, we use throw-depth analysis (T-z) to: (i) assess the role of dip linkage during normal fault growth, (ii) evaluate how the mechanical properties of the host rock influences fault growth, and (iii) identify periods of syn-sedimentary faulting and blind fault propagation (Mansfield and Cartwright, 1996; Nicol et al., 1996; Jackson and Rotevatn, 2013; Tvedt et al., 2013). Third, isochron (time-thickness) maps and expansion indices are used to investigate growth strata thickness variations, which can provide important information on the formation and growth of depocentres and, therefore, the kinematics of the bounding faults (Thorsen, 1963; Rouby et al., 2003; Jackson and Rotevatn, 2013; Tvedt et al., 2013).

Fault throw is recorded perpendicular to local fault strike every 100-200 m, depending on the degree of structural complexity and rapidity of along-strike throw variations. We have assigned an error of throw measurements in the Middle Jurassic and post-Aptian succession, within which the seismic quality is good-to-excellent, to ±4 ms. The

seismic quality within the Triassic and Tithonian–to-Aptian successions is poor-to-good, and we therefore estimated the throw measurement errors to be ±8 ms.

We use checkshot velocity data from five nearby wells (8/3-2, 9/1-1S, 17/12-1, 17/12-2 and 18/10-1; Table 1) to depth convert throw values recorded in milliseconds two-way time (ms TWT) to metres (Fig. 4b). Depth conversion indicates that the patterns and shapes of throw variations on T-z plots are the same in both the time and depth domains; throw values are therefore presented in milliseconds two-way time (ms TWT) rather than metres (cf. Baudon and Cartwright, 2008c). Taylor et al. (2008) demonstrate that differential compaction may influence calculation of fault throw in cases where the faulted growth sequence has a high shale content (>70%) and post-faulting burial is large (i.e. several kms). The faults we study have <2 km throw and are buried to relatively shallow depths (<0.5 km), and the host rock is comprised of a mixed sand-shale sequence with limited lateral sedimentological heterogeneity in the faulted succession. These observations suggest that differential compaction did not strongly influence throw variability on the studied faults, nor did it negatively impact our kinematic analysis derived from these throw data (Mansfield and Cartwright, 1996; Taylor et al., 2008).

4. Salt structures

The Egersund Basin contains a range of salt structures, including salt walls, stocks and anticlines (Figs. 5 and 6). Salt stocks are up to 2500 ms TWT tall (3550 m), typically extending up from the Upper Permian source layer into the Lower Palaeocene (SU11) (e.g. Omega Diapir; Mannie et al., 2014), or into the Upper Eocene-Middle Miocene (SU13) (e.g. Delta Diapir; Mannie et al., 2014) (Figs. 5 and 6). The Omega and Delta diapirs are per definition salt stocks, but for consistency with a previous naming convention established by (Mannie et al., 2014), we retain these names. Salt walls and anticlines are up to 700 ms TWT thick (1200 m) and 500 ms TWT thick (1019 m; e.g. the Xi anticline; Fig. 5), respectively. Between salt structures, the salt is relatively thin (typically <160 ms TWT or <300 m), or welded (Figs. 5 and 6).

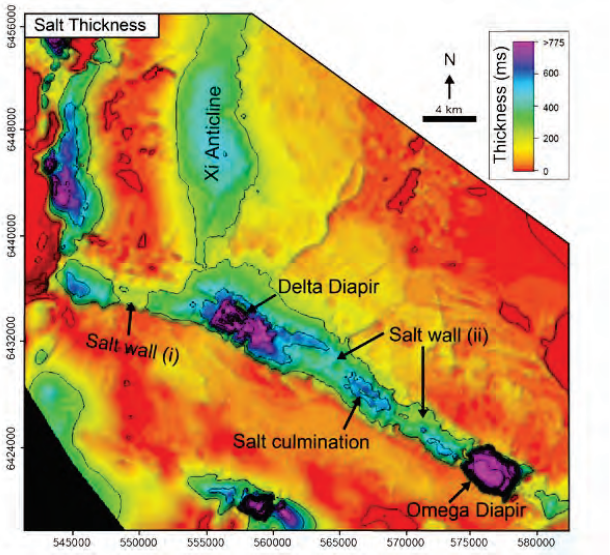

Fig. 5. Isochron map illustrating salt thickness in the studied part of the Egersund Basin, including major salt structures, such as salt walls, salt stocks and salt anticline.

In this study we focus on the supra-salt fault array that formed to the NW and SE of the Delta Diapir (Fig. 7). The salt walls underlying the studied supra-salt fault array trend SE and are divided into two parts, separated by the Delta Diapir; (i) a north-western wall that is 14 km long, 3.1 km wide and 490 ms TWT (1039 m) thick; and (ii) a south- eastern wall that is 18 km long, 3.7 km wide and up to 549 ms TWT (1004 m) thick, which is pinned between the Delta and Omega diapirs (Figs. 5 and 6). Both salt walls have relatively sharp triangular crests and occur in the footwall of major supra-salt normal faults (e.g. Fig. 8a). The south-eastern salt wall gradually increases in height towards the NW towards the Delta Diapir, where it pierces through the Jurassic strata. In contrast, on the north-western side of the Delta Diapir, the transition from salt wall to salt stock is steeper (Fig. 6a). A small salt accumulation, which may indicate an immature salt stock, is observed near the central part of the south-eastern salt wall (Fig. 5 and 6). The salt walls and the Delta and Omega diapirs are flanked to the NE and SW by salt welds.

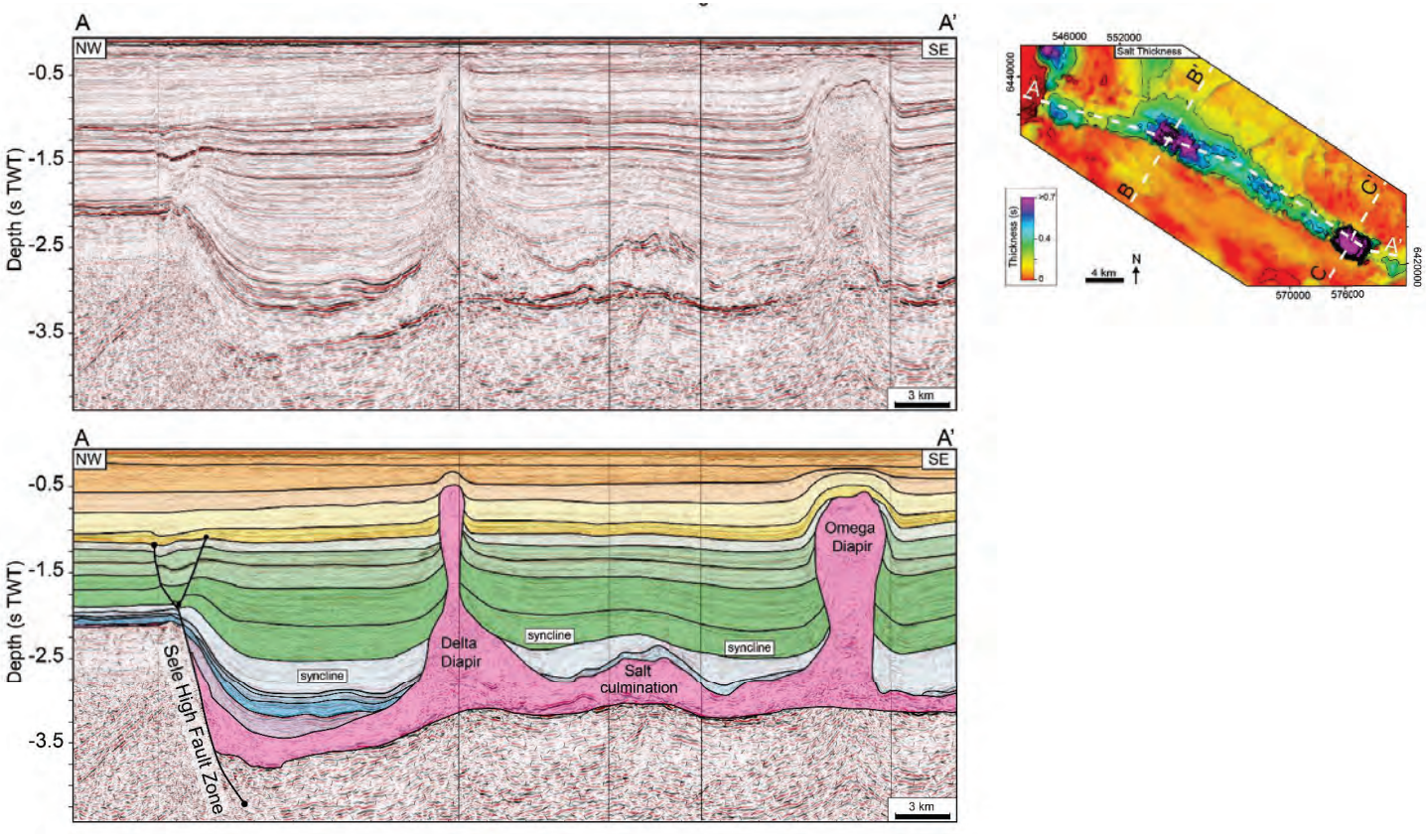
A
A'
NW
SE
-0.5
-1.5
-2.5
-3.5
Depth (s TWT)
3 km
Omega Diapir
Delta Diapir
syncline
syncline
syncline
Salt culmination
Sele High Fault Zone
546000
552000
Salt Thickness
6440000
6420000
570000
576000
Thickness (s)
>0.7
0.4
0
4 km
N

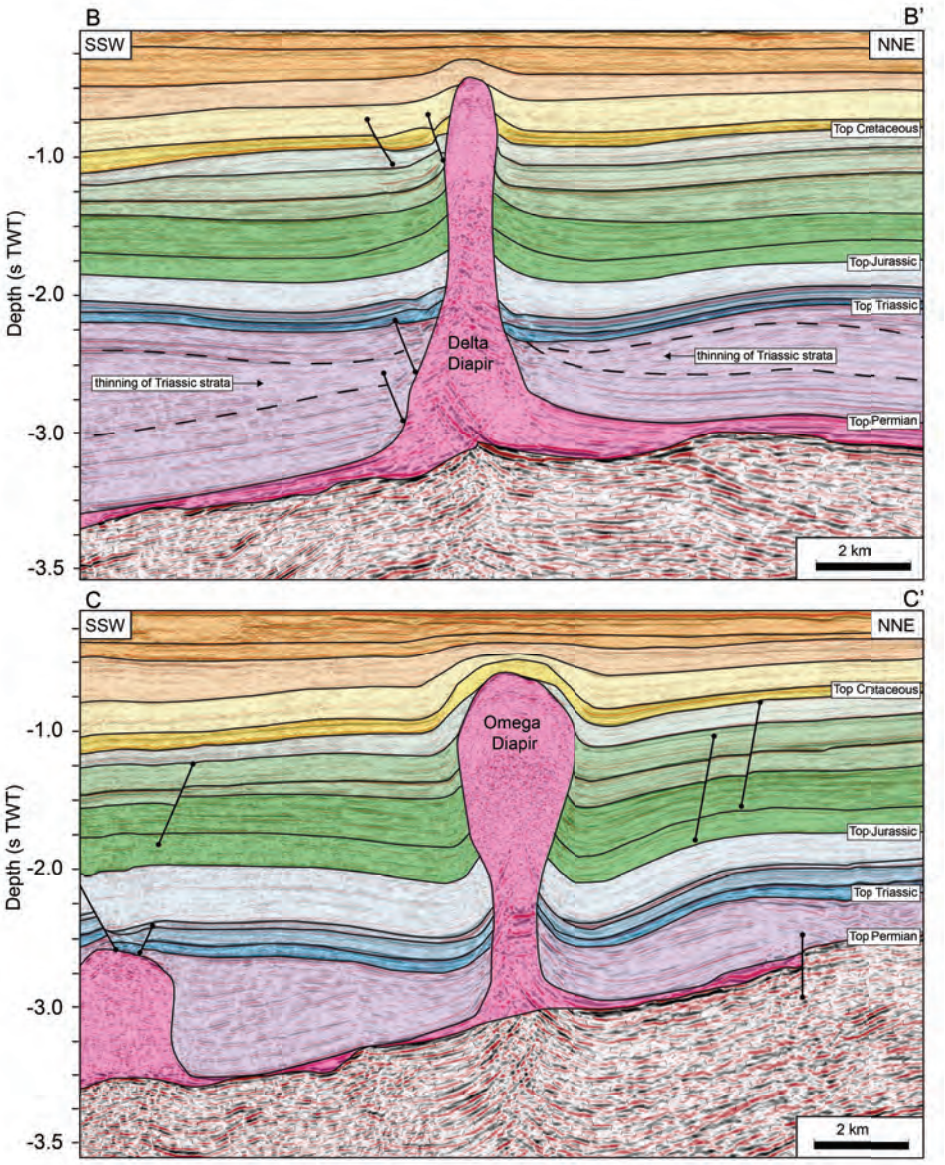

Fig. 6. Seismic profiles showing a cross section of the Delta and Omega diapirs perpendicular and parallel to strike of the studied supra-salt fault array, illustrating the graben configuration and stratigraphic sequences affected by growth of the fault array and salt stocks.

5. Geometry and kinematics of the supra-salt fault array

The studied supra-salt fault array trends SE, parallel to the underlying salt walls. The fault array is 36 km long and up to 7.5 km wide, and consists of a series of NE- and SW-dipping normal fault segments with throws up to 1190 ms TWT (2180 m; Figs. 7 and 8b). Individual fault segments are soft-linked or hard-linked, separated by breached or unbreached relay zones (Fig. 7a-f). Some faults bifurcate along strike and bound narrow fault lenses of host rock. The fault array on the NW side of the Delta Diapir, and between the Delta Diapir and the Omega Diapir, form the boundaries to relatively asymmetric half-grabens. Individual fault segments are up to 16 km long, slightly cuspate and convex-into-the-footwall in map-view; immediately adjacent (<2 km) to the salt stocks, however, fault strike abruptly changes by c. 90° and the faults terminate at c. 90° to the stock-sediment interface (Fig. 7a-f). In cross-section, the faults are relatively planar, although their dip locally decreases towards their lower tips as they approach and ultimately detach in the salt (Fig. 8b).

5.1. Graben-bounding faults: geometry and throw distribution

In this section we describe three of the major graben-bounding faults that display geometric features and growth histories characteristic of the three stages of fault growth we later define (F1, F2 and F7). The geometry and kinematics of some minor antithetic faults will also be briefly described in section 5.1.4.

Fault - F1

F1 is 16 km long and is laterally pinned between the Sele High Fault System in the NW and the Delta Diapir in the SE (Fig. 7). F1 strikes WNW-ESE, dips to the NNE and is mainly salt-detached, although locally, to the NW, the fault cross-cuts the salt and extends down into the pre-salt succession (Fig. 8). The faults upper tip is located within the Upper Cretaceous (Turonian-Danian; SU9-SU11) succession to the NW and the Eocene (Selandian-Lutetian; SU12) succession to the SE (Fig. 8a-c). Maximum throw (1190 ms TWT; 2180 m) is located near the fault centre, near the top of the Upper Triassic (SU1) (Fig. 8b). On T-x profiles for the lower, Triassic to Upper Jurassic units

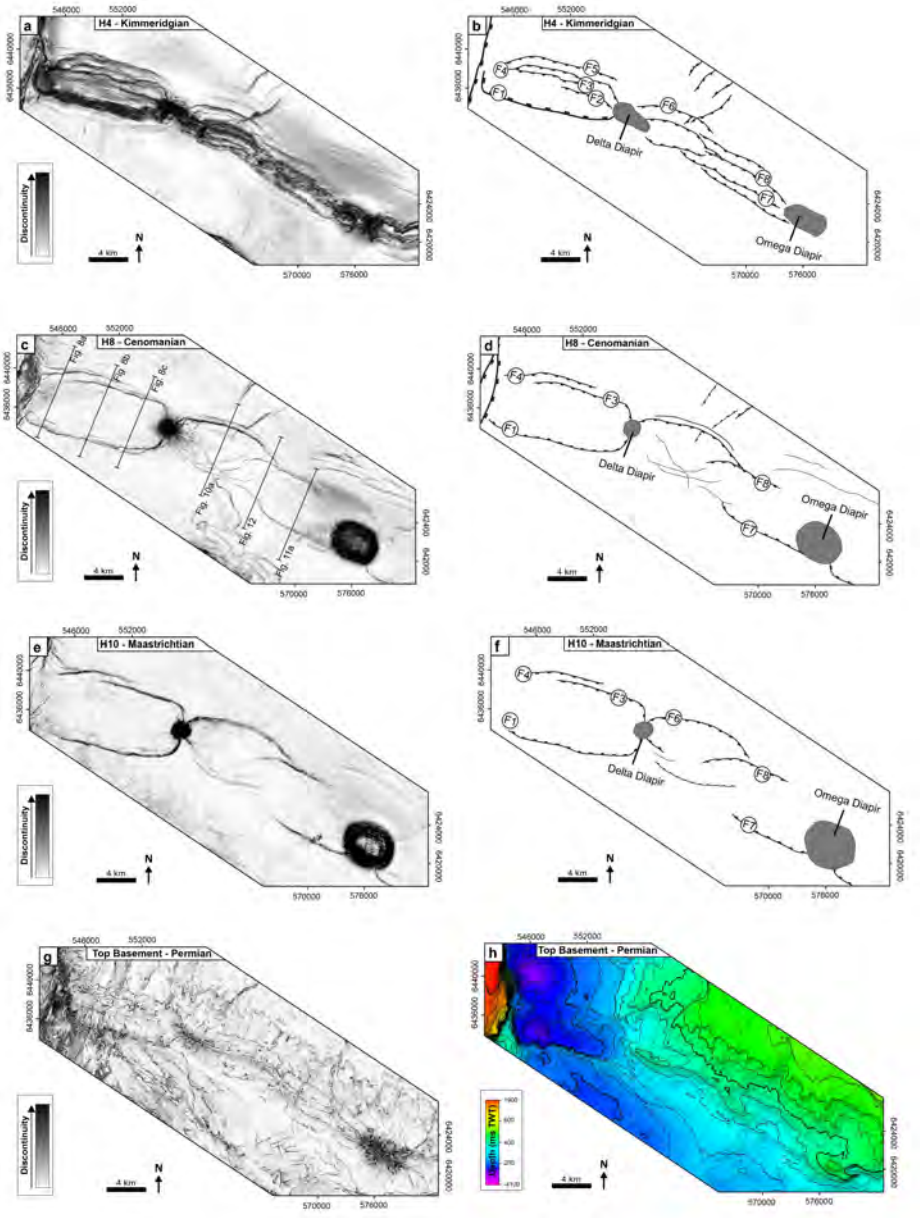

Fig. 7. Simplified maps of fault patterns based on fault interpretations and coherence discontinuities in the horizontal continuity of amplitude of the seismic (variance maps) for; (a) and (b) H4-Kimmeridgian; (c) and (d) Cover faults at H8 –Cenomanian level; (e) and (f) the cover fault array at H10 – Maastrichtian level. (g) Variance map of top Pre-salt. (h) Time structure-map of top basement. Locations of later seismic sections are included in Fig. 7c.

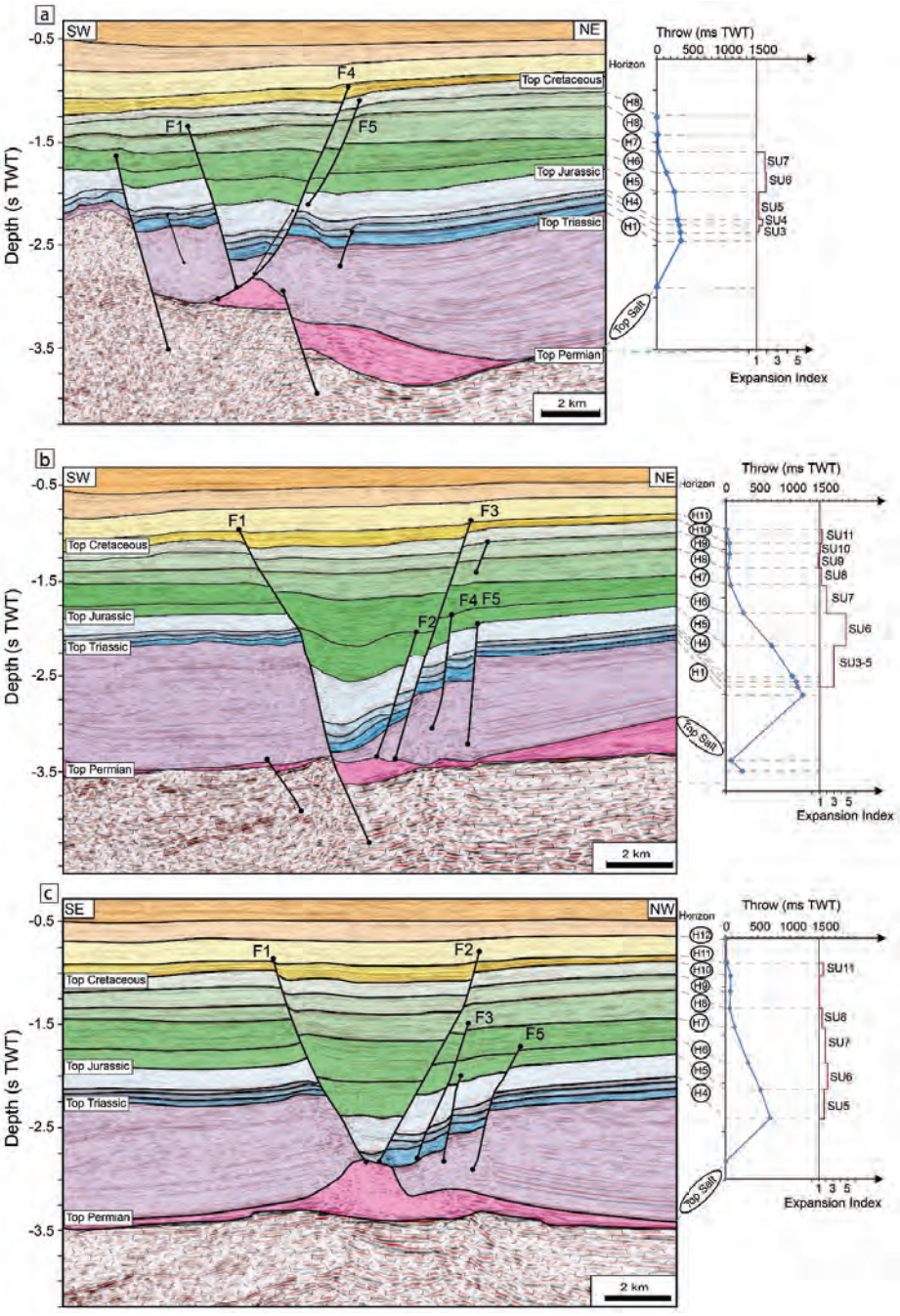
a
SW
NE
Depth (s TWT)
-0.5
-1.5
-2.5
-3.5
F1
F4
F5
Top Cretaceous
Top Jurassic
Top Triassic
Top Permian
2 km
Throw (ms TWT)
0 500 1000 1500
Horizon
H8
H8
H7
H6
H5
H4
H1
Top Salt
SU7
SU6
SU5
SU4
SU3
1 3 5
Expansion Index
b
SW
NE
F1
F3
F2
F4 F5
Top Cretaceous
Top Jurassic
Top Triassic
Top Permian
2 km
Throw (ms TWT)
0 500 1000 1500
Horizon
H11
H10
H9
H8
H7
H6
H5
H4
H1
Top Salt
SU11
SU10
SU9
SU8
SU7
SU6
SU3-5
1 3 5
Expansion Index
c
SE
NW
F1
F2
F3
F5
Top Cretaceous
Top Jurassic
Top Triassic
Top Permian
2 km
Throw (ms TWT)
0 500 1000 1500
Horizon
H12
H11
H10
H9
H8
H7
H6
H5
H4
Top Salt
SU11
SU8
SU7
SU6
SU5
1 3 5
Expansion Index

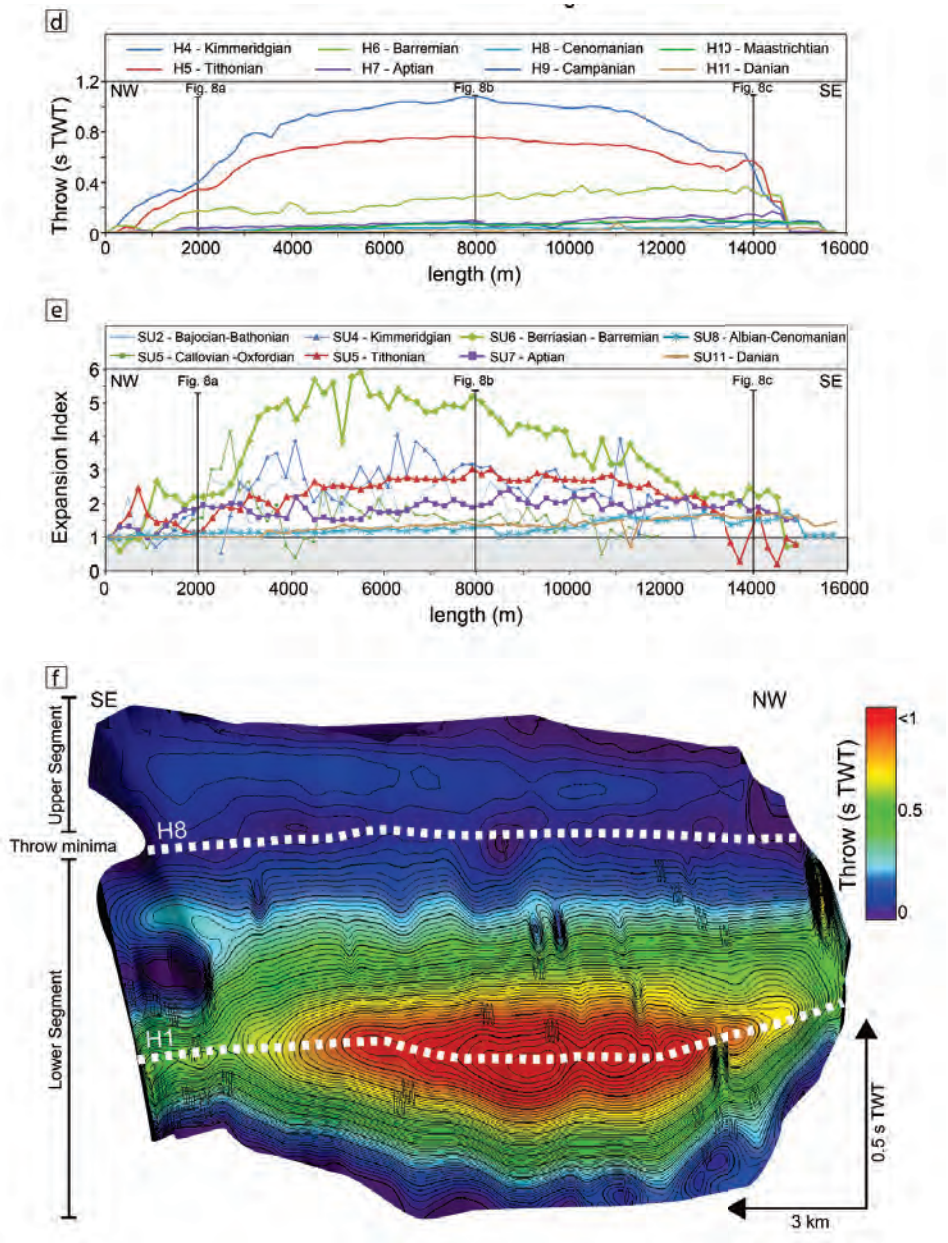

Fig. 8. (a-c) Seismic profiles illustrating the geometry of the fault F1, including T-z profiles and corresponding expansion indices. *T-z* plot shows an asymmetric, upward truncated vertical-throw profile where the maximum throw is at the transition between SU1 and SU2. (d) Throw-Distance plot illustrating the lateral variation in throw along strike of F1 for individual seismic units. (e) Expansion indices along strike of F1, indicating that the fault length was established during deposition of SU5 (Tithonian). (f) Throw strike-projections of F1 illustrating the three-dimensional throw distribution.

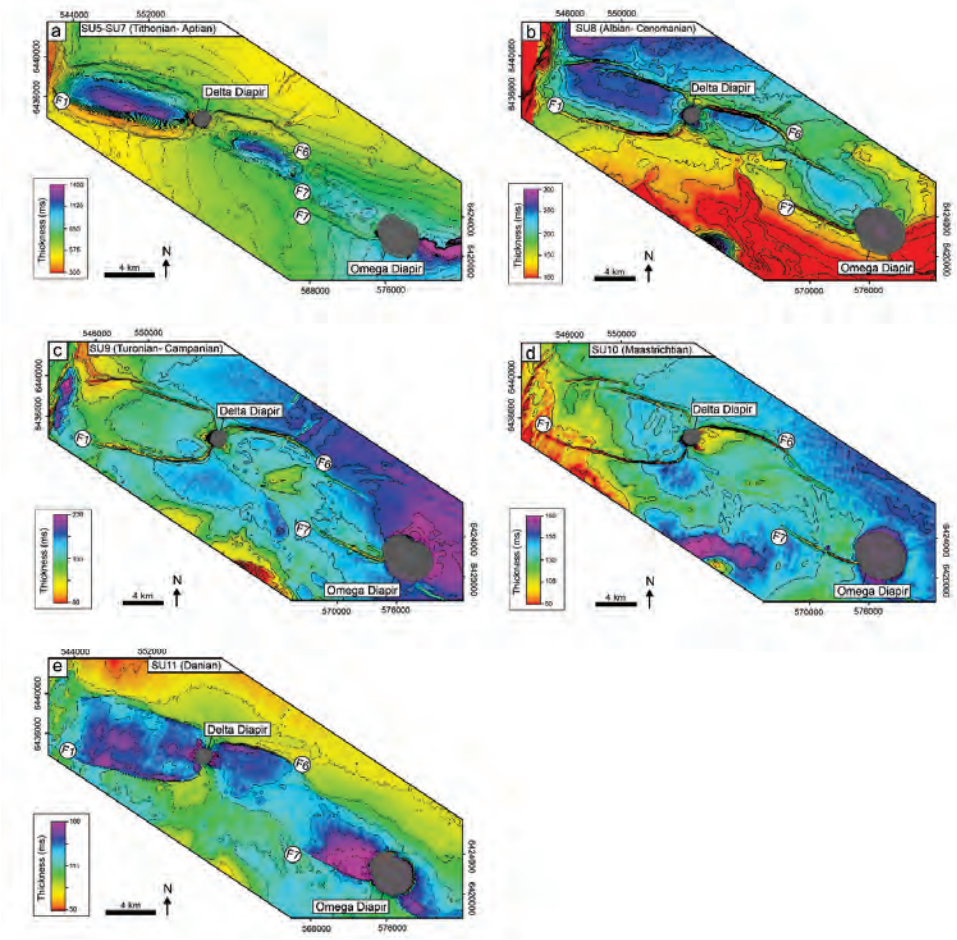

Fig. 9. Isochron maps of; (a) SU5-SU7 (Tithonian-Aptian), (b) SU8 (Albian-Cenomanian), (c) SU9 (Turonian-Campanian), (d) SU10 Maastrichtian and (e) SU11 (Danian) illustrating depocentre locations and fault growth.

(H1-H5), throw decreases relatively symmetrically away from the location of maximum throw, with high throw gradients occurring towards both lateral tips (e.g. up to 0.3 and 0.6 to the NW and SE, respectively, at the stratigraphic depth of H5; Fig. 8d). We also note that individual throw maxima for the upper units (Cretaceous; H6-H10) are located progressively closer to the Delta Diapir (Fig. 8d).

The T-z profile and throw strike-projections for F1 show an asymmetric vertical throw distribution characterised by two throw maxima: a lower maximum (1190 ms TWT; 2180 m) located near the top of the Triassic (SU1) and a minor upper maximum (63 ms TWT; 78 m) located near the top of the Maastrichtian (SU10) (Fig. 8b, c and f). The lower segment of the T-z plot, which contains the lower throw maximum, is characterised by high throw gradients (1.6) below the throw maximum towards the lower salt-confined tip. Relatively high throw gradients (1.0) also characterise the part of the fault surface located between the lower throw maximum and the top of the Albian-Cenomanian succession (SU8). From the Turonian (SU8) towards the top of the Campanian (SU9), throw decreases gradually upwards to the throw minimum separating the lower and upper maxima. Throw then increases upwards to the second throw maximum located near the top of the Maastrichtian (SU10); from here upwards towards the upper fault tip, throw gently decreases (gradient of 0.13).

Throw gradients are positively correlated with expansion indices (i.e. high throw gradients correlate with units characterised by large expansion indices; Fig. 8a-c). Furthermore, isochron maps confirm that across-fault stratal expansion occurs in the Aalenian-Cenomanian succession (SU2-SU8), indicating that F1 was active during deposition of these units (Fig. 8a-c and e). Across-fault expansion of relatively old growth strata (i.e. Bajocian-Tithonian; SU2-SU5; Fig. 8a,c and e) immediately inboard of the present lateral fault tips indicates that the early fault-controlled depocentre was nearly as long as the present length of F1; this indicates that the fault had established its length early, during deposition in the Tithonian (SU5) (cf. Walsh et al., 2002; Childs et al., 2003; Jackson and Rotevatn, 2013). The greatest across-fault stratal expansion (EI=3) occurs in the Tithonian-Aptian, suggesting this is the period when the fault was most active (SU5-SU7; Fig. 9a). No across-fault expansion (EI=1) occurs in the Turonian-Campanian (SU9), which we interpret to document a period of relatively minor fault activity. A subsequent period of syn-depositional faulting is recorded by across-fault expansion of the Danian (SU11) (EI=1.38) interval (Figs. 8b-c and 9c-e).

Fault - F6

F6 is 12 km long, dips to the SSW, strikes ESE-WNW and is pinned to the NW by the Delta Diapir (Fig. 7). F6 detaches downward into salt and its upper fault tip is located within the Eocene (Selandian-Lutetian) succession (SU12; Fig. 10a). Maximum throw (653 ms TWT; 1052 m) is located near the fault centre, near the top of the Tithonian (SU5) (Fig. 10a). At the stratigraphic depth of SU5, throw gradients towards the lateral tips are broadly similar, although lateral throw gradients are higher towards the NW and the Delta Diapir, than towards the SE (e.g. H4 and H5; Fig. 10c). In a similar manner to that observed for F1, individual throw maxima for the overlying Cretaceous and Palaeogene units (H6-H12) are located progressively closer to the Delta Diapir for F6 (Fig. 10c).

The vertical distribution of throw on F6 is broadly similar to that of F1. Overall, two zones of high throw are observed in the Tithonian (SU5) and Maastrichtian (SU10), with these being separated by a throw minimum in the Turonian-Campanian succession (SU9) (Fig. 10a-b). The stratigraphic depth of maximum throw is slightly shallower on F6 (near top Tithonian) than on F1 (near top Triassic) (Figs. 8a-c, e and 10a-b). SU1-SU3 (Triassic-Oxfordian) are however not present in the hangingwall of the fault, possibly due to tectonic thinning of the roof of the salt wall or no deposition here as a result of erosion of the lower most units as the salt was rising. The lower segment of the T-z plot, which contains the lower throw maximum (653 ms TWT; 1052 m), is characterised by high throw gradients away from this point of maximum throw, both downwards towards the lower salt-confined fault tip (0.78) and upwards towards the top of the Turonian-Campanian succession (SU9) (0.57) where the throw minimum occurs (Fig. 10a). From the throw minimum upward, throw steadily increases to the upper throw maxima (117 ms TWT; 134 m), and from here upwards towards the upper fault tip, which is located within the Selandian-Lutetian succession (SU12), throw decreases gently (gradient of 0.32).

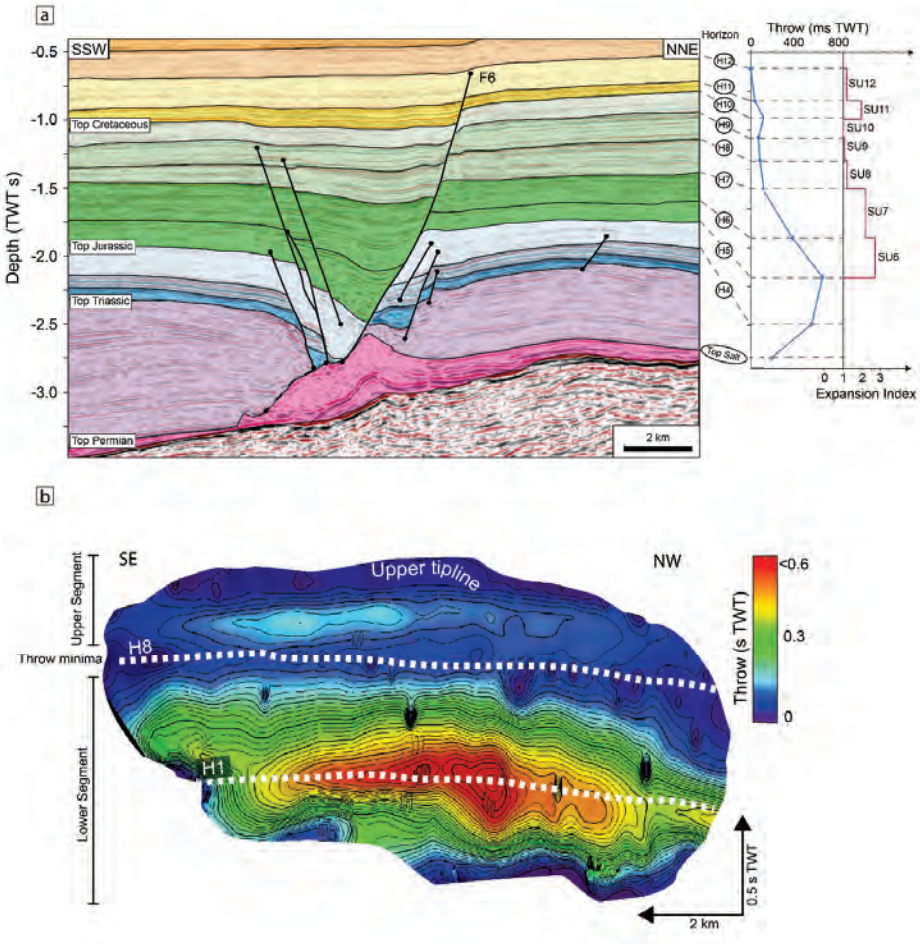
a
SSW
NNE
F6
Top Cretaceous
Top Jurassic
Top Triassic
Top Permian
Depth (TWT s)
-0.5
-1.0
-1.5
-2.0
-2.5
-3.0
2 km
Horizon
Throw (ms TWT)
0
400
800
H12
H11
H10
H9
H8
H7
H6
H5
H4
Top Salt
SU12
SU11
SU10
SU9
SU8
SU7
SU6
0 1 2 3
Expansion Index
b
SE
NW
Upper tipline
Upper Segment
Throw minima
H8
H1
Lower Segment
<0.6
0.3
0
Throw (s TWT)
0.5 s TWT
2 km

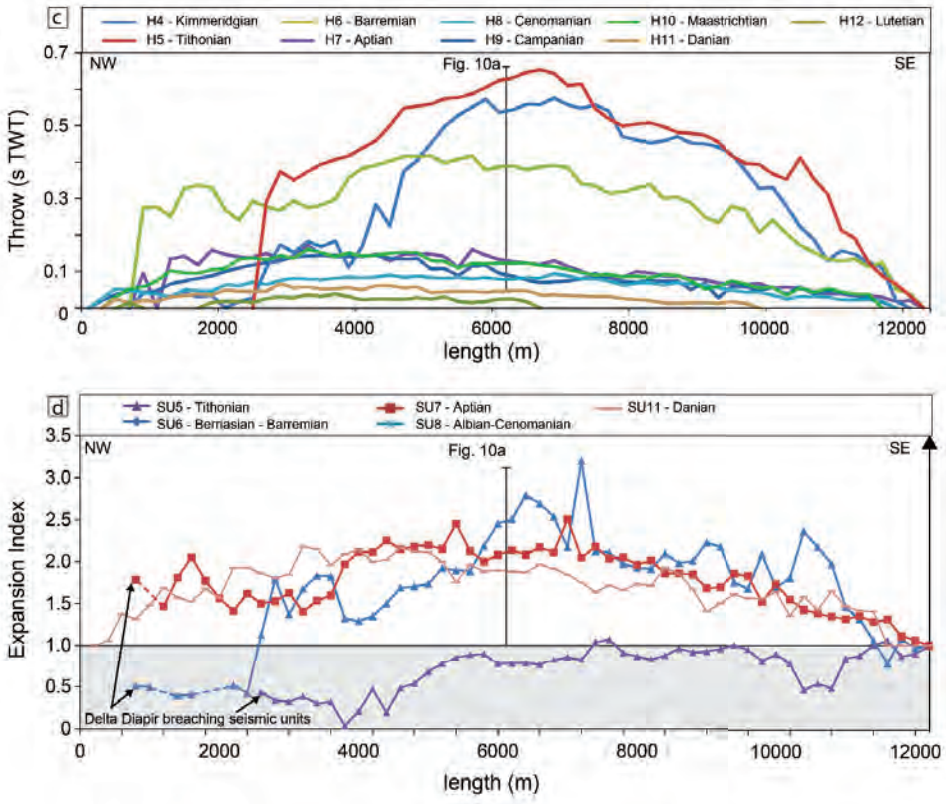

Fig. 10. (a) Seismic profiles illustrating the geometries of fault F6, with corresponding T-z profile and expansion index plot. (b) Throw strike-projections of F6 illustrating the three-dimensional throw distribution. (c) Throw-Distance plot illustrating the lateral variation in throw along strike of F6 for individual seismic units. (d) Expansion Indices along strike of F6, indicating that the fault length was established during deposition of SU6 – SU7 (Berriasian-Aptian).

As observed for F1, throw gradients on F6 are positively correlated with expansion indices. Expansion indices and isochron maps indicate that F6 broke surface during deposition of the Berriasian-Barremian succession (SU6) (EI=2.7; Fig. 10a). Expansion indices of >1.3 in the Berriasian-Barremian succession (SU6), immediately inboard of the lateral fault tips (Fig. 10d) suggest that the depocentre was nearly as long as the present length of F6, again demonstrating that the fault had established its near-full length early in its history, during the Berriasian-Barremian. Greatest across-fault stratal expansion occurs within the Berriasian-Aptian succession (SU6-SU7; EI=2.7-

2.2), thus we interpret this was a time of significant displacement accumulation. Minor across-fault stratal expansion characterises the Albian-Cenomanian succession (SU8) (EI=1.2), likely signifying a time of relatively minor fault activity and displacement accumulation. We interpret that interval characterized by relatively low across-fault expansion (SU9-10; Turonian-Maastrichtian) documents a period of relatively minor fault activity. Increased across-fault expansion of the Danian succession (SU11) (EI=2.0) is signifying a subsequent period of more significant displacement (Fig. 9e and 10a). The Upper Eocene-Middle Miocene succession (SU13) increases in thickness into the synclinal flexure developed on the hangingwall side of F6 (Fig. 10a); this observation suggests the fault grew by blind propagation during the Late Eocene-Middle Miocene, and since then, has been inactive.

Fault - F7

F7 is 16 km long, dips to the NNE and strikes WNW-ESE. F7 detaches downward into salt and is bound by the Omega Diapir to the SE (Figs. 7 and 11a). On the NW side of the salt culmination between the Delta Diapir and the Omega Diapir (Fig. 6a), the upper tip of F7 is located within the Lower Cretaceous (Berriasian-Barremian) succession (SU6), whereas on the SE side it is mainly located within the Eocene (Selandian-Lutetian) succession (SU12 or SU13; Fig. 11a-b). Maximum fault throw (414 ms TWT; 695 m) is observed at the centre of the fault near the top of the Tithonian (SU5; Fig. 11a; cf. F6). T-x profiles for F7 are relatively asymmetric at all stratigraphic levels. Furthermore, these profiles indicate that F7, on the NW side of the salt culmination between the Delta and Omega diapirs, only offsets the Kimmeridgian-Tithonian (SU4-SU5), whereas, on the SW side, it offsets strata as young as Salandian-Lutestian (SU12) (Fig. 11b). T-x profiles for H4 and H5 show higher lateral throw gradients towards the tip located adjacent to the Omega Diapir (0.51 and 1.05 respectively), whereas lower throw gradients occur towards the NW (0.15 and 0.9 respectively) (Fig. 11b). Individual throw maxima for the Cretaceous and Palaeogene units (H6-H12) are located progressively closer to the Omega Diapir (Fig. 11b; cf. F1 and F6; Figs. 8d and 10c).

T-z profiles for F7 show the same characteristics as for other supra-salt faults located further to the NW (e.g. F1 and F6; Figs. 8 and 10), with an asymmetric vertical throw distribution characterised by two throw maxima: a lower maximum (414 ms TWT; 695 m) located near the top of the Tithonian succession (SU5) and a more subtle, upper maximum (63 ms TWT; 78 m) located near the top of the Maastrichtian succession (SU10) (Fig. 11a). The lower segment of the T-z plot, which contains the lower throw maximum, is characterised by low throw gradients away from the throw maximum downwards towards the lower salt-confined fault tip (0.2), and upwards from the throw maximum towards the top of the Berriasian-Cenomanian succession (SU8) (0.4). From the top of the Berriasian-Cenomanian succession (SU8) towards the top of the Maastrichtian succession (SU10), throw increases gradually (0.1) upwards to the second throw maximum; from here upwards towards the upper fault tip within the Danian succession (SU11), throw decreases by a throw gradient of 0.4 (Fig. 11a).

Expansion indices and isochron maps indicate that F7 broke surface during deposition of the Berriasian-Barremian succession (SU6). Expansion indices for SU6 are >>1 immediately inboard of the present lateral fault tips (Fig. 11c), suggesting F7 established its near-full length early in its history, by Berriasian-Barremian times. Expansion indices and isochron maps indicate F7 was active during the Berriasian-Cenomanian (SU6-SU8), was inactive during the Turonian-Maastrichtian (SU9 and SU10; Fig. 11a), and was reactivated during deposition of SU11 (Danian) (Fig. 9 and 11a).

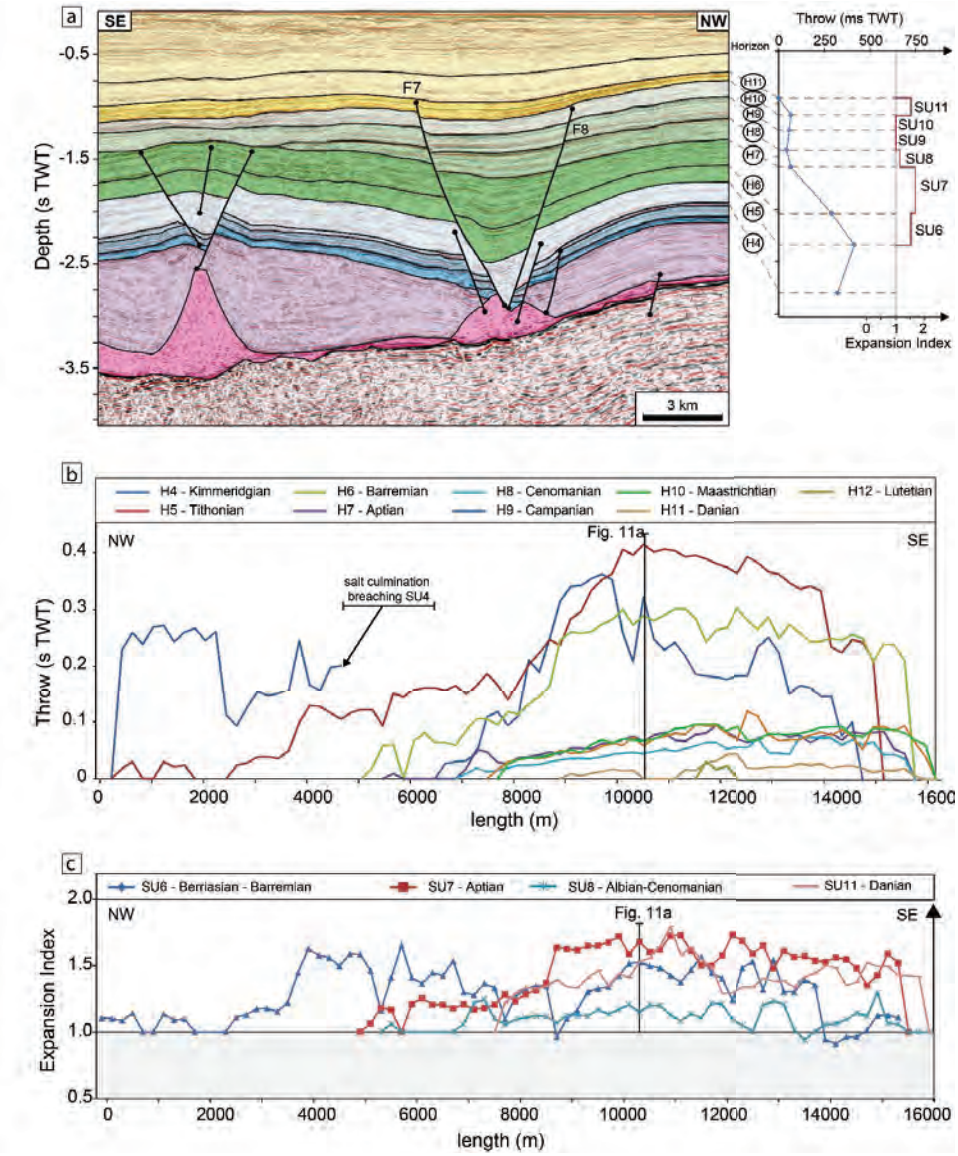

Fig. 11. (a) Seismic profile showing the F7 with corresponding T-z diagram and expansion index plot. (b) Throw-Distance plot illustrating the lateral variation in throw along strike of F7 for individual seismic units. (c) Expansion Indices along strike of F7, indicating that the fault length was established during deposition of SU6 (Berriasian-Barremian).

5.2. Secondary faults

Even though the large faults described above accommodated much of the strain associated with growth history of the supra-salt fault array, we feel it is necessary to at least briefly describe the structural style and kinematics of smaller, 'secondary' faults if we are to fully understand the whole growth history of the fault array. These faults strike broadly parallel to the large faults (i.e. WNW-ESE) and underlying salt walls, have up to 478 ms TWT (c. 800 m) throw and are up to 11 km long (e.g. F2-F5 and F8; Figs. 7, 8a-c, 11a, 12 and 13). Many of these faults are antithetic to the large faults, with maximum throw occurring at various stratigraphic levels (e.g. near the top of SU1 for F5, near the top of SU4 for F3, and near the top of SU5 for F2 and F9; Figs. 8 a-c, 12 and 13). These secondary faults are mainly progressively younger towards the crest of the salt walls (Figs. 12 and 13). Furthermore, whereas almost all secondary faults have their lower tips near the top of the salt, their upper tips lie at various stratigraphic levels, from as deep as the Tithonian (SU5; e.g. F11 in Fig. 12) to as shallow as the Upper Eocene-Lower Miocene succession (SU13; e.g. F8 in Fig. 12). Isochron maps and expansion indices indicate that the secondary faults initiated after and are thus slightly younger than F1, F6 and F7 (i.e. F5 formed during deposition of SU2, and F2 during deposition of SU6; Fig. 13).

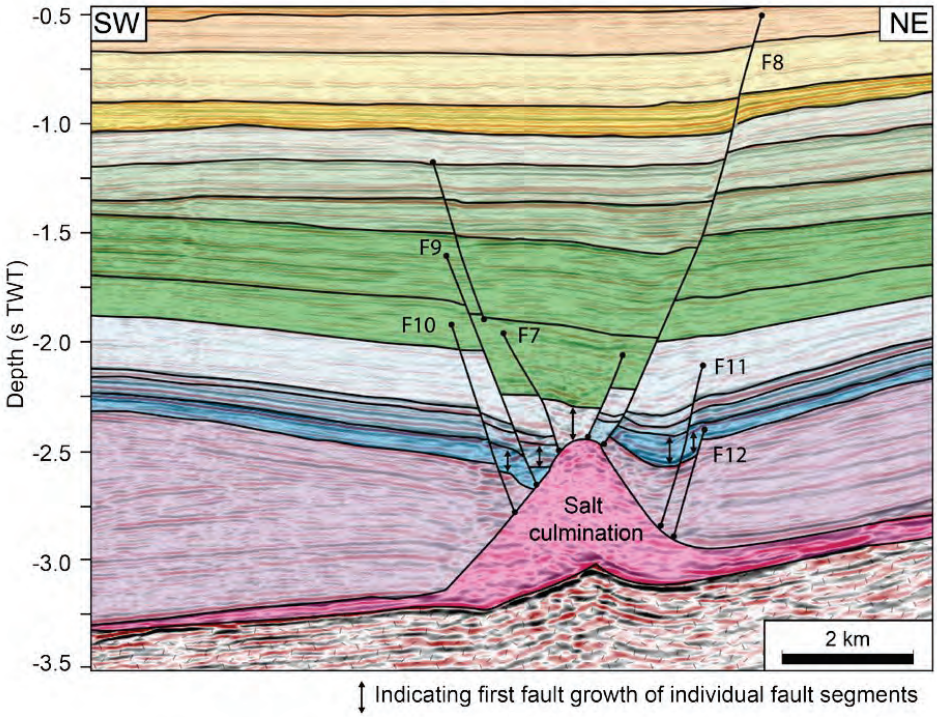

Fig. 12. Seismic profile perpendicular to strike of the fault array, crossing the salt culmination between the Delta and Omega diapirs, showing the geometries of Faults F7-F12. Arrows are indicating first seismic units showing fault related growth.

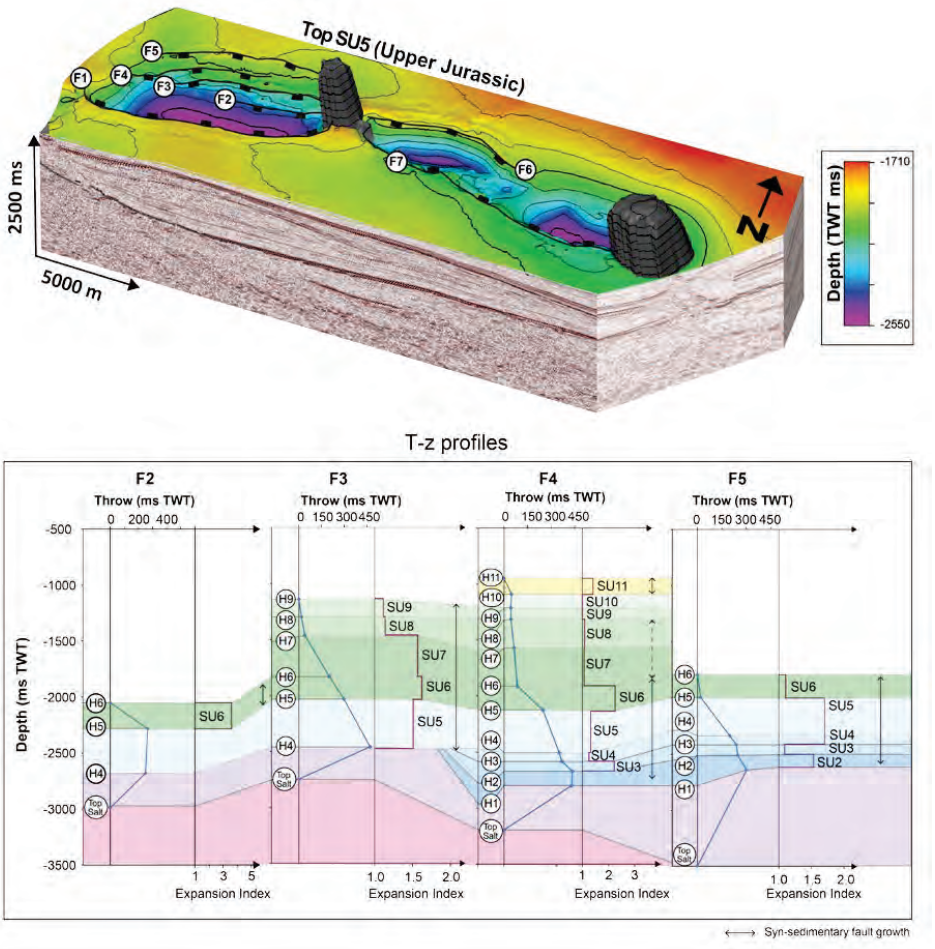

Fig. 13. Block diagram showing the fault array on top of SU5 (Tithonian) showing the map view geometries of faults and diapirs, with corresponding T-z profiles of smaller scale faults, F2-F5.

6. Growth of the supra-salt fault array; interpretation and discussion

By analysing salt body and fault geometry, fault throw patterns, and thickness variations in pre- and syn-kinematic strata, we here outline the trigger and driving mechanisms for, and growth history, of the supra-salt fault array described above. For each stage of salt-fault development, we begin by outlining the fault kinematics before focusing on how this relates to salt mobilisation and the growth of salt structures.

6.1. Initial fault growth, reactive diapirism and initial salt stock formation

6.1.1. Initial fault growth and fault length establishment

Based on T-z, T-x and EI plots, and thickness changes in syn-kinematic growth strata, we interpret that supra-salt fault initiation was strongly diachronous across the array, spanning the Late Triassic to Late Jurassic, and that the depth of fault nucleation varied. This interpretation is based on the following observations; (i) maximum throw occurs near the top Triassic (SU1) on F1 (Fig. 8b), suggesting this fault nucleated at this structural level. Across-fault thickening of immediately overlying Middle Jurassic strata suggest the fault nucleated in the very shallow subsurface and/or rapidly propagated upward to the free surface (Nicol et al., 1996; Baudon and Cartwright, 2008b; Jackson and Rotevatn, 2013; Tvedt et al., 2013); (ii) maximum throw on F6 and F7 occurs near the top of the Upper Jurassic succession (SU5), suggesting that these faults nucleated at this structural level (Figs. 10a and 11a). High throw gradients above the point of maximum throw (SU5 for both F6 and F7), and across-fault thickening of immediately overlying Lower Cretaceous strata into the early formed depocentres suggest the faults nucleated in the very shallow subsurface and/or rapidly propagated upward to the free surface (Figs. 9a, 10 and 11). Shallower and later nucleation of F6 and F7 compared to F1 further suggest the fault array nucleated earlier on the NW than the SE side of the Delta Diapir; and (iii) T-z profiles and expansion indices for the secondary faults indicate they nucleated at broadly the same time as the larger faults (i.e. Middle Jurassic to earliest Cretaceous), but at shallower stratigraphic levels towards the central parts of the graben and near the crests of the salt walls (e.g. F2-F5 and F8-F12; Fig. 8a-c, Fig. 12 and 13). Lower Jurassic strata are only locally preserved in the Egersund Basin due to the erosion related to growth of the Mid-North-Sea Dome, thereby making it difficult to determine how the faults evolved during the Early Jurassic.

Isochron maps and expansion indices suggest F1 had established its near-full length by the Tithonian (SU5), c. 21 Myr after its initiation, which equates to only 19% of its total c. 112 Myr slip history (Fig. 8d and 9a). F6 and F7 had established their near-full lengths by the Berriasian–Barremian (SU6), c. 20 Myr after they initiated, which

equates to c. 19% of their total c. 104 Myr slip history (Figs. 10d and 11c). The faults thus established their full lengths early in their growth history before progressively accumulating displacement (Figs. 8, 10 and 11) (cf. Walsh et al., 2002; Giba et al., 2012). Based on this observation, we elect to use the 'original method' of Chapman and Meneilly (1991) and Petersen et al. (1992) rather than the 'vertical throw subtraction method' of Dutton and Trudgill (2009) for throw backstripping and to analyse the kinematic history of the fault array in greater detail (Fig. 14) (see Jackson et al., in review). Our analysis indicates that F1 had attained c. 75% of its final length by the end of the Bathonian (SU2) (Fig. 14a) and its near-full length by the Tithonian; Likewise, F6 lengthened rapidly before accumulating displacement, attaining c. 79% of its final length by the end of the Barremian (SU6), with its near-full length established by the end of the Aptian (SU7) (Fig. 14b).

We suggest that lateral propagation of the fault array was impeded by intrabasin heterogeneities, which drove the switch to fault growth by displacement accumulation. The north-western part of the fault array terminates at the Sele High Fault System, which was active during the Triassic and Jurassic, and which became inactive during the Cretaceous (Jackson and Lewis, 2016). North-westwards termination of the supra-salt fault array at the Sele High Fault System suggest the latter was likely present before and thus may have restricted the north-westwards propagation of the former (Figs. 2a and 7). Expansion indices and isochron maps (Figs. 8e and 9a) indicate that the fault array established its full length relatively early in its development during the Late Jurassic and, therefore, that its lateral fault tip was located near the Sele High Fault System at this time (SU5). The significant (c. 90°) and abrupt change in fault strike immediately adjacent to the Delta and Omega diapirs (Fig. 7, 8, 9 and 10) suggests these structures were present, at least in an embryonic form, and forming lateral barriers to fault propagation and strike during the earliest stages of fault growth.

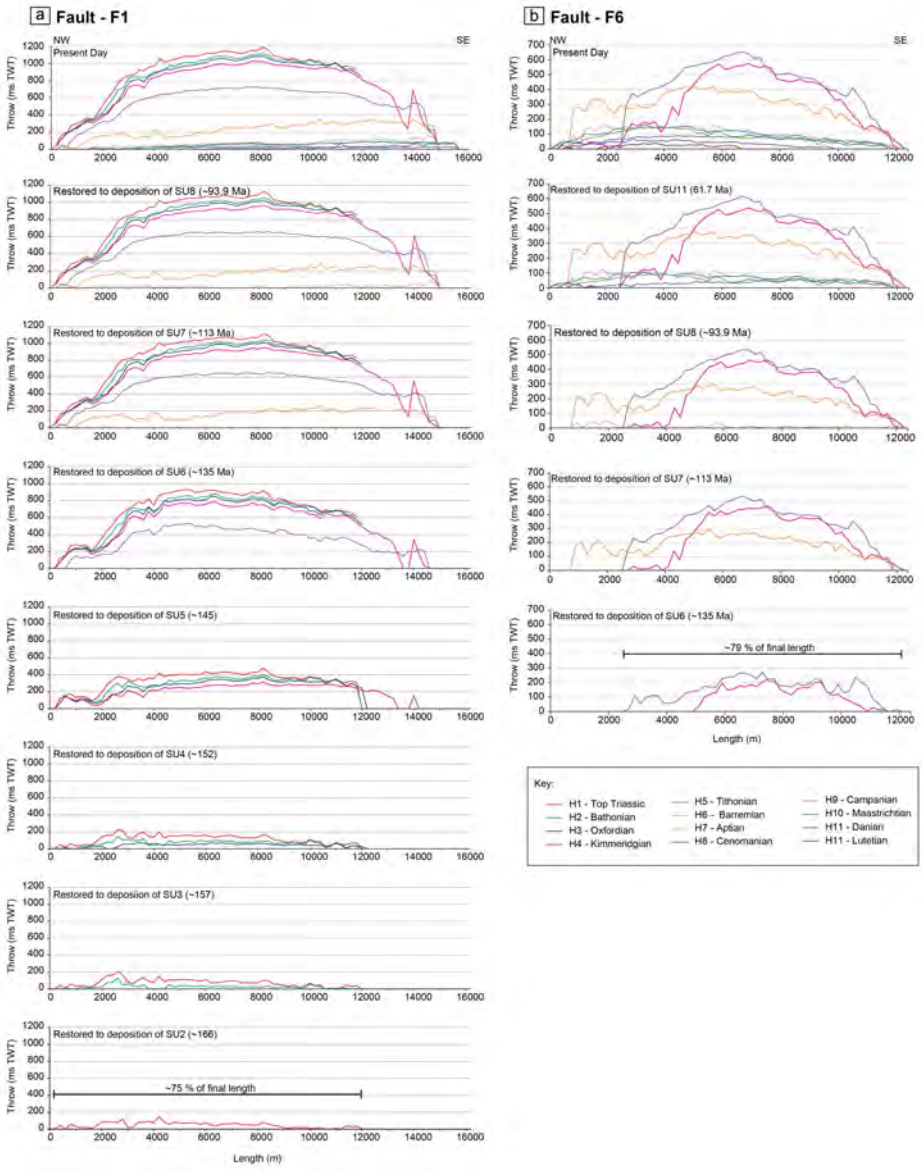

Fig. 14. Throw backstripping of the F1 (a) and F6 (b), illustrating early fault establishment. Note that H1, H2 and H3 cannot be mapped SE of c. 12000 m for F1, due to poor seismic imaging below the overhanging diapir flank.

6.1.2. Reactive rise and early stock nucleation

Having established that initial fault nucleation occurred in the Late Triassic to Late Jurassic, we here turn our attention to the impact this had on salt mobilisation and how this impacted further fault growth. We suggest that supra-salt faulting in the Late Triassic caused the initial reactive rise of salt in the form of rollers, which eventually grew to form salt walls (Fig. 15 and 16a). Our kinematic analysis (Figs. 10 and 11) indicate that faults initiated slightly later to the SE of the Delta Diapir than to the NW, and that reactive rise of the diapirs occurred until at least the Early Cretaceous, as indicated by the younging of faults towards the salt wall crest (Figs. 12, 15 and 16).

Younging of faults towards the salt wall crest (e.g. F1 and F2-F5; Fig. 8, and F7-F12; Fig. 12) suggest salt rose in response to reactive diapirism (Vendeville and Jackson, 1992b). This interpretation is further supported by the fact that F1, and F6 and F7 were surface-breaking growth faults during the Late Triassic-Late Jurassic (Fig. 8) and Late Jurassic (Figs. 10 and 11) respectively, which was coeval with regional thick-skinned

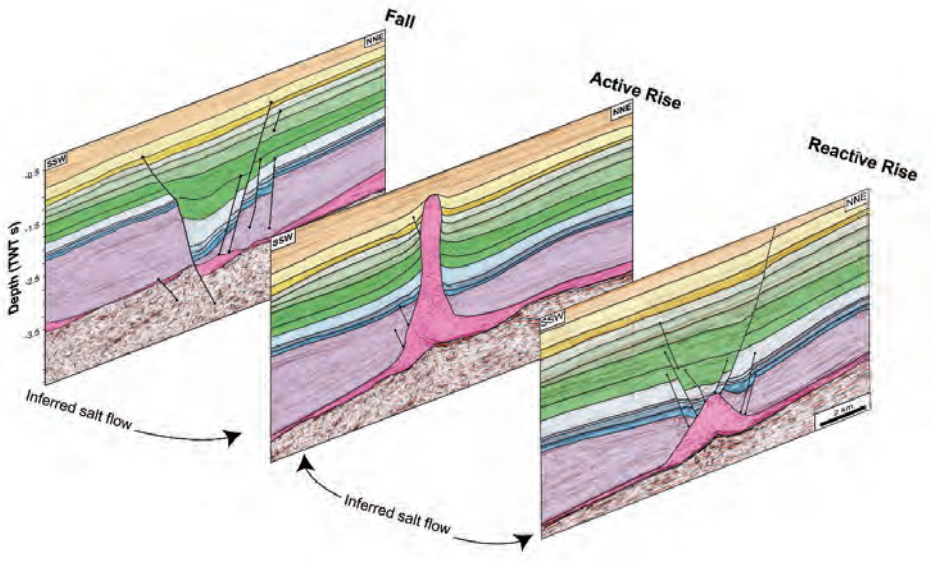

Fig. 15. Seismic profiles illustrating how different parts of the fault array reflect different stages of the growth history where reactive diapiric rise, collapse and active rise of salt have occurred simultaneously along strike, showing similarities with Vendeville and Jacksons (1992a) physical models.

extension (Sørensen et al., 1992; Vendeville and Jackson, 1992b; Jackson and Vendeville, 1994). Progressively younger faults occur towards the central part of the salt wall near the salt culmination between the Delta and Omega diapirs (Fig. 12). We interpret that the broadly triangular salt wall profile observed beneath F6 and F7 (Figs. 11a, 12a) and above the salt culmination between the Delta and Omega diapirs (Figs. 12 and 15), represent remnants of reactive diapirs, the geometries of which were modified during subsequent diapir extensional collapse (Vendeville and Jackson, 1992b; Mauduit and Brun, 1998) (see also section 6.2.2).

The physical models of Ge et al. (1995) show that reactive diapirs are capable of restricting lateral growth of supra-salt faults and causing a local change in fault strike near the salt-sediment interface (Y-shaped splay), the latter likely reflecting near-diapir stress perturbations. We observe similar salt-fault relationships in the Egersund Basin, with Kimmeridgian faults changing strike by c. 90° immediately adjacent to the Omega and Delta diapirs (Fig. 7a-b), suggesting these salt structures were present, at least in an immature form, and able to influence fault geometry and growth at this time. This observation also suggests that salt stock nucleation and initial inflation pre-date fault formation, explaining why the fault tips were pinned laterally at an early stage and why subsequently growth was thus primarily by displacement accrual. This is further supported by the observation that Middle-Upper Triassic strata are thin towards the Delta and Omega diapirs and the intervening salt walls (e.g. Fig. 6 and 12), suggesting early development of salt walls and stocks beneath the fault array.

6.2. Diapir collapse and continued fault growth

6.2.1. Continued fault growth and displacement accumulation

Expansion indices and isochron maps indicate that F1, F6 and F7 were most active during the latest Jurassic (Tithonian) to Early Cretaceous (Aptian) (SU5-SU7; Figs.9a). As discussed in section 6.1.1, the faults established their near-full lengths relatively early in the Tithonian-Barremian; further fault growth was dominated by displacement accrual rather than lateral tip propagation. During the Late Jurassic to Early Cretaceous, the main depocentre associated with the fault array on the north-western side of the

Delta Diapir was located directly above the salt wall (SU5-SU7; Fig. 9a). Further to the SE, between the Omega and Delta diapirs, two depocentres were present at this time (SU5-SU7; Fig. 9a), separated by a low-relief salt culmination across which a relatively thin sedimentary succession accumulated (Fig. 5); these thickness patterns indicate that the salt culmination was already established during the Late Jurassic. The faults continued to accumulate displacement during the Albian-Cenomanian (SU8), with the associated depocentres becoming asymmetric due to strain focusing along the NE margin (Fig. 9b). During the Turonian-Maastrichtian, only minor fault activity occurred as indicated by low across-fault expansion index values in strata of this age (SU9 and SU10).

6.2.2. Salt wall collapse

Based on the limited lateral thickness variations of the Upper Triassic-Quaternary strata NE and SW of the fault array and underlying salt wall, we propose that salt was nearly welded in these areas during the Late Triassic (Fig. 6b-c). As described by Vendeville and Jackson (1992a), diapir collapse can occur when diapirs widen and salt flow is too slow to maintain the height of the diapir. We propose that limited salt supply, linked to welding to the NE and SW of the main wall, caused the wall to begin to collapse during the Latest Jurassic-Early Cretaceous. Our interpretation that the diapir began to collapse at this time is indicated by the increased thickness of Jurassic and Lower Cretaceous sediments in the half-grabens and by the development of a series of relatively open synclines that developed in Triassic (SU1), Jurassic (SU2-5) and lower Cretaceous (SU6-SU7; Berriasian-Aptian) strata preserved in the following three areas; (i) the area between the Sele High Fault System and the Delta Diapir; (ii) the area between the Delta Diapir and the salt culmination; and (iii) the area between the salt culmination and the Omega Diapir (Figs. 6a and 9a). Thickening of Upper Jurassic-Lower Cretaceous strata in the graben between the salt diapirs and the salt culmination indicate salt withdrawal occurred from below the central part of the graben during this time; because this salt could not easily flow northwards or southwards into the already welded areas, it is likely it flowed laterally into and contributed to inflation of the Delta and Omega diapirs (Fig. 6 and 16). The style of stock growth at this time is cryptic,

with the Delta and Omega diapirs either growing as active structures below a thin roof or as emergent passive diapirs. Salt evacuation caused further subsidence of the crestal graben in the Early Cretaceous (Fig. 15 and 16), especially on the NW side of the Delta Diapir (Figs. 8b and 16).

6.3. Fault decay and growth of salt stocks

6.3.1. Decay and death of the fault-array

We interpret that dip linkage played a role in the latter stages of growth of the supra-salt fault array, with this process being recorded by two zones of relatively high throw (and expansion indices; i.e. Late Triassic to Early Cretaceous and the Early Palaeocene; Figs. 8b, 11a and Fig. 10a) located on the upper and lower parts of the fault surface being separated by a zone of relatively low throw (and low expansion indices; i.e. Turonian-Maastrichtian) (cf. Watterson, 1986; Walsh and Watterson, 1988; Mansfield and Cartwright, 2001; Rykkelid and Fossen, 2002; Baudon and Cartwright, 2008b; Baudon and Cartwright, 2008a; Jackson and Rotevatn, 2013; Tvedt et al., 2013; Rotevatn and Jackson, 2014). This throw pattern suggests that an early formed fault that was active in the Late Triassic to Early Cretaceous became inactive in the Turonian-Maastrichtian, with further extension in the Danian (SU11; e.g. Figs 8, 9e and 11a) resulting in the formation of a fault in Upper Cretaceous strata, and downward propagation of this fault to link with the pre-existing, underlying segment.

The Danian succession (SU11) thickens across most of the largest faults in the array (Figs. 8b-c, 9e, 10a, 11a and 12), especially on the NW side of the Omega Diapir. These thickness changes document the last period of true syn-sedimentary fault growth and half-graben subsidence in the Egersund Basin (Fig. 9e). Fault activity waned shortly after this period of Danian reactivation, with the last phase of faulting during the Late Eocene being documented by blind fault propagation into the lower part of the Bartonian-Serravalian (SU13) (F8; Fig. 12).

6.3.2. Collapse of salt walls and growth of salt stocks

The Turonian to Maastrichtian succession (SU9-SU10) thins towards the Delta and Omega diapirs (Figs. 6 and 9), likely reflecting the rise of salt due to differential loading (Vendeville and Jackson, 1992b; Schultz-Ela et al., 1993), or simple buoyancy (active diapirism; Hudec and Jackson, 2007). Just along strike of the salt stocks, Danian (SU11) strata are thicker immediately adjacent to the Omega and Delta diapirs, reflecting growth of the major graben-bounding faults (e.g. F1, F6 and F7; Figs. 9 and 10). Given this temporal relationship between fault-driven subsidence due to ongoing salt wall collapse, and salt stock rise due to passive or active diapirism, we infer that salt was flowing along the salt wall into the rising stocks. Our T-x plots and isochron maps indicate that, during deposition of Upper Cretaceous to lower Palaeogene growth strata, the locus of maximum throw migrated towards the diapir. This may indicate that, during the Late Cretaceous to early Palaeogene, salt stocks were fed by salt sourced from progressively closer locations within the collapsing wall.

Danian (SU11) to lowermost upper Neogene strata (SU14) are arched above the Delta and Omega diapir crests (Fig. 6). Arching of the overburden above these diapirs could either be caused by regional shortening or active diapirism; in fact, regional shortening may have triggered active diapirism (Schultz-Ela et al., 1993; Davison et al., 2000b; Hudec and Jackson, 2007), and it is known that regional shortening and basin inversion occurred during the Turonian-Maastrichtian (Wilson et al., 2013), leading to the formation of the teardrop-shaped diapirs (Jackson and Lewis, 2012). However, the presence of folded Neogene strata clearly indicate that the Delta and Omega diapirs were active and rising after the main period of basin shortening. Hudec and Jackson (2011) propose that, where the arched roof thickness is >20% of the diapir height, arching most likely reflects regional shortening. In contrast, where roof thickness is <20%, roof arching may simply reflect active diapirism. Present arched overburden thickness above the Delta and Omega diapirs are 4% and 5% of the diapir heights, respectively (Table 2), suggesting arching may simply reflect active diapiric rise in the absence of regional shortening. Cessation of active diapir rise during the Neogene likely reflect exhaustion of the source layer, perhaps due to welding (Ge et al., 1995).

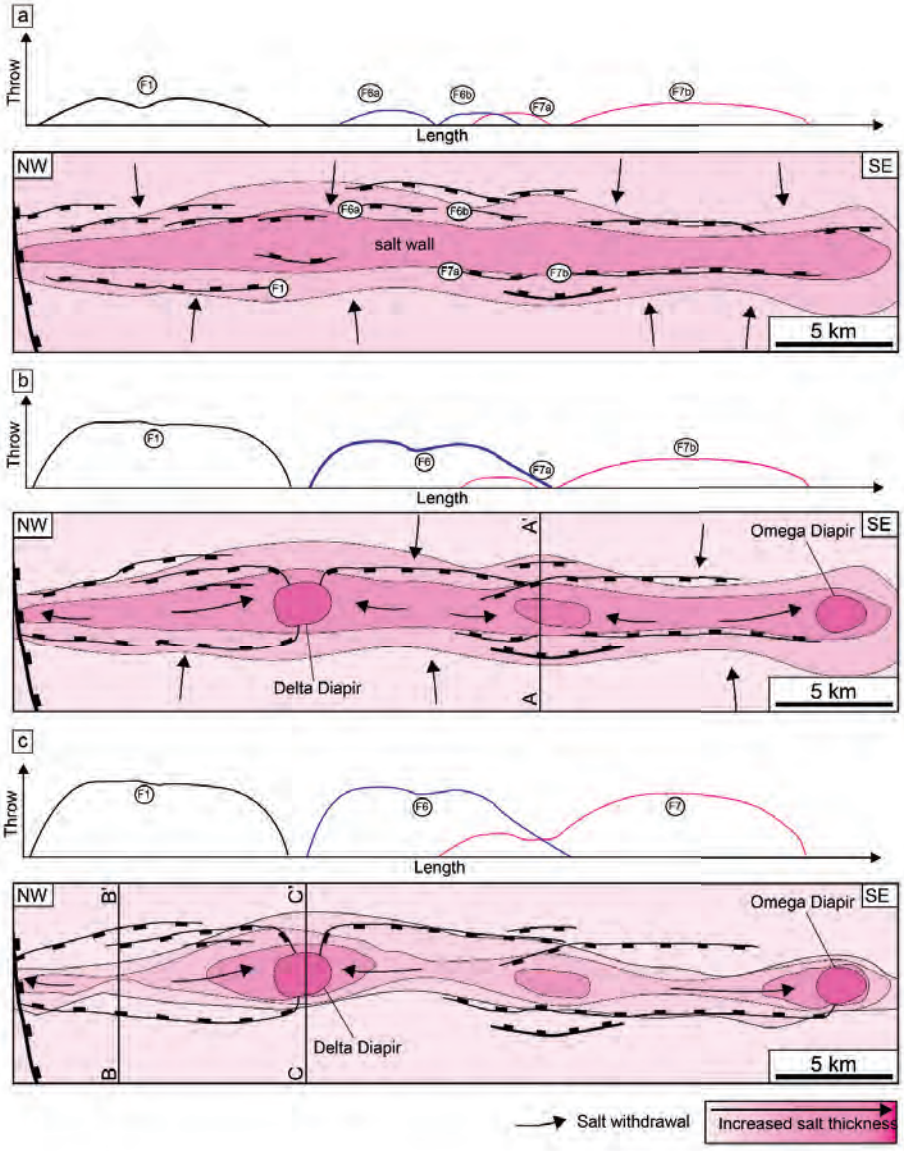
a
Throw
F1
F8a
F6b
F7a
F7b
Length
NW
SE
F6a
F6b
salt wall
F7a
F7b
F1
5 km
b
Throw
F1
F6
F7a
F7b
Length
NW
A'
Omega Diapir
SE
Delta Diapir
A
5 km
c
Throw
F1
F6
F7
Length
NW
B'
C'
Omega Diapir
SE
Delta Diapir
B
C
5 km
Salt withdrawal
Increased salt thickness

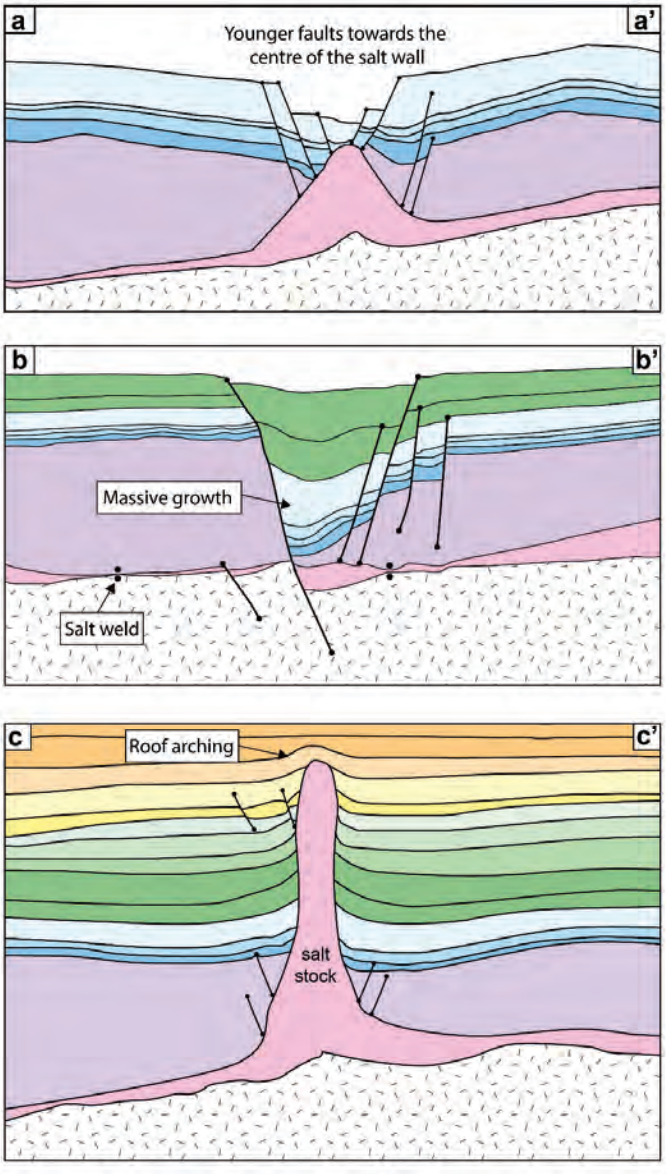

Fig. 18. Conceptual sketch of how the fault array evolved through time; (a) Late Triassic-Middle Jurassic: Salt wall formation, reactive diapirism and fault nucleation; (b) Jurassic: Salt stock nucleation, continued reactive diapirism and fault linkage; and (c) Cretaceous: Major collapse, continued fault growth and diapirism along strike. These mechanisms are shown in seismic profiles; reactive rise of salt diapirs (profile a-a'), collapse (profile b-b') and active diapirism (profile c-c') occurring simultaneously along strike, where salt withdrew from beneath collapsing parts of the salt walls into the emerging diapirs.

7. A genetic four dimensional model for the evolution of supra-salt fault arrays during the rise and fall of salt diapirs

The growth of the supra-salt fault array and the flow of Zechstein salt were intimately coupled for ca. 171 Myr, spanning the Late Triassic to Neogene. Reactive diapirism (Late Triassic–Early Cretaceous) was followed by diapir collapse (Late Jurassic-middle Palaeogene) and, eventually, growth of salt stocks by passive and active diapirism (Late Jurassic-Neogene) driven by the along-strike flow of salt within collapsing walls. These processes partly overlapped in time, occurring simultaneously along strike of a single salt wall-stock system and genetically related supra-salt fault arrays. These processes are documented in physical models (Vendeville and Jackson, 1992a; Vendeville and Jackson, 1992b; Ge et al., 1995) but, until now, has not been documented in a natural example.

Based on our observations from the Egersund Basin we here propose a genetic model for the four-dimensional development of a supra-salt fault array forming during the birth, growth and death of a series of physically and kinematically linked salt diapirs. The initial formation of a supra-salt fault array may be caused by a range of processes, including; (i) gravity-gliding and thin-skinned extension; (ii) regional thick-skinned extension; or (iii) gravity spreading. Irrespective of the exact trigger, overburden faulting causes reactive rise of salt walls (Fig. 16). Fault growth may follow the isolated or coherent fault model (Walsh et al., 2002; Jackson and Rotevatn, 2013), with the wall being of broadly similar length to the overlying fault array. At this time, new faults form as reactive diapirs inflate and widen, with younger overburden faults progressively initiating closer to the crest of the rising salt walls. Stocks may nucleate on the wall crest where the roof is thinnest (Ge et al., 1995; Guglielmo et al., 1997). Early formed stocks may impede lateral propagation of the faults, resulting in high throw gradients at their tips and abrupt changes in their strike due to local perturbation of the regional extensional stress by hoop stresses flanking the inflating stocks. If the autochthonous salt layer is very thin or welded, inflating stocks may be fed by salt flowing along strike within flanking walls, which begin to collapse due to ongoing overburden extension related to thin-skinned or regional thick-skinned tectonics

(1992b; Vendeville and Jackson, 1992a; Ge et al., 1995). Grabens develop above collapsing walls and the degree of collapse will then drive the feeding of the growing salt stocks. Even if true regional thin- or thick-extension ceases, thin-skinned faults may continue to be active and the crestal graben may continue to subside due to widening of the previously reactive diapirs and the along-strike flow within the walls. At this time, diapir collapse is accommodated in the overburden by progressively fewer faults that are located progressively nearer the crest of the salt walls (Fig. 16). As stocks begin to cannibalise salt from increasingly proximal locations in the flanking walls, faults may initiate progressively closer to and the locus of maximum subsidence may migrate along-strike towards, this area. During the latter stages of their development, salt stocks may grow by active or passive diapirism.

Our genetic four-dimensional model shows many geometric and kinematic similarities to the physical models of Vendeville and Jackson (1992a; 1992b), Ge et al. (1995) and Guglielmo et al. (1997; 1999). More specifically, our model highlights the structural style and kinematic variability that can occur simultaneously along strike of a salt body in response to coeval wall collapse and stock rise (Figs. 1, 15 and 16). However, as may be predicted, our natural example is more complex than the physical models, with multiphase diapirism and fault growth, and fault dip linkage, in particular, being key processes. This complexity reflects the fact that salt mobilisation and fault growth reflect regional, far-field tectonic events such as whole crust extension and contraction, as well as local events related to thin-skinned extension. We have shown that 3D seismic reflection and borehole data allow us to investigation the dynamics of overburden deformation above salt, allowing us to track the four-dimensional flow of salt; this study thus provides us with a better understanding of the tectono-stratigraphic evolution of salt-influenced sedimentary basins.

8. Conclusions

We have used 3D seismic reflection and borehole data to illustrate how multiphase salt mobilisation influences the structural style and growth of supra-salt fault arrays. More specifically, this natural example has allowed us to test, in fully three-dimensions and

for the first time, the predictions of previous physical models focused on normal fault structural style and kinematic development during the rise and fall of salt diapirs. Our main conclusions are:

1. We recognise three stages of salt mobilisation and associated fault growth; (i) thick-skinned extension in the Late Triassic to Middle Jurassic, which caused base-of-salt and overburden tilting, overburden stretching, the nucleation and initial syn-sedimentary growth of a supra-salt fault array, and reactive diapirism; (ii) syn-sedimentary fault growth during the Early Cretaceous, which was triggered by extensional collapse of underlying salt walls driven by continued thin-skinned extension; (iii) passive and active diapirism from the Jurassic until the Neogene, with salt being fed into the stock by along-strike flow within the flanking walls; hence wall collapse and stock rise were coeval, with these processes being recorded in the growth histories of the genetically related supra-salt fault array.
2. Near-final fault lengths were established at an early stage in their development (i.e. after up to only 20% of their growth histories), with fault growth being dominated by displacement accumulation and not lateral tip propagation.
3. For much (i.e. c. 80%) of the fault growth history, lateral tip propagation was inhibited by extant, albeit low-relief salt diapirs, and thick-skinned, basement-involved faults.
4. The natural example documented herein show-cases how a fault array can grow through reactive rise, collapse, and active piercement of salt, and how this can occur simultaneously through time. This variation along strike of the system reflects the interplay between several different mechanisms such as differential loading, and salt flow along the salt wall. The growth history and fault geometries of the natural example documented herein, are far more complex than that predicted by the physical models, with multiphase salt diapirism and fault growth, and fault dip linkage in particular, being key processes.
5. This study illustrates how 3D seismic reflection and borehole data allow us to investigate the dynamics of supra-salt overburden deformation, and how this

can be used to track the three-dimensional flow of salt, and providing us with a better understanding of the tectonostratigraphic evolution of salt-influenced sedimentary basins.

Acknowledgements

We thank PGS, in particular Richard Lamb and Mike Keavney, for providing access to seismic reflection data and for granting permission to publish the results of our study. We also thank Schlumberger for providing access to Petrel software and Badleys Geosciences for providing access to Traptester software.

Chapter 3. Synthesis

This research focuses on how and why supra-salt normal fault arrays form and the extent to which salt may control the geometry and growth of such fault arrays. Our research provides detailed investigations of the techniques used to determine the style of growth of seismic-scale syn-sedimentary normal faults and three case studies of the three-dimensional growth of supra-salt normal fault arrays, where fault growth is related to multiphase salt diapirism. The case studies illustrate how several different triggering and driving mechanisms may operate simultaneously along strike, as well as how they can change through time. In this study, we show how supra-salt fault arrays evolve above thin and thick salt in extensional basins and downslope on passive margins. The fault arrays are initiated and driven by several mechanisms, including basement faulting and salt mobilisation. The fault arrays are triggered by extension and/or contraction causing gravity gliding, resulting in reactive diapirism, collapse, and passive and active rise of salt etc. In the following we synthesize and discuss the main findings of the present study, and assess their implications for investigation of supra-salt fault arrays and the tectono-stratigraphic evolution of salt-basins.

3.1 Synthesis of main findings and key implications of the study

3.1.1 Techniques used to track fault growth and the flow of salt

In this research, a wide range of techniques have been applied to fully understand the growth of supra-salt fault arrays. The fault arrays exemplified herein (Paper II-IV) are analysed by using methods describing the three dimensional throw distribution, such as throw-depth and throw-length analysis and strike-throw projections, combined with isochrons and expansion indices to determine the three-dimensional growth history of individual faults, as well as the supra-salt fault arrays. In paper I we describe these different methods and exemplify their use and their limitations, while in Paper II-IV we apply these methods to illustrate different aspects of salt related fault growth. To analyse the evolution of such supra-salt fault arrays exemplified herein, extensive fault

analysis is needed to understand their evolution of the and how the growth is related to salt mobilisation.

To determine how the faults have lengthened and accumulated displacement, two throw backstripping methods (the 'original' and 'modified' methods; Paper I & Paper IV) can be used. As stated in Paper I, *a priori* knowledge of which fault growth model is most likely is needed when choosing which method to apply. In Paper IV we used expansion indices along strike of individual fault segments to identify syn-sedimentary faulting near the lateral fault tips and thereby establishing that the near-final fault length established relatively early in the growth history. These observations lead to the conclusion that the 'original' method was the most applicable when performing backstripping of the faults.

We have here shown how different techniques be used to describe the temporal and spatial evolution of a supra-salt fault array and salt mobilisation, where e.g. the lateral change in maximum throw for younger strata can illustrate where collapse occurs at a given time, where fault length analysis can shed light on when salt stocks start to nucleate, and where expansion indices can indicate e.g. when salt anticlines were forming and when a fault established its near-final length. The combination of different analyses such as displacement-length profiles, including backstripping of those, vertical throw distribution, throw strike-projections, thickness maps and expansion indices can yield important knowledge about the temporal and spatial evolution of a supra-salt fault array, and lead to a better understanding of the flow of salt. Detailed quantitative fault analysis in combination with a qualitative approach, as exemplified herein, has a range of other applications and is essential in the assessment of displacement distribution, fault zone geometry as well as growth- and linkage history. Comprehensive three-dimensional fault displacement analysis is therefore important, capturing a level of detail in displacement distribution and fault history that would otherwise be lost.

3.1.2 The complexity of triggers and driving mechanisms of fault growth in a salt influenced basin

The recent improvement of seismic acquisition has resulted in high quality 3D seismic datasets that have given us new insight into the interplay between salt mobilisation and supra-salt cover deformation and sedimentation patterns (e.g. Richardson et al., 2005; Marsh et al., 2010; Lewis et al., 2013; Wilson et al., 2013; Harding and Huuse, 2015; Jackson et al., 2015; Jackson and Lewis, 2016). Even though research during the past decades have increased our knowledge about salt tectonics, there are still unresolved questions regarding triggering and driving mechanisms. This thesis presents three studies of fault arrays in two different basins. In both basins the fault arrays display complex growth histories that are clearly influenced by the flow of salt.

The research conducted within the Egersund Basin allowed us to investigate the growth of two supra-salt fault arrays. The three-dimensional growth histories of the two supra-salt fault arrays (Paper II and IV) are quite different even though they are oriented nearly perpendicular to one another (Fig. 3.1). The fault array in Paper II, is developed above a relatively thin (c. 100 m) salt layer and a sub-salt fault array, whereas the fault array studied in Paper IV, is located above an up to c. 600 m thick salt wall separated by tall (2.7 km) salt stocks. Even though the fault arrays were active during broadly the same time period and both initiated by cover stretching related to activity on the large, thick-skinned, basin-bounding faults, their mechanisms of fault growth are different.

The fault array studied in Paper II was initiated by re-activation of a pre-existing sub-salt fault array during the Late Triassic and was deactivated after burial of the fault tips during the Late Jurassic to Turonian times. Salt re-mobilisation triggered by basin inversion initiated in the Turonian, led to blind reactivation of some of the faults in parts of the fault array. The reactivated faults are located where the underlying salt is thicker, while the non-reactivated faults are found where salt is depleted, indicating that salt was at least controlling much of the later phases of fault growth. The supra-salt fault array is *geometrically decoupled* through the salt along most of its extent, but locally physically linked where strains were sufficiently large to discretely breach the Zechstein Supergroup. Despite the large extent of geometric decoupling across the

Zechstein Supergroup, deformation was *kinematically coupled*, in the sense that the basement faults still affected the nucleation, localization and geometry of the supra-salt faults.

The supra-salt fault array studied in Paper IV was initiated by movement on a thick-skinned, basin bounding fault in the Late Triassic, causing salt mobilisation by base salt tilting and gliding, which in turn caused the nucleation and initial fault growth by thin-skinned extension. Overburden gravity gliding and stretching drove reactive diapirism and salt wall growth that continued into the Late Jurassic, when the salt stocks nucleated. The faults reached their near-full length during this time, caused by lateral restriction by the Delta and Omega diapirs and the Sele High Fault System. The

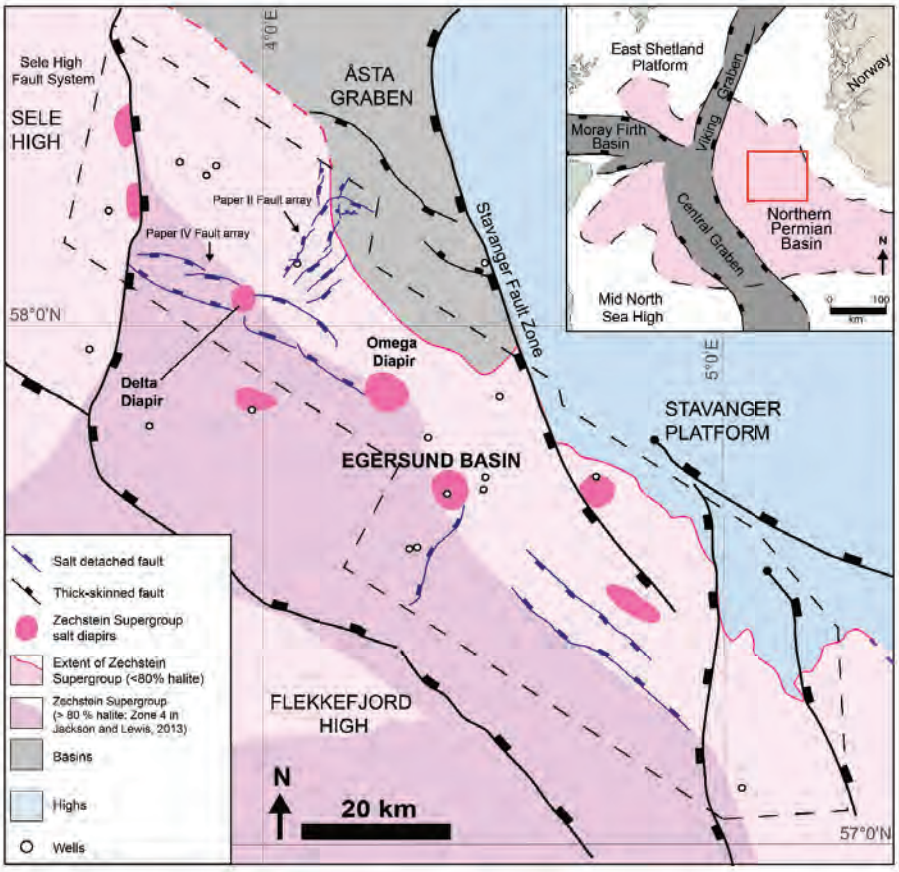

Fig. 3.1. The localisation of fault arrays relative to each other and relative to halite rich salt (Zone 4 (>80 % halite; Jackson and Lewis, 2016)

amount of fault growth during reactive diapirism during the Late Triassic-Late Jurassic was controlled by salt flow into the widening salt walls (though extension was driving the reactive diapirism). Subsequent to reactive diapirism, diapir collapse due to along-strike migration of salt within the wall drove further fault growth, principally by displacement accrual in the Early Cretaceous, with active diapirism occurring simultaneously along strike. Active diapirism occurred until the Neogene, which drove further salt wall collapse and fault growth near the diapirs (Figs. 16 and 17 in Paper IV).

The research of the supra-salt fault arrays in the Egersund Basin illustrates how two closely related supra-salt fault arrays may evolve differently in response to different salt-related forcing mechanisms. The different mechanisms of fault growth in the two fault arrays in the Egersund Basin is most likely a result of the salt thickness and composition. Jackson and Lewis (2016) illustrate how salt thickness and composition can impact the structural style and growth of supra-salt faults by the use of the Sele High Fault System (Fig. 3.1). Their study of the Zechstein Supergroup indicates that the salt beneath Paper IV fault array is containing more halite than beneath Paper II fault array. The higher content of halite result in a lower viscosity for the salt, hence more mobile salt (Jordan, 1987; Jackson and Talbot, 1989; van Keken et al., 1993; Hudec and Jackson, 2007; Wagner III and Jackson, 2011). The increased salt mobility will then in turn result in different growth patterns and structural styles. The Zechstein Supergroup is also much thicker beneath Paper IV fault array. Duffy et al. (2013) showed that thin salt (c.100 m) can result in variable degree of decoupling between basement and overburden deformation and provide a detachment for gravity-gliding of the cover, while thicker salt can to a larger extent control the structural styles and syn-rift stratal geometries. Overall, the difference in the growth patterns and structural styles of the two fault arrays studied in the Egersund Basin is suggested to be a result of thickness and composition variations of the salt, in addition to the fact that the supra-salt fault array to the north (Paper II) in its early growth history was largely controlled by basement faulting, while the fault array to the south (Paper IV) was controlled by gravity gliding and reactive diapirism.

Within the Santos Basin on the São Paulo Plateau the salt is thick and have much larger control on the structural style compared to the Egersund Basin where salt is thinner. The mechanisms of initiation of growth of the supra-salt fault arrays are also much more complex and harder to elucidate within this part of the Santos Basin. Existing models describing the relationship between extensional faulting and salt mobilisation on passive margins are largely focused in the up-slope part (often referred to as the extensional domain) or the downslope domain (often referred to as the contractional domain). The case study of the fault array within the Santos Basin on the São Paulo Plateau showed in Paper III are within what is often referred to as the contractional province of the Santos Basin (Cobbold and Szatmari, 1991; Demercian et al., 1993; Garcia et al., 2012; Rowan et al., 2012). However, this specific study provide an example of supra-salt-salt fault arrays formed in an area where salt mobilisation is cryptic and may be 'translational', or at least locally moving at different rates causing both compressional (i.e. folding; Fig 5 in Paper III) and extensional deformation (i.e. reactive diapirism; Fig 4b in Paper III). This suggests that the 'contractional domain' is at least locally extensional or may actually be termed a 'transtensional domain' in this part of the São Paulo Plateau. Differences in the style of supra-salt faulting observed within São Paulo Plateau may be related to variability in the rate and divergence of salt mobilisation. In contrast to the up-slope 'extensional domain' and the 'contractional domain' of a passive margin where the typical structures observed are often related to textbook examples of e.g. rafts, reactive diapirs and downdip buckle folding and thrusts, the complexity of movement of salt in the 'translational domain' may cause enigmatic mechanisms of fault growth both related to local extension and shortening. Furthermore, the research of the supra-salt fault arrays within the Santos Basin demonstrates that, based on the fault and salt body geometry, and fault displacement distributions alone, it may be difficult to confidently constrain the mechanisms triggering fault nucleation and/or driving fault slip accumulation.

The mechanisms of supra-salt normal fault growth, both in rift basins and on passive margins, are generally well described in 2D and by analogue physical experiment (Vendeville and Jackson, 1992b; Vendeville and Jackson, 1992a; Schultz-Ela et al.,

1993; Ge et al., 1995; Guglielmo et al., 1997; Hudec and Jackson, 2007; Brun and Fort, 2011), and several studies during the past decades have studied supra-salt fault arrays in 3D (Rowan et al., 1998; Richardson et al., 2005; Marsh et al., 2010), but there has been little focus on the multiphase salt mobilisation and the possible different trigger and driving mechanisms of supra-salt fault growth. This research has shown how seismic reflection data can be used to document the structural style and growth of supra-salt extensional fault arrays during the subsurface flow of salt and how this can be used to differentiate between different mechanisms.

3.1.3 Implications for models of normal fault growth and fault length establishment

An accepted model is that faults lengthen during accumulation of displacement (e.g. Watterson, 1986; Cowie and Scholz, 1992b; Gillespie et al., 1992). The displacement-length ratios of normal-faults are well documented from numerous studies in the literature (e.g. Muraoka and Kamata, 1983; Krantz, 1988; Walsh and Watterson, 1988; Gudmundsson and Bäckström, 1991; Cowie and Scholz, 1992b; Dawers et al., 1993; Cartwright et al., 1995; Schlische et al., 1996; Schultz and Fossen, 2002) and are often represented in a logarithmic diagram (Fig. 3.2a). This diagram has commonly been used in favour of the 'isolated fault' model (e.g. Watterson, 1986; Walsh and Watterson, 1988; Dawers et al., 1993; Cartwright et al., 1995), resulting in a linear displacement-length ratio (g = 1.0; Fig. 3.2a) for normal, strike-slip, and thrust faults.

Recent studies (e.g. Walsh et al., 2002; Childs et al., 2003; Giba et al., 2012; Jackson and Rotevatn, 2013) have shown that some faults reach their near-full length early in their growth history, and that subsequent strain is accommodated through displacement accrual accompanied by limited tip propagation only. In both the Santos and Egersund basins (Paper II, III & IV) we have observed faults that have established their lengths early in the growth history, in accordance to the 'coherent' growth model (*see* Paper I). However, individual fault segments studied in this research do not differ in present-day length-displacement ratios from non-salt influenced fault segments (Fig. 3.2a) and their final throw-length ratios are within the established trend (Krantz, 1988; Gudmundsson and Bäckström, 1991; Cowie and Scholz, 1992b; Dawers et al., 1993;

Cartwright et al., 1995; Schlische et al., 1996; Schultz and Fossen, 2002). This raises the question of whether faults behaving according to the ‘coherent fault’ model are hidden in the logarithmic displacement-length diagram. To address this, we have backstripped some of the faults that Papers II-IV revealed to have established their near-final lengths early. When inserting the backstripped values into the logarithmic displacement-length diagram (Fig. 3.2a), these faults end up on the common trend on this diagram despite the fact that they were 'underdisplaced' early in their growth histories in contrast to predictions of the 'isolated fault model'. Hence, the complex growth history of the faults is not justified when plotting displacement-length ratios in the logarithimic diagram. The logarithmic way of showing displacement and length data may result in that the finite displacement-length distributions of faults behaving according to the ‘isolated fault’ or the ‘coherent fault’ models will not differ significantly. In Figure 3.2b, showing the same values on a regular diagram without the logarithmic scale, it becomes very clear that the faults attained their lengths early in the growth history, and mainly accumulated throw after early length establishment. Walsh et al. (2002) demonstrated the power of showing the cumulative displacement and length versus time of faults from the Timor Sea, which indicate that these fault attained their near-full length early in their growth history. The same observations can be made of faults showed in this research (Fig. 3.3).

A question arising from these analyses is “*Why did the faults establish their lengths so early?” R*ecent studies (Walsh et al., 2002; Childs et al., 2003; Giba et al., 2012; Jackson and Rotevatn, 2013) have shown that some faults reach their near-full length, early in their growth history, and that subsequent strain is accommodated through displacement accrual accompanied by limited tip propagation. Studies by Walsh et al. (2002), Giba et al. (2012) and Jackson and Rotevatn (2013) indicate that the fault arrays inherited their fault length from underlying structures, resulting in near-final fault lengths, early in their growth history.

Neither the fault array studied in Paper IV in the Egersund Basin or the Santos Basin indicate inheritance of fault length from underlying structures. According to Schultz et al. (2006) the displacement-length ratio for faults depends primarily on three factors: the Youngs' modulus, the magnitude of shear driving stress, and the yield strength. For example will a stiffer rock such as a granite require greater near-tip stresses to break than a sandstone, leading to larger values of displacement along the fault (Schultz and Fossen, 2002; Schultz et al., 2006). If the fault frictional strength is low, this will result in reduced displacement gradients along the fault (Cowie and Scholz, 1992a; Schultz et al., 2006). In both the Santos and Egersund Basins we know that the faults were surface breaching during their early growth history, meaning that the sediments in which they formed were unconsolidated or weakly consolidated and thereby most likely had a low shear modulus (low rock strength or hardness). This in combination with the low viscosity of the salt below could maybe result in rapid propagation of the faults as the shear yield strength near the fault tips is low.

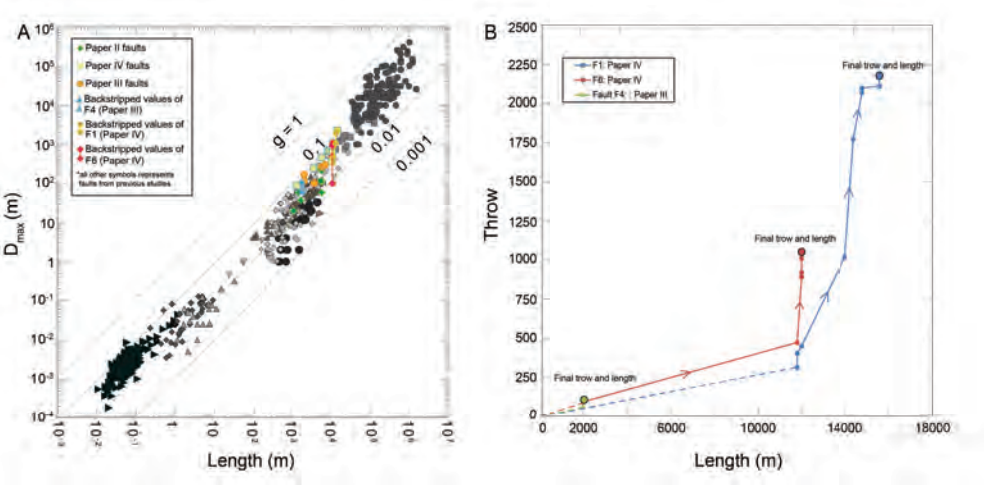

Fig. 3.2. (a) Logarithmic plot of lengths against maximum displacement for faults in this research, including the backstripped values of three faults from this research and their corresponding growth paths through time. The grey coloured data points represent displacement-length relations of faults from previous studies (Krantz, 1988; Gudmundsson and Bäckström, 1991; Cowie and Scholz, 1992b and references therein; Dawers et al., 1993; Cartwright et al., 1995; Schlische et al., 1996; Schultz and Fossen, 2002). (b) Non-logarithmic overview of the the backtripped values of three faults from this research showing the how the throw-length relationship has evolved through time.

Retardation of further fault-lengthening within the fault array studied in Paper IV is suggested to be a result of lateral restriction by early emplacement of salt stocks and presence of the Sele High Fault System. Within the research area within the Santos Basin there are not any significant lateral restrictions except for the possibility of it being the salt itself. The ability of salt to flow easily and form an undulating surface quite rapidly allows for possible restriction in the lateral direction. The lateral retardation of further lengthening can also be a result of interaction between the established faults (Nicol et al., 1996; Childs et al., 2003).

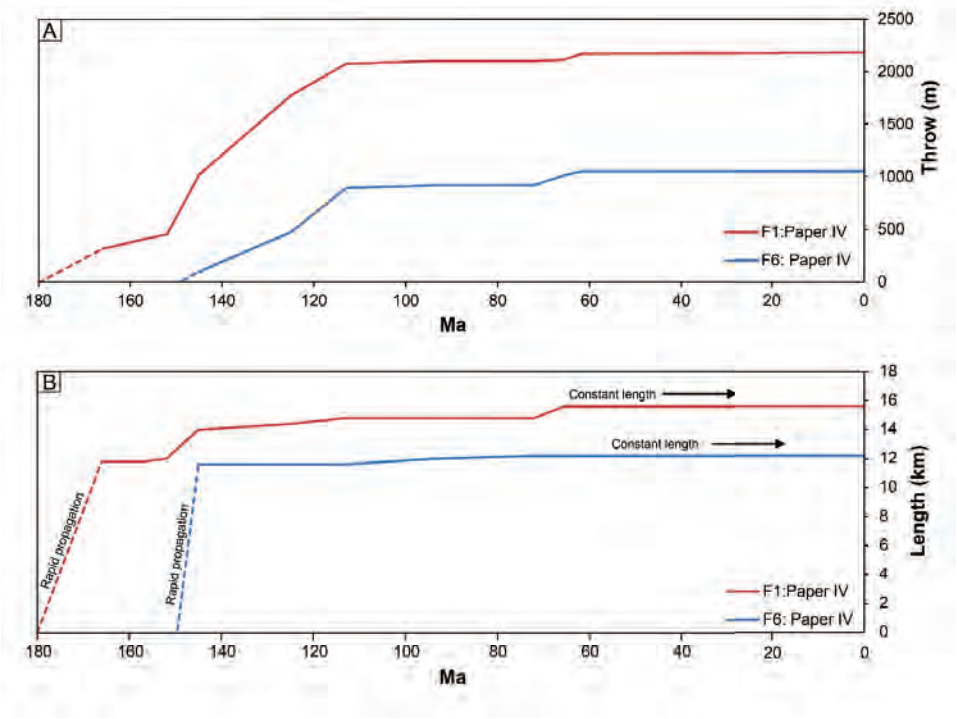

Fig. 3.3. Growth curves for two of the faults in the Egersund Basin (Paper IV) showing the changes in fault throw (a) and fault length (b) through time. The dashed lines indicate approximation of early length and throw evolution.

3.2 Concluding remarks

Over the past decades, the interest in salt tectonics has increased dramatically. Despite that 3D-seismic data have been available for a few decades, the understanding of supra-salt faulting has mainly been based on observations in the cross-sectional plane of observation, whereas the lateral variability in salt movement and fault evolution have mainly been considered in analogue physical experiments. The research presented in this thesis has demonstrated the strength of using three-dimensional data and combining quantitative and qualitative analyses to investigate supra-salt faulting and its relationship to salt mobilisation through time. The main findings and implications are summarized below:

- The detailed quantitative and qualitative fault analysis, as exemplified herein, has a range of applications and is essential in the assessment of displacement distribution, fault zone geometry as well as growth- and linkage history. Comprehensive three-dimensional fault displacement analysis is therefore important, capturing a level of detail in displacement distribution and fault history that would otherwise be lost.

- All three case studies indicate that as soon as a fault has formed, nevertheless the mechanism, the fault can more easily reactivate due to remobilisation of salt without relation to regional extension. As a fault is formed by extension, the salt mobilisation during late stages may affect the supra-salt faulting, e.g. allowing normal reactivation of faults even though the stress is on a regional scale contractional.

- The tectonic regime of the salt basin has an important influence on the character of supra-salt deformation, mainly in terms of complexity of mechanisms initiating and driving supra-salt faulting.

- The driving mechanism behind supra-salt fault nucleation in this study support previous observations that faults can form by direct extension related to basement faults or only be kinematically linked. Basement faults can control the nucleation and localization of cover faults through salt without being geometrically linked.

- The results presented in this study provide new insight into how supra-salt fault array can grow in terms if mechanisms, and give important knowledge to take into account when investigating a salt basins' evolution. This research is important both for the general salt tectonic understanding, but also for understanding the formation of e.g. hydrocarbon traps in the supra-salt overburden.

- The growth of a supra-salt fault array can be influenced by changes in salt wall geometry along strike, from reactive walls to collapse and active diapirism along strike, with immature salt rollers and ridges, to mature active diapirs. This variation along strike of the array reflects the interplay between several different mechanisms such as differential loading, and salt flow along the salt wall, and show-cases how a fault array can grow through reactive rise, collapse, and active piercement of salt, and how this can occur simultaneously through time. The natural example from the Egersund Basin shows a far more complex geometry and evolution than that predicted by previous physical models, with multiphase salt diapirism and fault growth and fault dip linkage in particular, being key processes.

- From this research, it is clear that some of the supra-salt normal faults both in the Egersund Basin (Paper IV) and Santos Basin (Paper III) established their lengths early. In the Egersund Basin, rapid length establishment could be a result of lateral restrictions by basin bounding faults and the pre-existing/contemporaneous growth of salt stocks. The faults in the Santos Basin are suggested to have established their lengths early either because of

possible retardation in the lateral direction by the undulating top salt surface itself or interaction between the established faults.

- This study provides a contribution to the understanding of overburden deformation linked to salt mobilisation, with specific focus on how salt has moved through time by investigating the overburden and how that can track the flow of salt, offering insight into the complex interplay between salt diapirism and faulting, showcasing three-dimensional examples of how protracted, multiphase salt diapirism can influence the structure and growth of normal fault arrays.

- Detailed investigation of the dynamics of overburden deformation above salt, have implications for the prediction the four-dimensional flow of salt study and can thereby provide us with a better understanding of the tectono-stratigraphic evolution of salt-influenced sedimentary basins. This in turn may have implications for understanding fault seal capacity and thus, fluid flow dynamics during production or the delineation and risking of fault controlled traps in hydrocarbon exploration and production.

3.3 Perspectives

In light of our observations and results throughout the project, new research possibilities arose for expanding and improving this knowledge:

Fault length establishment

Further detailed research on supra-salt normal fault arrays focusing on the fault length establishment in different salt basins could investigate whether there is a trend that supra-salt normal faults establish their lengths early, and if so where and why. This can have implications for the understanding of syn-sedimentary fault growth in salt basins, and have implication for the understanding of sedimentary routing patterns, depocentre locations through time, reservoir distribution, hydrocarbon traps in the supra-salt overburden and can help quantify where to expect sand-on sand juxta positioning due to fault growth. This can also be expanded to normal faults in general, to better understand where faults lengthen early. Detailed investigation of both timing of fault growth and establishment of their lengths should also be considered to get a better understanding of the common trends of the 'coherent' and 'isolated' fault models. Detailed investigation should include expansion indices, isochron maps and three-dimensional fault throw analysis, aided by relay zone and throw backstripping through time.

Internal salt mobilisation and supra-salt faulting

The current limitation of the seismic resolution within the salt has made it quite hard to determine how the salt flow has occurred through time and this have largely been based on field examples from outcrops and mines, and physical experiments. With the improved imaging of internal salt geometries the recent years, it has been possible to investigate the internal movement within the salt and thereby better constrain the different mechanisms responsible for the growth of salt structures (e.g. Van Gent et al., 2011; Strozyk et al., 2012; Dooley et al., 2015; Jackson et al., 2015). As the seismic resolution has improved we can now better combine analyses of internal salt movement and supra-salt fault analyses to better understand the interplay between the salt and the

supra-salt overburden through time and thereby get a more detailed understanding of a salt basin's evolution.

Stress field perturbation associated with salt diapirism

In the Egersund Basin, the faults near the Omega and Delta diapirs are changing strike with almost 90 degrees close to the salt stocks. This change of strike is similar to the '*hoop stresses*' around salt stocks in the Central Graben, North Sea, investigated by Carruthers et al. (2013) using the geometry of polygonal fault patterns to reconstruct the evolving stress state of salt stocks. To further investigate this stress field modification associated with the propagating and interacting tips of salt-related fault systems (e.g. radial faults interacting with collapse graben bounding faults) using numerical modelling to simulate the stress field modification through time could be beneficial to better constrain the timing of diapir growth.

Supra-salt sub-seismic deformation related to salt mobilisation

This research is limited by the resolution of three-dimensional seismic data. To further constrain the growth mechanisms of supra-salt wall faults, analogue studies in the field can provide details about sub-seismic deformation related to growth of such supra-salt fault arrays and may provide further insights into how to constrain the trigger and driving mechanisms. Further, this can have implications for the understanding of reservoir segmentation and trap configurations in hydrocarbon exploration and production. Possible analogues in the field suggested are e.g. at Qushm Island and Bon e Kooh Chahar Berkeh in Iran or near the Ellesmere Island in the northern Canada.

Postface

Some rocks are special, and behave quite differently from the stable rocks we encounter every day. Salt is not only a supplement to make your popcorn taste better or make your drive home safe when the roads are icy. Salt is one of those unique rocks, which almost like a magic trick has the ability to dissolve, travel by water and then appear again somewhere completely different in the world. It can in solid state move very fast! It can glide down the slope, it can rise higher than any human building built, and if the salt has been placed somewhere cramped with more solid friends, salt is the first to leave the party and move away to somewhere more convenient. Salt can be a stylist, controlling the apparent looks of its surrounding more solid friends. Who would have thought that the salt we put in our mouth every day is one of the fastest on the track when comparing solid rocks? Salt is the solid rocks' Ferrari; it can move so fast that the other rocks cannot keep up, and collapse as they try to keep pace, leaving them tremendously deformed. Only every now and then, the quick gumbo clay tries its best to show off some of its speed, but he is more like a sprinter, he cannot keep up for long. Salt is fascinating, salt is complex, salt is quite unique.

References

Adam, J., Ge, Z., Sanchez, M. (2012). Salt-structural styles and kinematic evolution of the Jequitinhonha deepwater fold belt, central Brazil passive margin. *Marine and Petroleum Geology*, **37**, 101-120.

Anderson, N., Brown, R., Hinds, R. (1988). Geophysical aspects of Wabamun salt dissolution in southern Alberta: Can. *J. Exp*, 166-178.

Anderson, N., Franseen, E. (1991). Differential compaction of Winnipegosis reefs: A seismic perspective. *Geophysics*, **56**, 142-147.

Anderson, N., Knapp, R. (1993). An overview of some of the large scale mechanisms of salt dissolution in western Canada. *GEOPHYSICS*, **58**, 1375-1387.

Athmer, W., Groenenberg, R.M., Luthi, S.M., Donselaar, M.E., Sokoutis, D., Willingshofer, E. (2010). Relay ramps as pathways for turbidity currents: a study combining analogue sandbox experiments and numerical flow simulations. *Sedimentology*, **57**, 806-823.

Athmer, W., Luthi, S.M. (2011). The effect of relay ramps on sediment routes and deposition: A review. *Sedimentary Geology*, **242**, 1-17.

Bahorich, M., Farmer, S. (1995). 3-D seismic discontinuity for faults and stratigraphic features: The coherence cube. *The leading edge*, **14**, 1053-1058.

Baudon, C., Cartwright, J.A. (2008a). The kinematics of reactivation of normal faults using high resolution throw mapping. *Journal of Structural Geology*, **30**, 1072-1084.

Baudon, C., Cartwright, J.A. (2008b). Early stage evolution of growth faults: 3D seismic insights from the Levant Basin, Eastern Mediterranean. *Journal of Structural Geology*, **30**, 888-898.

Baudon, C., Cartwright, J.A. (2008c). 3D seismic characterisation of an array of blind normal faults in the Levant Basin, Eastern Mediterranean. *Journal of Structural Geology*, **30**, 746-760.

Benedicto, A., Schultz, R., Soliva, R. (2003). Layer thickness and the shape of faults. *Geophysical Research Letters*, **30**.

Bertoni, C., Cartwright, J.A. (2005). 3D seismic analysis of circular evaporite dissolution structures, Eastern Mediterranean. *Journal of the Geological Society*, **162**, 909-926.

Bishop, D.J., Buchanan, P.G., Bishop, C.J. (1995). Gravity-driven thin-skinned extension above Zechstein Group evaporites in the western central North Sea: an application of computer-aided section restoration techniques. *Marine and Petroleum Geology*, **12**, 115-135.

Bouroullec, R., Cartwright, J.A., Johnson, H.D., Lansigu, C., Quémener, J.-M., Savanier, D. (2004). Syndepositional faulting in the Grés d'Annot Formation, SE France: high-resolution kinematic analysis and stratigraphic response to growth faulting. *In: Joseph, P. & Lomas, S.A. (eds) Deep-water sedimentation in the Alpine Basin of SE France: new perspectives on the Grès d'Annot and related systems. Geological Society, London, Special Publications*, **221**, 241-265.

Brown, A.R. (2003). Interpretation of three-dimensional seismic data. *American Association of Petroleum Geologists Memoir 42, 6th edition, 541 p.*

Brun, J.-P., Mauduit, T.P.-O. (2009). Salt rollers: structure and kinematics from analogue modelling. *Marine and Petroleum Geology*, **26**, 249-258.

Brun, J.P., Fort, X. (2011). Salt tectonics at passive margins: Geology versus models. *Marine and Petroleum Geology*, **28**, 1123-1145.

Carruthers, D., Cartwright, J., Jackson, M.P., Schutjens, P. (2013). Origin and timing of layer-bound radial faulting around North Sea salt stocks: New insights into the evolving stress state around rising diapirs. *Marine and Petroleum Geology*, **48**, 130-148.

Cartwright, J.A., Trudgill, B.D., Mansfield, C.S. (1995). Fault growth by segment linkage: an explanation for scatter in maximum displacement and trace length data from the Canyonlands Grabens of SE Utah. *Journal of Structural Geology*, **17**, 1319-1326.

Cartwright, J.A., Bouroullec, R., James, D., Johnson, H. (1998). Polycyclic motion history of some Gulf Coast growth faults from high-resolution displacement analysis. *Geology*, **26**, 819-822.

Cartwright, J.A., Stewart, S.A., Clark, J. (2001). Salt dissolution and salt-related deformation of the Forth Approaches Basin, UK North Sea. *Marine and Petroleum Geology*, **18**, 757-778.

Cartwright, J.A. (2007). The impact of 3D seismic data on the understanding of compaction, fluid flow and diagenesis in sedimentary basins. *Journal of the Geological Society*, **164**, 881-893.

Cartwright, J.A. (2011). Diagenetically induced shear failure of fine-grained sediments and the development of polygonal fault systems. *Marine and Petroleum Geology*, **28**, 1593-1610.

Chang, H.K., Kowsmann, R.O., Figueiredo, A.M.F., Bender, A. (1992). Tectonics and stratigraphy of the East Brazil Rift system: an overview. *Tectonophysics*, **213**, 97-138.

Chapman, T., Meneilly, A. (1991). The displacement patterns associated with a reverse-reactivated, normal growth fault. *Geological Society, London, Special Publications*, **56**, 183-191.

Childs, C., Easton, S.J., Vendeville, B.C., Jackson, M.P.A., Lin, S.T., Walsh, J.J., Watterson, J. (1993). Kinematic analysis of faults in a physical model of growth faulting above a viscous salt analogue. *Tectonophysics*, **228**, 313-329.

Childs, C., Watterson, J., Walsh, J.J. (1995). Fault overlap zones within developing normal fault systems. *Journal of the Geological Society*, **152**, 535-549.

Childs, C., Nicol, A., Walsh, J.J., Watterson, J. (1996). Growth of vertically segmented normal faults. *Journal of Structural Geology*, **18**, 1389-1397.

Childs, C., Nicol, A., Walsh, J.J., Watterson, J. (2003). The growth and propagation of synsedimentary faults. *Journal of Structural Geology*, **25**, 633-648.

Childs, C., Manzocchi, T., Walsh, J.J., Bonson, C.G., Nicol, A., Schöpfer, M.P. (2009). A geometric model of fault zone and fault rock thickness variations. *Journal of Structural Geology*, **31**, 117-127.

Cobbold, P.R., Szatmari, P. (1991). Radial gravitational gliding on passive margins. *Tectonophysics*, **188**, 249-289.

Cobbold, P.R., Meisling, K.E., Mount, V.S. (2001). Reactivation of an obliquely rifted margin, Campos and Santos basins, southeastern Brazil. *AAPG bulletin*, **85**, 1925-1944.

Contreras, J., Anders, M.H., Scholz, C.H. (2000). Growth of a normal fault system: observations from the Lake Malawi basin of the east African rift. *Journal of Structural Geology*, **22**, 159-168.

Cosgrove, J.W., Hillier, R. (2000). Forced-fold development within Tertiary sediments of the Alba Field, UKCS: evidence of the differential compaction and post-depositional sandstone remobilization. *Special Publication - Geological Society of London*, **169**, 61-72.

Cowie, P.A., Scholz, C.H. (1992a). Physical explanation for the displacement-length relationship of faults using a post-yield fracture mechanics model. *Journal of Structural Geology*, **14**, 1133-1148.

Cowie, P.A., Scholz, C.H. (1992b). Displacement-length scaling relationship for faults: data synthesis and discussion. *Journal of Structural Geology*, **14**, 1149-1156.

Crider, J.G., Pollard, D.D. (1998). Fault linkage; three-dimensional mechanical interaction between echelon normal faults. *Journal of Geophysical Research*, **103**, 24,373-324,391.

Davison, I., Alsop, G., Evans, N., Safaricz, M. (2000a). Overburden deformation patterns and mechanisms of salt diapir penetration in the Central Graben, North Sea. *Marine and Petroleum Geology*, **17**, 601-618.

Davison, I., Alsop, I., Birch, P., Elders, C., Evans, N., Nicholson, H., Rorison, P., Wade, D., Woodward, J., Young, M. (2000b). Geometry and late-stage structural evolution of Central Graben salt diapirs, North Sea. *Marine and Petroleum Geology*, **17**, 499-522.

Davison, I. (2007). Geology and tectonics of the South Atlantic Brazilian salt basins. *Geological Society, London, Special Publications*, **272**, 345-359.

Davison, I., Anderson, L., Nuttall, P. (2012). Salt deposition, loading and gravity drainage in the Campos and Santos salt basins. *Geological Society, London, Special Publications*, **363**, 159-174.

Dawers, N.H., Anders, M.H., Scholz, C.H. (1993). Growth of normal faults: Displacement-length scaling. *Geology*, **21**, 1107-1110.

Dawers, N.H., Anders, M.H. (1995). Displacement-length scaling and fault linkage. *Journal of Structural Geology*, **17**, 607-614.

Dawers, N.H., Underhill, J.R. (2000). The role of fault interaction and linkage in controlling synrift stratigraphic sequences: Late Jurassic, Statfjord East area, northern North Sea. *AAPG bulletin*, **84**, 45-64.

Demercian, S., Szatmari, P., Cobbold, P. (1993). Style and pattern of salt diapirs due to thin-skinned gravitational gliding, Campos and Santos basins, offshore Brazil. *Tectonophysics*, **228**, 393-433.

Dooley, T.P., Jackson, M.P.A., Hudec, M.R. (2009). Inflation and deflation of deeply buried salt stocks during lateral shortening. *Journal of Structural Geology*, **31**, 582-600.

Dooley, T.P., Jackson, M.P.A., Jackson, C.A.L., Hudec, M.R., Rodriguez, C.R. (2015). Enigmatic structures within salt walls of the Santos Basin—Part 2: Mechanical explanation from physical modelling. *Journal of Structural Geology*, **75**, 163-187.

Duffy, O.B., Gawthorpe, R.L., Docherty, M., Brocklehurst, S.H. (2013). Mobile evaporite controls on the structural style and evolution of rift basins: Danish Central Graben, North Sea. *Basin Research*, **25**, 310-330.

Dutton, D.M., Trudgill, B.D. (2009). Four-dimensional analysis of the Sembo relay system, offshore Angola: Implications for fault growth in salt-detached settings. *AAPG bulletin*, **93**, 763-794.

Erratt, D., Thomas, G.M., Wall, G.R.T. (1999). The evolution of the Central North Sea Rift. *Geological Society, London, Petroleum Geology Conference series*, **5**, 63-82.

Evans, D., Graham, C., Armour, A., Bathurst, P., (2003). The millennium atlas: Petroleum geology of the central and northern North Sea. The Geological Society of London.

Ferrill, D.A., Morris, A.P. (2001). Displacement gradient and deformation in normal fault systems. *Journal of Structural Geology*, **23**, 619-638.

Ferrill, D.A., Morris, A.P., McGinnis, R.N. (2012). Extensional fault-propagation folding in mechanically layered rocks: The case against the frictional drag mechanism. *Tectonophysics*, **576**, 78-85.

Fiduk, J.C., Rowan, M.G. (2012). Analysis of folding and deformation within layered evaporites in Blocks BM-S-8 & -9, Santos Basin, Brazil. *Geological Society special publication*, **363**, 471-488.

Ford, M., Le Carlier de Veslud, C., Bourgeois, O. (2007). Kinematic and geometric analysis of fault-related folds in a rift setting: The Dannemarie basin, Upper Rhine Graben, France. *Journal of Structural Geology*, **29**, 1811-1830.

Fossen, H., (2010). Structural geology. Cambridge University Press.

Garcia, S.F.d.M., Letouzey, J., Rudkiewicz, J.-L., Danderfer Filho, A., Frizon de Lamotte, D. (2012). Structural modeling based on sequential restoration of gravitational salt deformation in the Santos Basin (Brazil). *Marine and Petroleum Geology*, **35**, 337-353.

Gawthorpe, R., Hurst, J. (1993). Transfer zones in extensional basins: their structural style and influence on drainage development and stratigraphy. *Journal of the Geological Society*, **150**, 1137-1152.

Gawthorpe, R.L., Sharp, I., Underhill, J.R., Gupta, S. (1997). Linked sequence stratigraphic and structural evolution of propagating normal faults. *Geology*, **25**, 795-798.

Gawthorpe, R.L., Leeder, M.R. (2000). Tectono-sedimentary evolution of active extensional basins. *Basin Research*, **12**, 195-218.

Gawthorpe, R.L., Jackson, C.A.-L., Young, M.J., Sharp, I.R., Moustafa, A.R., Leppard, C.W. (2003). Normal fault growth, displacement localisation and the evolution of normal fault populations: the Hammam Faraun fault block, Suez rift, Egypt. *Journal of Structural Geology*, **25**, 883-895.

Ge, H., Jackson, M.P., Vendeville, B.C. (1995). Rejuvenation and subsidence of salt diapirs by regional extension. *Gulf Coast Assiciation of Geological Societies Transactions*, **XLV**, 211-218.

Ge, H., Jackson, M.P., Vendeville, B.C. (1997). Kinematics and dynamics of salt tectonics driven by progradation. *AAPG bulletin*, **81**, 398-423.

Ge, H., Jackson, M.P. (1998). Physical modeling of structures formed by salt withdrawal: Implications for deformation caused by salt dissolution. *AAPG bulletin*, **82**, 228-250.

Gemmer, L., Beaumont, C., Ings, S.J. (2005). Dynamic modelling of passive margin salt tectonics: effects of water loading, sediment properties and sedimentation patterns. *Basin Research*, **17**, 383-402.

Giba, M., Walsh, J.J., Nicol, A. (2012). Segmentation and growth of an obliquely reactivated normal fault. *Journal of Structural Geology*, **39**, 253-267.

Gibbs, A.D. (1984). Structural evolution of extensional basin margins. *Journal of the Geological Society*, **141**, 609-620.

Gillespie, P., Walsh, J.t., Watterson, J. (1992). Limitations of dimension and displacement data from single faults and the consequences for data analysis and interpretation. *Journal of Structural Geology*, **14**, 1157-1172.

Glennie, K.W., (1998). Petroleum geology of the North Sea: basic concepts and recent advances. Blackwell Science, Oxford.

Glennie, K.W., Higham, J., Stemmerik, L., (2003). Permian, in: Evans, D., Graham, C., Armour, A., Bathurst, P. (Eds.), The Millennium Atlas: Petroleum Geology of the Central and Northern North Sea. The Geological Society of London, London, pp. 91-103.

Goldsmith, P., Hudson, G., Van Veen, P., (2003). Triassic, in: Evans, D., Graham, C., Armour, A., Bathurst, P. (Eds.), The Millennium Atlas: Petroleum Geology of the Central and Northern North Sea. The Geological Society of London, London, pp. 105-127.

Goldstein, A., Collins, E. (1984). Deformation of Permian strata overlying a zone of salt dissolution and collapse in the Texas Panhandle. *Geology*, **12**, 314-317.

Gudmundsson, A., Bäckström, K. (1991). Structure and development of the Sveinagja graben, Northeast Iceland. *Tectonophysics*, **200**, 111-125.

Guglielmo, G., Jackson, M.P.A., Vendeville, B.C. (1997). Three-dimensional visualization of salt walls and associated fault systems. *Aapg Bull*, **81**, 46-61.

Guglielmo, G., Vendeville, B.C., Jackson, M.P.A. (1999). Isochores and 3-D visualization of rising and falling slat diapirs. *Marine and petroleum geology*, **16**, 849-861.

Gupta, A., Scholz, C.H. (2000). A model of normal fault interaction based on observations and theory. *Journal of Structural Geology*, **22**, 865-879.

Gupta, S., Cowie, P.A., Dawers, N.H., Underhill, J.R. (1998). A mechanism to explain rift-basin subsidence and stratigraphic patterns through fault-array evolution. *Geology*, **26**, 595-598.

Gutiérrez, F. (2004). Origin of the salt valleys in the Canyonlands section of the Colorado Plateau: Evaporite-dissolution collapse versus tectonic subsidence. *Geomorphology*, **57**, 423-435.

Harding, R., Huuse, M. (2015). Salt on the move: Multi stage evolution of salt diapirs in the Netherlands North Sea. *Marine and Petroleum Geology*, **61**, 39-55.

Hemelsdaël, R., Ford, M. (2016). Relay zone evolution: a history of repeated fault propagation and linkage, central Corinth rift, Greece. *Basin Research*, **28**, 34-56.

Higgins, S., Clarke, B., Davies, R.J., Cartwright, J.A. (2009). Internal geometry and growth history of a thrust-related anticline in a deep water fold belt. *Journal of Structural Geology*, **31**, 1597-1611.

Hillier, R., Cosgrove, J. (2002). Core and seismic observations of overpressure-related deformation within Eocene sediments of the Outer Moray Firth, UKCS. *Petroleum Geoscience*, **8**, 141-149.

Hodgson, N.A., Farnsworth, J., Fraser, A.J. (1992). Salt-related tectonics, sedimentation and hydrocarbon plays in the Central Graben, North Sea, UKCS. *Geological Society, London, Special Publications*, **67**, 31-63.

Hongxing, G., Anderson, J.K. (2007). Fault Throw Profile and Kinematics of Normal Fault.-Conceptual Models and Geologic Examples. *Geological Journal of China Universities*, **13**, 75-88.

Hospers, J., Rathore, J.S., Jianhua, F., Finnstrøm, E.G., Holthe, J. (1988). Salt tectonics in the Norwegian—Danish Basin. *Tectonophysics*, **149**, 35-60.

Hudec, M.R., Jackson, M.P.A. (2002). Structural segmentation, inversion, and salt tectonics on a passive margin: Evolution of the Inner Kwanza Basin, Angola. *Geological Society of America Bulletin*, **114**, 1222-1244.

Hudec, M.R., Jackson, M.P.A. (2004). Regional restoration across the Kwanza Basin, Angola: Salt tectonics triggered by repeated uplift of a metastable passive margin. *AAPG Bulletin*, **88**, 971-990.

Hudec, M.R., Jackson, M.P.A. (2006). Advance of allochthonous salt sheets in passive margins and orogens. *Aapg Bulletin*, **90**, 1535-1564.

Hudec, M.R., Jackson, M.P.A. (2007). Terra infirma: Understanding salt tectonics. *Earth-Sci Rev*, **82**, 1-28.

Hudec, M.R., Jackson, M.P.A. (2011). The salt mine: a digital atlas of salt tectonics. The University of Texas at Austin, Bureau of Economic Geology, Udden Book Series No. 5. *AAPG Memoir*, **99**, 305.

Huggins, P., Watterson, J., Walsh, J., Childs, C. (1995). Relay zone geometry and displacement transfer between normal faults recorded in coal-mine plans. *Journal of Structural Geology*, **17**, 1741-1755.

Husmo, T., Hamar, G., Høiland, O., Johannessen, E.P., Rømuld, A., Spencer, A., Titterton, R., (2003). Lower and Middle Jurassic, in: Evans, D., Graham, C., Armour, A., Bathurst, P. (Eds.), The Millennium Atlas: Petroleum Geology of the Central and Northern North Sea. The Geological Society of London, London, pp. 129-155.

Isaksen, D., Tonstad, K., (1989). A Revised Cretaceous and Tertiary lithostratigraphic nomenclature for the Norwegian North Sea. Oljedirektoratet, Stavanger.

Jackson, C.A.L., Gawthorpe, R.L., Sharp, I.R. (2002). Growth and linkage of the East Tanka fault zone, Suez rift: structural style and syn-rift stratigraphic response. *Journal of the Geological Society*, **159**, 175-187.

Jackson, C.A.L. (2012). The initiation of submarine slope failure and the emplacement of mass transport complexes in salt-related minibasins: A three-dimensional seismic-reflection case study from the Santos Basin, offshore Brazil. *Geological Society of America Bulletin*, **124**, 746-761.

Jackson, C.A.L., Lewis, M.M. (2012). Origin of an anhydrite sheath encircling a salt diapir and implications for the seismic imaging of steep-sided salt structures, Egersund Basin, Northern North Sea. *Journal of the Geological Society*, **169**, 593-599.

Jackson, C.A.L., Chua, S.-T., Bell, R., Magee, C. (2013). Structural style and early stage growth of inversion structures: 3D seismic insights from the Egersund Basin, offshore Norway. *Journal of Structural Geology*, **46**, 167-185.

Jackson, C.A.L., Lewis, M.M. (2013). Physiography of the NE margin of the Permian Salt Basin: new insights from 3D seismic reflection data. *Journal of the Geological Society*, **170**, 857-860.

Jackson, C.A.L., Rotevatn, A. (2013). 3D seismic analysis of the structure and evolution of a salt-influenced normal fault zone: A test of competing fault growth models. *Journal of Structural Geology*, **54**, 215-234.

Jackson, C.A.L., Jackson, M.P.A., Hudec, M.R., Rodriguez, C. (2014a). Internal structure, kinematics, and growth of a salt wall: Insights from 3-D seismic data. *Geology*, **42**, 307-310.

Jackson, C.A.L., Rodriguez, C.R., Rotevatn, A., Bell, R.E. (2014b). Geological and geophysical expression of a primary salt weld: An example from the Santos Basin, Brazil. *Interpretation*, **2**, SM77-SM89.

Jackson, C.A.L., Jackson, M.P.A., Hudec, M.R., Rodriguez, C.R. (2015). Enigmatic structures within salt walls of the Santos Basin—Part 1: Geometry and kinematics from 3D seismic reflection and well data. *Journal of Structural Geology*, **75**, 135-162.

Jackson, C.A.L., Lewis, M.M. (2016). Structural style and evolution of a salt-influenced rift basin margin; the impact of variations in salt composition and the role of polyphase extension. *Basin Research*, **28**, 81-102.

Jackson, C.A.L. (in press). Growth of a Salt-Detached Normal Fault and Controls on throw Rate Variability; Gudrun Field, South Viking Graben, Offshore Norway. *AAPG Memoir*.

Jackson, C.A.L., Bell, R.E., Rotevatn, A., Tvedt, A.B.M. (in review). Techniques to determine the style of growth of seismic-scale syn-sedimentary normal faults. *Geological Society, London, Special Publications*.

Jackson, J., McKenzie, D. (1983). The geometrical evolution of normal fault systems. *Journal of Structural Geology*, **5**, 471-482.

Jackson, J.A. (1987). Active normal faulting and crustal extension. *Geological Society, London, Special Publications*, **28**, 3-17.

Jackson, M.P.A., Talbot, C.J. (1989). Anatomy of mushroom-shaped diapirs. *Journal of Structural Geology*, **11**, 211-230.

Jackson, M.P.A., Vendeville, B.C. (1994). Regional extension as a geologic trigger for diapirism. *Geological society of America bulletin*, **106**, 57-73.

Jackson, M.P.A., Vendeville, B.C., Schultzela, D.D. (1994). Structural Dynamics of Salt Systems. *Annu Rev Earth Pl Sc*, **22**, 93-117.

Jackson, M.P.A., Hudec, M.R. (2005). Stratigraphic record of translation down ramps in a passive-margin salt detachment. *Journal of Structural Geology*, **27**, 889-911.

Jordan, P.G. (1987). The deformational behaviour of bimineralic limestone-halite aggregates. *Tectonophysics*, **135**, 185-197.

Kane, K.E., Jackson, C.A.L., Larsen, E. (2010). Normal fault growth and fault-related folding in a salt-influenced rift basin: South Viking Graben, offshore Norway. *Journal of Structural Geology*, **32**, 490-506.

Karner, G.D. (2000). Rifts of the Campos and Santos Basins, Southeastern Brazil: Distribution and Timing, in: Mello, M.R., Katz, B. (Eds.), Petroleum Systems of South Atlantic Margins. *AAPG Memoir*, **73**, 301-315.

Kattenhorn, S.A., Aydin, A., Pollard, D.D. (2000). Joints at high angles to normal fault strike: an explanation using 3-D numerical models of fault-perturbed stress fields. *Journal of Structural Geology*, **22**, 1-23.

Kim, Y.-S., Sanderson, D.J. (2005). The relationship between displacement and length of faults: a review. *Earth-Sci Rev*, **68**, 317-334.

Koyi, H., Petersen, K. (1993). Influence of basement faults on the development of salt structures in the Danish Basin. *Marine and Petroleum Geology*, **10**, 82-94.

Krantz, R.W. (1988). Multiple fault sets and three-dimensional strain: theory and application. *Journal of Structural Geology*, **10**, 225-237.

Lewis, M.M., Jackson, C.A.L., Gawthorpe, R.L. (2013). Salt-influenced normal fault growth and forced folding: The Stavanger Fault System, North Sea. *Journal of Structural Geology*, **54**, 156-173.

Mannie, A.S., Jackson, C.L., Hampson, G.J. (2014). Structural controls on the stratigraphic architecture of net-transgressive shallow-marine strata in a salt-influenced rift basin: Middle-to-Upper Jurassic Egersund Basin, Norwegian North Sea. *Basin Research*, **26**, 1-26.

Mansfield, C.S., Cartwright, J.A. (1996). High resolution fault displacement mapping from three-dimensional seismic data: evidence for dip linkage during fault growth. *Journal of Structural Geology*, **18**, 249-263.

Mansfield, C.S., Cartwright, J.A. (2001). Fault growth by linkage: observations and implications from analogue models. *Journal of Structural Geology*, **23**, 745-763.

Marsh, N., Imber, J., Holdsworth, R.E., Brockbank, P., Ringrose, P. (2010). The structural evolution of the Halten Terrace, offshore Mid-Norway: extensional fault growth and strain localisation in a multi-layer brittle-ductile system. *Basin Research*, **22**, 195-214.

Mauduit, T., Guerin, G., Brun, J.-P., Lecanu, H. (1997). Raft tectonics: the effects of basal slope angle and sedimentation rate on progressive extension. *Journal of Structural Geology*, **19**, 1219-1230.

Mauduit, T., Brun, J.P. (1998). Growth fault/rollover systems: Birth, growth, and decay. *Journal of Geophysical Research: Solid Earth (1978–2012)*, **103**, 18119-18136.

Maurin, J.-C., Niviere, B. (2000). Extentional forced folding and decollement of the pre-rift series along the Rhine graben and their influence on the geometry of the syn-rift sequences. *Special publication - Geological Society of London*, **169**, 73-86.

McClay, K.R. (1990). Extensional fault systems in sedimentary basins: a review of analogue model studies. *Marine and Petroleum Geology*, **7**, 206-233.

McLeod, A.E., Underhill, J. (2000). The propagation and linkage of normal faults: insights from the Strathspey–Brent–Statfjord fault array, northern North Sea. *Basin Research*, **12**, 263-284.

Meisling, K.E., Cobbold, P.R., Mount, V.S. (2001). Segmentation of an Obliquely Rifted Margin, Campos and Santos Basins, Southeastern Brazil. *AAPG Bulletin*, **85**, 1903-1924.

Modica, C.J., Brush, E.R. (2004). Postrift sequence stratigraphy, paleogeography, and fill history of the deep-water Santos Basin, offshore southeast Brazil. *Aapg Bulletin*, **88**, 923-945.

Mohriak, W., Nemčok, M., Enciso, G. (2008). South Atlantic divergent margin evolution: rift-border uplift and salt tectonics in the basins of SE Brazil. *Geological Society, London, Special Publications*, **294**, 365-398.

Montaron, B., Tapponnier, P. (2010). A quantitative model for salt deposition in actively spreading basins. *AAPG Search and Discovery*, Article #30117.

Morley, C., Back, S., Van Rensbergen, P., Crevello, P., Lambiase, J. (2003). Characteristics of repeated, detached, Miocene–Pliocene tectonic inversion events, in a large delta province on an active margin, Brunei Darussalam, Borneo. *Journal of structural geology*, **25**, 1147-1169.

Morley, C.K. (2002). Evolution of large normal faults: Evidence from seismic reflection data. *AAPG bulletin*, **86**, 961-978.

Muraoka, H., Kamata, H. (1983). Displacement distribution along minor fault traces. *Journal of Structural Geology*, **5**, 483-495.

Møller, J.J., Rasmussen, E.S. (2003). Middle Jurassic–Early Cretaceous rifting of the Danish Central Graben. *Geological Survey of Denmark and Greenland Bulletin*, **1**, 247-264.

Nalpas, T., Brun, J.-P. (1993). Salt flow and diapirism related to extension at crustal scale. *Tectonophysics*, **228**, 349-362.

Nicol, A., Watterson, J., Walsh, J.J., Childs, C. (1996). The shapes, major axis orientations and displacement patterns of fault surfaces. *Journal of Structural Geology*, **18**, 235-248.

Pascoe, R., Hooper, R., Storhaug, K., Harper, H., (1999). Evolution of extensional styles at the southern termination of the Nordland Ridge, Mid-Norway: a response to variations in coupling above Triassic salt, Geological Society, London, Petroleum Geology Conference series. Geological Society of London, pp. 83-90.

Peacock, D.C.P., Sanderson, D.J. (1991). Displacements, segment linkage and relay ramps in normal fault zones. *Journal of Structural Geology*, **13**, 721-733.

Peacock, D.C.P., Sanderson, D.J. (1994). Geometry and development of relay ramps in normal fault systems. *AAPG Bulletin*, **78**, 147-165.

Penge, J., Taylor, B., Huckerby, J., Munns, J., (1993). Extension and salt tectonics in the East Central Graben, Geological Society, London, Petroleum Geology Conference series. Geological Society of London, pp. 1197-1209.

Petersen, K., Clausen, O., Korstgård, J. (1992). Evolution of a salt-related listric growth fault near the D-1 well, block 5605, Danish North Sea: displacement history and salt kinematics. *Journal of Structural Geology*, **14**, 565-577.

Pollard, D.D., Johnson, A.M. (1973). Mechanics of growth of some laccolithic intrusions in the Henry mountains, Utah, II: Bending and failure of overburden layers and sill formation. *Tectonophysics*, **18**, 311-354.

Quirk, D.G., Schødt, N., Lassen, B., Ings, S.J., Hsu, D., Hirsch, K.K., Von Nicolai, C. (2012). Salt tectonics on passive margins: examples from Santos, Campos and Kwanza basins. *Geological Society, London, Special Publications*, **363**, 207-244.

Richard, P., Krantz, R.W. (1991). Experiments on fault reactivation in strike-slip mode. *Tectonophysics*, **188**, 117-131.

Richardson, N.J., Underhill, J.R., Lewis, G. (2005). The role of evaporite mobility in modifying subsidence patterns during normal fault growth and linkage, Halten Terrace, Mid-Norway. *Basin Research*, **17**, 203-223.

Rotevatn, A., Jackson, C.A.-L. (2014). 3D structure and evolution of folds during normal fault dip linkage. *Journal of the Geological Society*, **171**, 821-829.

Rouby, D., Guillocheau, F., Robin, C., Bouroullec, R., Raillard, S., Castelltort, S., Nalpas, T. (2003). Rates of deformation of an extensional growth fault/raft system (offshore Congo, West African margin) from combined accommodation measurements and 3-D restoration. *Basin Research*, **15**, 183-200.

Rowan, M.G. (1993). A systematic technique for the sequential restoration of salt structures. *Tectonophysics*, **228**, 331-348.

Rowan, M.G. (1997). Three-dimensional geometry and evolution of a segmented detachment fold, Mississippi Fan foldbelt, Gulf of Mexico. *Journal of Structural Geology*, **19**, 463-480.

Rowan, M.G., Hart, B.S., Nelson, S., Flemings, P.B., Trudgill, B.D. (1998). Three-dimensional geometry and evolution of a salt-related growth-fault array: Eugene Island 330 field, offshore Louisiana, Gulf of Mexico. *Marine and Petroleum Geology*, **15**, 309-328.

Rowan, M.G., Jackson, M.P.A., Trudgill, B.D. (1999). Salt-related fault families and fault welds in the northern Gulf of Mexico. *AAPG Bulletin*, **83**, 1454-1484.

Rowan, M.G., Lawton, T.F., Giles, K.A., Ratliff, R.A. (2003). Near-salt deformation in La Popa basin, Mexico, and the northern Gulf of Mexico: A general model for passive diapirism. *AAPG bulletin*, **87**, 733-756.

Rowan, M.G., Peel, F.J., Vendeville, B.C. (2004). Gravity-driven fold belts on passive margins, in: K. R. McClay, ed., Thrust tectonics and hydrocarbon systems. *AAPG Memoir*, **82**, 157-182.

Rowan, M.G., Vendeville, B.C. (2006). Foldbelts with early salt withdrawal and diapirism: physical model and examples from the northern Gulf of Mexico and the Flinders Ranges, Australia. *Marine and Petroleum Geology*, **23**, 871-891.

Rowan, M.G., Peel, F.J., Vendeville, B.C., Gaullier, V. (2012). Salt tectonics at passive margins: Geology versus models – Discussion. *Marine and Petroleum Geology*, **37**, 184-194.

Rykkelid, E., Fossen, H. (2002). Layer rotation around vertical fault overlap zones: observations from seismic data, field examples, and physical experiments. *Marine and Petroleum Geology*, **19**, 181-192.

Schlische, R.W. (1995). Geometry and origin of fault-related folds in extensional settings. *AAPG bulletin*, **79**, 1661-1678.

Schlische, R.W., Young, S.S., Ackermann, R.V., Gupta, A. (1996). Geometry and scaling relations of a population of very small rift-related normal faults. *Geology*, **24**, 683-686.

Schultz-Ela, D.D., Jackson, M.P.A., Vendeville, B.C. (1993). Mechanics of active salt diapirism. *Tectonophysics*, **228**, 275-312.

Schultz, R.A., Fossen, H. (2002). Displacement–length scaling in three dimensions: the importance of aspect ratio and application to deformation bands. *Journal of Structural Geology*, **24**, 1389-1411.

Schultz, R.A., Okubo, C.H., Wilkins, S.J. (2006). Displacement-length scaling relations for faults on the terrestrial planets. *Journal of Structural Geology*, **28**, 2182-2193.

Schöpfer, M.P., Childs, C., Walsh, J.J. (2006). Localisation of normal faults in multilayer sequences. *Journal of structural geology*, **28**, 816-833.

Soliva, R., Benedicto, A. (2005). Geometry, scaling relations and spacing of vertically restricted normal faults. *Journal of Structural Geology*, **27**, 317-325.

Soliva, R., Benedicto, A., Schultz, R., Maerten, L., Micarelli, L. (2008). Displacement and interaction of normal fault segments branched at depth: Implications for fault growth and potential earthquake rupture size. *Journal of Structural Geology*, **30**, 1288-1299.

Stewart, S.A., Coward, M.P. (1995). Synthesis of salt tectonics in the southern North Sea, UK. *Marine and Petroleum Geology*, **12**, 457-475.

Stewart, S.A., Harvey, M.J., Otto, S.C., Weston, P.J. (1996). Influence of salt on fault geometry: examples from the UK salt basins. *Geological Society, London, Special Publications*, **100**, 175-202.

Stewart, S.A., Ruffell, A.H., Harvey, M.J. (1997). Relationship between basement-linked and gravity-driven fault systems in the UKCS salt basins. *Marine and Petroleum Geology*, **14**, 581-604.

Stewart, S.A. (1999). Geometry of thin-skinned tectonic systems in relation to detachment layer thickness in sedimentary basins. *Tectonics*, **18**, 719-732.

Stovba, S.M., Stephenson, R.A. (2002). Style and timing of salt tectonics in the Dnieper-Donets Basin (Ukraine): implications for triggering and driving mechanisms of salt movement in sedimentary basins. *Marine and Petroleum Geology*, **19**, 1169-1189.

Strozyk, F., Van Gent, H., Urai, J., Kukla, P. (2012). 3D seismic study of complex intra-salt deformation: An example from the Upper Permian Zechstein 3 stringer, western Dutch offshore. *Geological Society, London, Special Publications*, **363**, 489-501.

Sørensen, S., Morizot, H., Skottheim, S. (1992). A tectonostratigraphic analysis of the Southeast Norwegian North Sea basin. *Special Publication - Norwegian Petroleum Society, NPF*, **1**, 19-42.

Taylor, S.K., Nicol, A., Walsh, J.J. (2008). Displacement loss on growth faults due to sediment compaction. *Journal of Structural Geology*, **30**, 394-405.

Thorsen, C.E. (1963). Age of growth faulting in southeast Louisiana. *Gulf Coast Association of Geological Societies* **13**, 103-110.

Trudgill, B., Cartwright, J.A. (1994). Relay-ramp forms and normal-fault linkages, Canyonlands National Park, Utah. *Geological Society of America Bulletin*, **106**, 1143-1157.

Turner, S., Regelous, M., Kelley, S., Hawkesworth, C., Mantovani, M. (1994). Magmatism and continental break-up in the South Atlantic: high precision40Ar-39Ar geochronology. *Earth and Planetary Science Letters*, **121**, 333-348.

Tvedt, A.B.M., Rotevatn, A., Jackson, C.A.L., Fossen, H., Gawthorpe, R.L. (2013). Growth of normal faults in multilayer sequences; a 3D seismic case study from the Egersund Basin, Norwegian North Sea. *Journal of Structural Geology*, **55**, 1-20.

Tvedt, A.B.M., Rotevatn, A., Jackson, C.A.-L., Fossen, H. (in review). Growth of Supra-Salt Normal Fault Arrays in the Santos Basin. *Journal of Structural Geology*.

Underhill, J.R., Partington, M.A. (1993). Jurassic thermal doming and deflation in the North Sea: implications of the sequence stratigraphic evidence. *Geological Society, London, Petroleum Geology Conference series*, **4**, 337-345.

Van Gent, H., Urai, J.L., De Keijzer, M. (2011). The internal geometry of salt structures–A first look using 3D seismic data from the Zechstein of the Netherlands. *Journal of Structural Geology*, **33**, 292-311.

van Keken, P.E., Spiers, C.J., van den Berg, A.P., Muyzert, E.J. (1993). The effective viscosity of rocksalt: implementation of steady-state creep laws in numerical models of salt diapirism. *Tectonophysics*, **225**, 457-476.

Van Rensbergen, P., Morley, C., Ang, D., Hoan, T., Lam, N. (1999). Structural evolution of shale diapirs from reactive rise to mud volcanism: 3D seismic data from the Baram delta, offshore Brunei Darussalam. *Journal of the Geological Society*, **156**, 633-650.

Vejbæk, O., Andersen, C. (2002). Post mid-Cretaceous inversion tectonics in the Danish Central Graben—regionally synchronous tectonic events. *Bulletin of the Geological Society of Denmark*, **49**, 129-144.

Vendeville, B.C., Jackson, M.P.A. (1992a). The fall of diapirs during thin-skinned extension. *Marine and Petroleum Geology*, **9**, 354-371.

Vendeville, B.C., Jackson, M.P.A. (1992b). The rise of diapirs during thin-skinned Extension. *Marine and Petroleum Geology*, **9**, 331-353.

Vendeville, B.C., Ge, H., Jackson, M.P.A. (1995). Scale models of salt tectonics during basement-involved extension. *Petroleum Geoscience*, **1**, 179-183.

Viana, A.R. (2001). Seismic expression of shallow-to deep-water contourites along the south-eastern Brazilian margin. *Marine Geophysical Researches*, **22**, 509-521.

Vollset, J., Doré, A.G. (1984). A revised Triassic and Jurassic lithostratigraphic nomenclature for the Norwegian North Sea. *Norwegian Petroleum Directorate Bulletin*, **3**.

Wagner III, B.H., Jackson, M.P.A. (2011). Viscous flow during salt welding. *Tectonophysics*, **510**, 309-326.

Walsh, J.J., Watterson, J. (1988). Analysis of the relationship between displacements and dimensions of faults. *Journal of Structural Geology*, **10**, 239-247.

Walsh, J.J., Watterson, J. (1990). New methods of fault projection for coalmine planning. *Proceedings of the Yorkshire Geological and Polytechnic Society*, **48**, 209-219.

Walsh, J.J., Watterson, J. (1991). Geometric and kinematic coherence and scale effects in normal fault systems. *Geological Society, London, Special Publications*, **56**, 193-203.

Walsh, J.J., Nicol, A., Childs, C. (2002). An alternative model for the growth of faults. *Journal of Structural Geology*, **24**, 1669-1675.

Walsh, J.J., Bailey, W., Childs, C., Nicol, A., Bonson, C. (2003). Formation of segmented normal faults: a 3-D perspective. *Journal of Structural Geology*, **25**, 1251-1262.

Watterson, J. (1986). Fault dimensions, displacements and growth. *Pure and Applied Geophysics*, **124**, 365-373.

Williams, G., Powell, C., Cooper, M. (1989). Geometry and kinematics of inversion tectonics. *Geological Society, London, Special Publications*, **44**, 3-15.

Wilson, P., Elliott, G.M., Gawthorpe, R.L., Jackson, C.A.-L., Michelsen, L., Sharp, I.R. (2013). Geometry and segmentation of an evaporite-detached normal fault array: 3D seismic analysis of the southern Bremstein Fault Complex, offshore mid-Norway. *Journal of Structural Geology*, **51**, 74-91.

Withjack, M.O., Olson, J., Peterson, E. (1990). Experimental Models of Extensional Forced Folds (1). *AAPG Bulletin*, **74**, 1038-1054.

Withjack, M.O., Callaway, S. (2000). Active Normal Faulting Beneath a Salt Layer: An Experimental Study of Deformation Patterns in the Cover Sequence. *AAPG Bulletin*, **84**, 627-651.

Withjack, M.O. (2002). Rift-basin structure and its influence on sedimentary systems. *In: Sedimentation in Continental Rifts. SEPM Special Publication*, **73**, 57-81.

Young, M.J., Gawthorpe, R.L., Hardy, S. (2001). Growth and linkage of a segmented normal fault zone; the Late Jurassic Murchison–Statfjord North Fault, northern North Sea. *Journal of Structural Geology*, **23**, 1933-1952.

Zanella, E., Coward, M., (2003). Structural framework, in: Evans, D., Graham, C., Armour, A., Bathurst, P. (Eds.), The Millennium Atlas: Petroleum Geology of the Central and Northern North Sea. The Geological Society of London, London, pp. 45-59.

Ziegler, P.A. (1992). North Sea rift system. *Tectonophysics*, **208**, 55-75.

Appendix

Poster Presentation: Annual Convention and Exhibition AAPG
31st of May – 3rd of June 2015, Denver

Growth of Supra-Salt Normal Fault Arrays

Anette Broch Mathisen Tvedt [1, 2], Atle Rotevatn [2], Christopher A-L. Jackson[3] and Haakon Fossen [2, 4]

[1] Centre for Integrated Petroleum Research, University of Bergen, Allégaten 41, 5007 Bergen, Norway
[2] Department of Earth Science, University of Bergen, Allégaten 41, 5007 Bergen, Norway
[3] Basins Research Group (BRG), Department of Earth Science and Engineering, Imperial College, Prince Consort Road, London SW7 2BP, UK
[4] Museum of Natural History, University of Bergen, PO BOX 7803, N-5007 Bergen, Norway

The structural style and evolution of normal fault systems above mobile salt is less understood compared to those developed in rifts where strong variations in mechanical stratigraphy are absent. In this study we examine how extensional fault arrays evolve during the reactive rise, collapse and subsequent active rise of salt diapirs. We use 3D seismic data from the Egersund Basin, offshore Norway to investigate the three-dimensional growth history of supra-salt fault arrays. We study two fault arrays that are orientated nearly perpendicular to one another; Fault Array 1 (FA1), which trends NW, is located above a c. 600 m thick salt wall separated by tall (2.7 km) salt stocks, whereas Fault Array 2 (FA2), trends N and is developed above a relatively thin (c. 100 m) salt layer and a sub-salt fault array. FA1 is c. 35 km long and comprises segments up to 16 km long with throws up to 2 km. FA2 is 16 km long, comprises segments up to 6 km long with throws up to 230 m. The evolution of these two fault arrays is divided into four main stages; (1) initial syn-sedimentary fault growth during the Late Triassic–to-Middle Jurassic; (2) continued growth of FA1 during the Late Jurassic–to-Early Cretaceous at a time activity on FA2 has ceased; (3) Late Cretaceous reactivation of FA1 and FA2; and (4) death of FA2 by the end of the Late Cretaceous, whereas FA1 continued to grow until the Neogene. Even though the fault arrays were active during broadly the same time period and both initiated by cover stretching related to activity on the large, thick-skinned, basin-bounding faults, their growth mechanisms are different; FA1 was initiated through gliding, with further slip controlled by reactive

diapirism, diapir collapse and active diapirism, which occurred simultaneously along strike during stages 2 to 4. FA2 was initiated by re-activation of a pre-existing sub-salt fault array, mainly through kinematic coupling, during stage 1, before being buried during stage 2. Parts of FA2 were then reactivated during stage 3, in response to salt mobilization driven by basin inversion. The reactivated faults are located where the underlying salt is thick, while the non-reactivated faults are found where salt is depleted. This study illustrates how two closely related supra-salt fault arrays may evolve differently in response to different salt-related forcing mechanisms.

Poster Presentation: Geometry and growth of normal faults conference
25th-27th of June 2014, Geological Society of London

Normal fault growth related to multi-phase salt diapirism and thin skinned extension, Egersund Basin, Norwegian North Sea

Anette Broch Mathisen Tvedt [1, 2], Atle Rotevatn [2], Christopher A-L. Jackson[3], Haakon Fossen2, 4, Robert L. Gawthorpe 2

1 Centre for Integrated Petroleum Research, University of Bergen, Allégaten 41, 5007 Bergen, Norway
2 Department of Earth Science, University of Bergen, Allégaten 41, 5007 Bergen, Norway
3 Basins Research Group (BRG), Department of Earth Science and Engineering, Imperial College, Prince Consort Road, London SW7 2BP, UK
4 Museum of Natural History, University of Bergen, PO BOX 7803, N-5007 Bergen, Norway

Many salt diapirs are accompanied by crestal graben structures in overlying sedimentary layers. The growth and style of such supra-salt grabens are controlled by the evolution of the underlying diapir. Structures related to the rise and fall of diapirs during thin-skinned extension are particularly well studied in cross-sections, but although a number of recent studies focus on the 3D evolution of normal fault growth in salt-influenced settings, the effects of salt on lateral fault growth and map-view fault geometries are clearly far less constrained than those observed in cross-section. The reason for this is probably that high-resolution 3D seismic data have only become extensively used in geological research over the past decade or so. In this study we present a three-dimensional analysis of the structural style and growth history of supra-salt normal fault arrays that have formed in response to growth and demise of an array of salt walls and stocks in the Egersund Basin, Norwegian North Sea. More specifically we assess fault kinematics and salt wall evolution through time, and investigate the effect that lateral migration of salt along the salt walls and into the salt stocks has on the evolution of the overlying fault systems. We use: (i) 3D seismic mapping of faults and age-constrained growth strata; (ii) mapping of three-dimensional throw distributions on fault surfaces; and (iii) expansion indices and thickness maps.

The studied thin-skinned ENE-WSE striking normal fault system is developed above a salt wall, bounding two c. 15 km long, 8 km wide grabens separated by a large (3.5 km

tall) salt stock. Individual fault segments are up to 15 km long and are relatively planar in cross-section. In map-view the faults are relatively straight, although they change strike by c. 90° immediately adjacent to the central salt stock. We interpret the change in fault strike immediately adjacent to the salt stock to reflect perturbation of the regional stress field driving thin-skinned by hoop stresses surrounding the stock. Our quantitative analysis of fault kinematics, based on the construction of throw-distance (T-x) and throw-depth (T-z) plots in addition to strike projection of fault throw, lead us to conclude that thin-skinned fault systems developed in two stages; i) nucleation and initial growth in Middle to Late Jurassic times, contemporaneous with reactive diapirism and salt wall growth, and ii) renewed fault growth in the Lower Cretaceous linked with extensional collapse of walls. Furthermore, thickness maps and expansion indices indicate that the salt stock started to grow in the Lower Cretaceous, contemporaneous with the most rapid accumulation of displacement on the overlying fault array.

This study showcases a three-dimensional example of how multi-phase salt diapirism may influence lateral fault growth and fault geometry both vertically and laterally during reactive diapirism and extensional collapse of salt walls. Furthermore, this study tests previous analogue models of fault kinematics and salt tectonics during the rise and fall of salt diapirs.

Poster Presentation: Annual Convention and Exhibition AAPG
19th-22nd of May 2013, Pittsburgh

Supra-salt extensional fault evolution in the Santos Basin (Brazil)

Anette Broch Mathisen Tvedt [1, 2], Atle Rotevatn [1, 2], Christopher A-L Jackson[3], Rob Gawthorpe 1,Haakon Fossen[1, 2]

1 Department of Earth Science, University of Bergen, Allégaten 41, 5007 Bergen, Norway
2 Centre for Integrated Petroleum Research, University of Bergen, Allégaten 41, 5007 Bergen, Norway
3 Department of Earth Science & Engineering, Imperial College, London SW7 2AZ, UK

The structural style and evolution of normal fault arrays related to salt-mobilization is less well understood than crustal scale rift basins. In this study we use three-dimensional seismic data from the Santos Basin to characterize supra-salt extensional fault arrays and assess the influence of mobile evaporites on their evolution. To evaluate the structural style and growth history of the fault arrays we apply the following methods: 1) 3D mapping of faults and age-constrained growth strata, 2) geometric and kinematic classification of fault segments, and 3) mapping of three-dimensional displacement distributions on fault surfaces. The supra-salt fault arrays develop either along the edge of, or at the center along the top of, the flat-topped salt stocks. The fault arrays tip out downward into large salt stocks and display relatively long, hard-linked segments, up to . Throw analyses suggest a staged evolution of (1) rapid developed surface-breaching faults (2) which then as a consequence have propagated laterally and have caused hard linkage of fault segments and development of fault arrays. Salt rollers are present in the footwall of the faults, and increase in amplitude with increasing displacement. We hypothesize that the localization of the fault arrays may result from (i) internal collapse of an enigmatic sequence within the salt stock (ii) related to salt heterogeneity, (iii) salt stock geometry and flank steepness, or (iv) pre-existing irregularities at the top of the salt stocks at the time of deposition of the overlying strata.

In this study we will highlight the importance of detailed structural analyses for determining the structural evolution of salt- influenced fault arrays. The studied fault

arrays above the salt stocks in the Santos Basin seem affected by local mobilization of salt. Based on the three-dimensional displacement analyses we conclude that salt mobilization allows faults to develop laterally where strain is accommodated for by the salt rather than the surrounding rocks.

Presentation: Winter Conference - Norwegian Geological Society
8-10th of January 2013, Oslo

Growth and linkage of a salt-influenced extensional fault array: Egersund Basin, Norwegian North Sea

Anette Broch Mathisen Tvedt [1, 2], Atle Rotevatn [1, 2], Christopher A-L Jackson [3], Haakon Fossen [1, 2], Robert L. Gawthorpe [1]

[1] Department of Earth Science, University of Bergen, Allégaten 41, 5007 Bergen, Norway
[2] Centre for Integrated Petroleum Research, University of Bergen, Allégaten 41, 5007 Bergen, Norway
[3] Department of Earth Science & Engineering, Imperial College, London SW7 2AZ, UK

In this this study we illustrate the structural style and growth history of a fault array in response to salt-mobilization by the use of 3D seismic reflection and well data from the Egersund Basin, Norwegian North Sea. The studied thin-skinned NE-SW striking normal fault array (c. 16 km long and approximately 6 km wide) developed in response to the growth of a low-relief salt pillow. General mapping, geometric analysis and fault displacement analysis reveal differences between the fault evolution in the southern part of the area where salt is thick, and the northern part, where salt is thin or depleted, in terms of geometry, timing and fault linkage or coupling between faults in the subsalt section and the cover. Present-day throw distributions suggest both lateral and vertical growth and linkage. Furthermore, the intricate but systematic style of displacement and growth suggests a staged evolution of; (1) initial syn-sedimentary fault growth during the late Triassic- middle Jurassic contemporaneous with growth of a salt pillow to the west, and (2) subsequent fault initiation at a shallower level contemporaneous with remobilization of the salt, with downward fault propagation and linkage with pre-existing stage 1 faults, resulting in reactivated fault surfaces in the late Cretaceous-early Tertiary. Based on the three-dimensional displacement analyses we conclude that salt mobilization controls the development of the fault array, where reactivation only occurs where salt is not depleted. A close connection is observed between pre-salt (sub-salt) fault occurrence and the localization of shallower faults formed during salt

mobilization, showing that strain was largely transferred through the salt layer during the fault development.

Three-dimensional seismic data have provided important insights into the development of salt-influenced normal fault arrays; in particular, we will highlight the lateral growth and linkage and the importance of dip linkage and blind fault reactivation. Comprehensive three-dimensional fault displacement analysis is therefore important, capturing a level of detail in displacement distribution and fault history that would otherwise be lost.

Poster presentation: Industrial Structural Geology Principles, Techniques & Integrations 28-30th of November 2012, London

Industry applications of quantitative fault analysis illuminated by a case study from the Egersund Basin, offshore southern Norway

Anette Broch Mathisen Tvedt 1, 2, Christopher A-L Jackson3, Atle Rotevatn 1, 2, Haakon Fossen1, 2, Rob Gawthorpe 1

1 Department of Earth Science, University of Bergen, Allégaten 41, 5007 Bergen, Norway
2 Centre for Integrated Petroleum Research, University of Bergen, Allégaten 41, 5007 Bergen, Norway
3 Department of Earth Science & Engineering, Imperial College, London SW7 2AZ, UK

In this this study we illustrate how fault displacement- and sedimentary growth analyses can be integrated to document the three-dimensional structural style and growth history of a fault array. The combination of different analyses such as displacement-length profiles, vertical throw distribution, thickness maps and expansion indices can yield important knowledge about the temporal and spatial evolution of a fault array. The application and integration of these methods will be illustrated by a case study utilizing three-dimensional reflection seismic in the analysis of a fault array in the Egersund Basin, Norwegian North Sea. The studied thin-skinned NE-SW striking normal fault array (c. 16 km long and approximately 6 km wide) developed as a response to the growth of a low-relief salt pillow. General mapping and analysis of fault displacement distribution and geometry were undertaken, revealing differences in the geometric and temporal evolution between the southern part of the array where salt is thick, and the northern part of the array, where salt is thin or depleted. The intricate but systematic style of displacement and growth suggest a staged evolution of; (1) initial syn-sedimentary fault growth during the late Triassic- middle Jurassic contemporaneous with growth of a salt pillow to the west and (2) subsequent fault initiation at a shallower level, which then propagated down and vertically linked with pre-existing deeper faults (formed during stage 1) resulting in reactivated fault surfaces. Further, these analyses indicate that reactivation of the faults in the late Cretaceous- early Tertiary is a result of contemporaneous remobilization of the salt. Based on the three-dimensional displacement analyses we conclude that salt

mobilization controlled the development of the fault array, where reactivation the buried late Triassic to middle Jurassic faults is only observed where salt is not depleted. A close connection is observed between pre-salt ('basement') fault arrays and the localization of shallower ('cover') faults formed during salt mobilization. One of the cover faults is coupled with one of the pre-salt faults, while the majority of faults are decoupled and show that strain was largely transferred through the salt layer during the fault development.

In hydrocarbon exploration and production, detailed quantitative fault analysis, as exemplified herein, has a range of other applications and is essential in the assessment of displacement distribution, fault zone geometry as well as growth- and linkage history. This in turn may have implications for understanding fault seal capacity and thus, fluid flow dynamics during production or the delineation and risking of fault controlled traps in exploration. Comprehensive three-dimensional fault displacement analysis is therefore important, capturing a level of detail in displacement distribution and fault history that would otherwise be lost.

Oral Presentation: Tectonic Studies Group meeting
4th-6th of January 2012, Edenborough

The growth and linkage of salt-influenced extensional faults: Egersund Basin, Norwegian North Sea

Anette Broch Mathisen Tvedt 1, 2, Christopher A-L Jackson3, Atle Rotevatn 1, 2, Rob Gawthorpe 1

1 Department of Earth Science, University of Bergen, Allégaten 41, 5007 Bergen, Norway
2 Centre for Integrated Petroleum Research, University of Bergen, Allégaten 41, 5007 Bergen, Norway
3 Department of Earth Science & Engineering, Imperial College, London SW7 2AZ, UK

The structural style and evolution of normal fault systems above thick, mobile salt layers is less well understood compared to the normal faults developed in rifts where strong variations in mechanical stratigraphy are absent. This study uses 3D seismic reflection and well data from the Egersund Basin, Norwegian North Sea, to document the structural style and growth history of a salt-related normal faults array. To evaluate the evolution and morphology of the salt-influenced faults we apply the following methods: 1) 3D mapping of faults and age-constrained growth strata, 2) geometric and kinematic classification of the fault segments, and 3) three-dimensional mapping of displacement distributions on the fault surfaces. Our analysis indicates that several of the faults exhibit linkage geometries that differ from segmented faults in basins that lack salt. In the northern part of the basin, the growth of a low-relief salt pillow led to the development of a thin-skinned normal fault array, c. 16 km long and approximately 6 km wide, where the general dip directions of the faults are either northwest or southeast. Throw generally increases northward along the fault array from 40-60 ms, in the south, to a maximum of c. 140 ms in the north. Present-day throw distributions suggest both lateral and dip growth and linkage. Furthermore, the intricate, but systematic style of displacement and growth, suggest a staged evolution of (1) initial syn-sedimentary fault growth and (2) subsequent reactivation and blind propagation of some structures. Growth strata indicate syn-sedimentary faulting at the transition between Skagerrak and Bryne formations (Late Triassic - Early Jurassic), which is

contemporaneous with growth of a salt pillow to the west. The reactivation of the faults may either be caused by later salt mobilization or a later tectonic event. Three-dimensional seismic data have provided important insights into the development of salt-influenced normal fault arrays; in particular, we will highlight the lateral growth and linkage and the importance of dip linkage and blind fault reactivation.